A TWO-LAYER BOX MODEL FOR THE STRAIT OF ISTANBUL USING RADIAL BASIS FUNCTION COLLOCATION

by

Cenk Güngör

B.S., C.E., Yıldız Technical University, 2000

Submitted to the Institute for Graduate Studies in
Science and Engineering in partial fulfillment of
the requirements for the degree of
Master of Science

Graduate Program in Civil Engineering

Boğaziçi University

2005

ACKNOWLEDGEMENTS

I would like to express my sincere gratitude to Dr. Osman S. Börekçi for accepting to supervise my thesis and also for teaching, orienting, and motivating me throughout my studies, and for his friendly attitude above all.

I would like to thank the members of my thesis committee, Dr. Cem Avcı, Dr. Esin Cevik, Dr. Yasin Fahjan and Dr. Emre Otay.

I am grateful to Dr. Emre Otay, and Dr. Akın Tezel for their both direct and indirect contributions to my intellectual development.

I benefited greatly from the criticism, suggestions and support of Dr. Emin Özsoy, Dr. Haluk Örs and Dr. Orhan Yenigün during this study.

I am indebted to my friends and the members of the coastal group-Yavuz Tokmak, Arzu Samancı, Bilge Tutak- in the Civil Engineering Department, and my girl friend Beril Gökan, who rendered my M.S. period a great experience!

Finally, I am grateful to my family who were always by me at every stage of this study. I dedicate this thesis to them as this would not have been possible without their love and devotion

ABSTRACT

A TWO-LAYER BOX MODEL FOR THE STRAIT OF ISTANBUL USING RADIAL BASIS FUNCTION COLLOCATION

A one-dimensional, two-layer, depth averaged box model was developed to simulate the surface gradient driven steady flow occurring in the Strait of Istanbul (Bosphorus). An efficient meshless numerical scheme based on the Radial Basis Function Collocation method has been employed in the model.

In the model, the currents are driven by the hydrostatic pressure gradient and the bottom slope. Flow resistance is introduced through the bottom shear stress and interfacial shear stress between the layers. Transfer of momentum in the vertical direction is neglected.

The model was tested by specifying layer thickness and discharge values at the Black Sea and the Sea of Marmara ends of the strait. The results, presented in the form of graphs of layer depths and velocities along the length of the strait, were found to be in close agreement with those of previous studies and, where available, measurements. The Radial Basis Function Collocation method was found to be a promising method for two- and possibly three-dimensional models of the strait.

ÖZET

İSTANBUL BOĞAZI AKINTILARININ RADYAL BAZ FONKSIYON KOLLAKASYONU İLE İKİ KATMANLI KUTU MODELİ

İstanbul Boğazı'nda su yüzeyinin eğimli olması sonucu oluşan, zamanda değişmeyen yüzey akıntısını simule etmek için, tek boyutlu, iki katmanlı ve derinlik boyunca ortalama alınmış bir kutu model geliştirilmiştir. Modelde, radyal baz fonksiyonları nokta atama metodunu esas alan, verimli, ağsız bir sayısal şema kullanılmıştır.

Modelde akıntılar, hidrostatik basınç değişimleri ve taban eğimi ile hareket etmektedirler. Taban sürtünmesi ve katmanlar arası sürtünmeler akıma karşı koymaktadırlar. Dikey yönde momentum transferi dikkate alınmamıştır.

Model, Karadeniz ve Marmara Denizi girişlerinde, katman kalınlıkları ve akım değerleri belirtilerek test edilmiştir. Boğaz boyunca çizilen tabaka kalınlığı ve hız grafiklerinden çıkan sonuçlar, daha önceki çalışmalar ve elde olan ölçümlerle yakın ilişki içindedirler. Radyal baz fonksiyonları nokta atama yöntemi iki ve muhtemelen üç boyutlu boğaz modelleri için ümit vaadedici bulunmuştur.

TABLE OF CONTENTS

LIST OF FIGURES

LIST OF TABLES

LIST OF SYMBOLS/ABBREVIATIONS

A	Eddy viscosity
A_h	Horizontal eddy viscosity
A_z	Vertical eddy viscosity
C	Chezy coefficient
c	Shape parameter
C_{10}	Wind drag coefficient
d	Depth
d_1	Depth of upper layer
d_2	Depth of lower layer two
f	Coriolis parameter
f_b	Frictional parameter
g	Gravitational acceleration
H	Channel depth
h	Depth
Δh	Elevation difference
L	Channel length
N_h	Horizontal eddy viscosity per unit density
p	Pressure
p_a	Atmospheric pressure
p_0	Hydrostatic pressure
Q	Flow rate
Q_1	Flow rate of the upper layer
Q_2	Flow rate of the lower layer
ΔQ	Net barotropic flow
ΔQ_f	Seasonal fresh water influx deviation
r	Bottom drag coefficient

S_0^x	Bottom slope along direction x
S_0^y	Bottom slope along direction y
u	Horizontal velocity component
$\overline{u}$	Depth averaged horizontal velocity component
u_1	Horizontal velocity component of layer one
u_2	Horizontal velocity component of layer two
$\lvert V_t \rvert$	Magnitude of the fluid velocity
v	Transverse velocity component
$\overline{v}$	Depth averaged transverse velocity component
v_1	Transverse velocity component of layer one
v_2	Transverse velocity component of layer two
W	Wind speed
w	Vertical velocity component
$\Delta\varsigma_b$	Sea level deviation from the mean value
Θ	Latitude
Ω	Earth's angular velocity
α	Frictional parameter
γ	Unit weight of water
η	Free surface displacement
λ	Interpolation coefficient
ν	Order of Bessel function
ρ	Density of water
$\overline{\rho}$	Average density
ρ'	Density fluctuation
ρ_1	Density of layer one
ρ_2	Density of layer two
τ_i	Interfacial shear stress
τ_b^x	Bottom shear stress along x

τ_s^x	Surface shear stress along x
4^{th}OS	4^{th} order spline
BBJ	Black Sea junction
MQ	Multiquardic
PDEs	Partial differential equations
ppt	Parts per thousand
RBFs	Radial basis functions
SWE	Shallow water equation

1. INTRODUCTION

Two-layer exchange flows often occur when a constriction separates two bodies of water with different densities. The density difference may arise owing to differences in temperature, salinity and/or sediment concentration. Understanding exchange flow is important when addressing water quality issues in semi-enclosed bodies such as bays, fjords and inlets. A classic example is the exchange of more saline Mediterranean water with Atlantic water through the Strait of Gibraltar (e.g. Armi and Farmer, 1988). Important exchange flows occur in other straits including the Bosphorus and Dardanelles which connect the Aegean and Black Seas via the Marmara Sea (Oğuz and Sur, 1989; Gregg and Özsoy, 2002) and the Bab-el-Mandeb which connects the Indian Ocean to the Red Sea (Murray and Johns, 1997). Understanding exchange flow can be important in engineering problems. For example, the design of a bridge linking Denmark and Sweden required zero reduction in exchange flow through the Great Belt between the Baltic and North Seas (Ottesen Hansen and Moller, 1990). Another exchange of environmental concern is that of heavily polluted water from Hamilton Harbor with Lake Ontario water through the Burlington Ship Canal (Hamblin and Lawrence, 1990).

The Bosphorus Strait provides the only mechanism of communication between the Black Sea and the Sea of Marmara. For this important reason, the geographic importance has been recognized since the earliest times. In the 17th century, Count Marsilli was the first one to make scientific observations in the Bosphorus and perform insightful experiments establishing the existence of counter-currents underneath the surface currents. Modern observations have revealed persistent exchange flows, specific and general understanding of the flow patterns. A detailed chronological review of the oceanographic investigations of the Turkish Straits can also be found in DAMOC Report (1971). A brief account of these investigations will be presented in the appendices.

With the advancement of computers, numerical methods have been widely used in flow modeling. The hydrodynamic-numerical models can be safely used to compute dynamic processes when a close correlation between the numerical results and the results of field measurements yields.

Meshfree methods for the solution of partial differential equations (PDEs) gained much attention in recent years, not only in the engineering but also in the mathematics community. One of the reasons for this development is the fact that meshfree discretizations and particle models are often better suited to cope with geometric changes of the domain of interest, e.g. free surfaces and large deformations, than classical discretization techniques such as finite differences, finite elements or finite volumes. Another obvious advantage of meshfree discretizations is of course their independence of a mesh. Mesh generation is still the most time consuming part of any mesh based numerical simulation. Since meshfree discretization techniques are based only on a set of independent points these costs of mesh generation are eliminated. Finally, the coupling of particle models to continuous models gained enormous interest in recent years from a theoretical as well as from a practical point of view.

Using Radial Basis Functions (RBFs) for the solutions of PDEs gained enormous interest after Kansa (1990a; 1990b). Numerical computing with RBFs concentrates on the rebuilding of unknown functions from known data. Data depended functions may be solutions of PDEs. More advantages of RBFs are,

- Decrease the computational time,
- Use with hyperbolic, elliptic and parabolic equations,
- Formulated easily in non-linear problems,
- Save time in adjustable domains,
- Use in irregular domains.

In this study, the depth averaged equations of motion and continuity, satisfying certain additional conditions on the boundaries are presented. In the model developed here, the shallow water equations (SWE) were driven by a free surface gradient between the Black Sea and the Marmara Sea to determine both the velocity field and the variations of layer thicknesses by a meshless method using RBF collocation method which is a convergent new technique.

2. CHARACTERISTICS OF THE BOSPHORUS STRAIT

2.1. Geometrical Features

The Bosphorus is a meandering strait located at the northern part of the Turkish Strait System (Figure 2.1) which forms a passageway connecting the Black Sea to the Mediterranean Sea. It is assumed that the Bosphorus is an ancestral valley which has formed under the control of joint sets and faults in the North West-South West and East directions. It is also assumed that during the Pleistocene age it was drowned and became a sea connection. From then to our time it has undergone some changes brought about by the effects of surface and sea-bottom erosion. It can be characterized as a drowned ancestral valley.

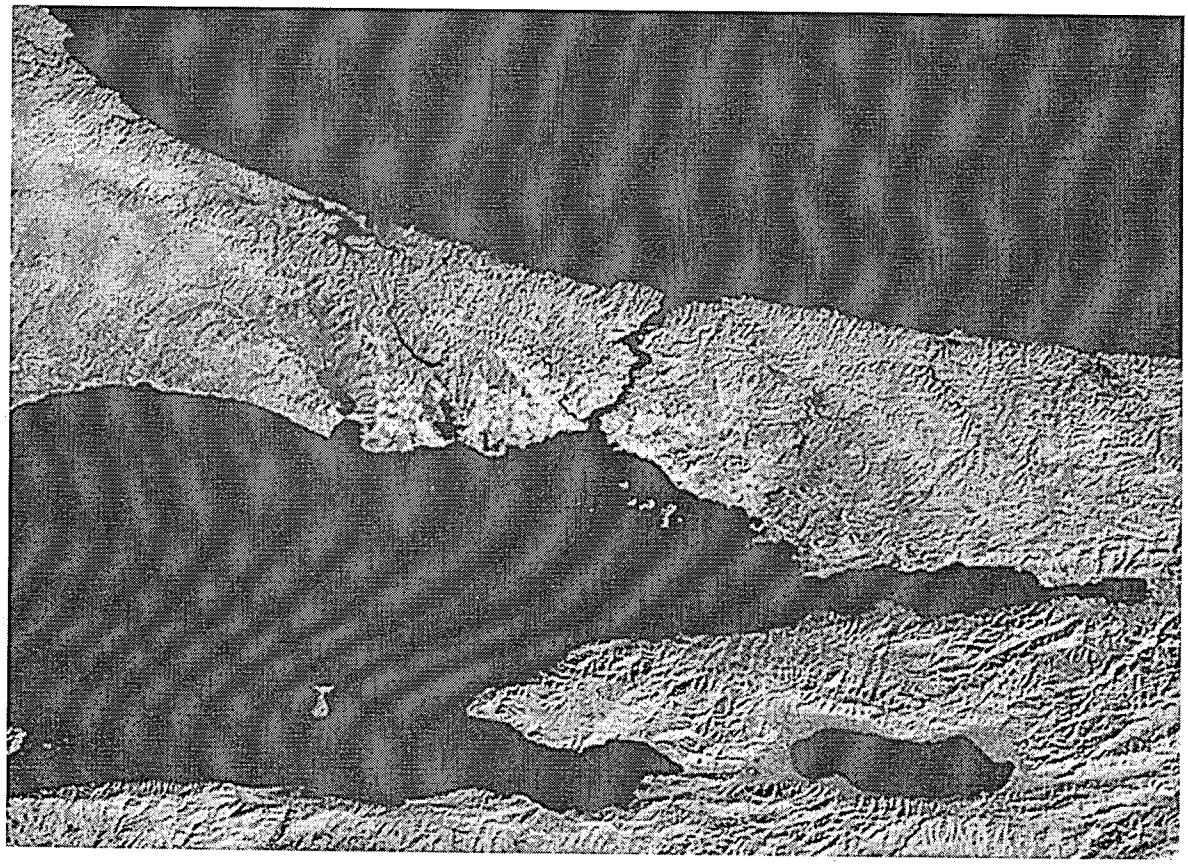

Figure 2.1. Northern part of the Turkish Strait System (NASA, 2003)

The length of the Bosphorus is about 35 km and its width varies between 600 and 3500 m (Turkish Navy Department of Navigation, Hydrography and Oceanography (TNHO) Map No: 2921 a, b). The Bosphorus is, therefore, one of the straits over the world having the smallest width to length ratio. A small estuary, the Golden Horn, joins it at the southern tip of the strait.

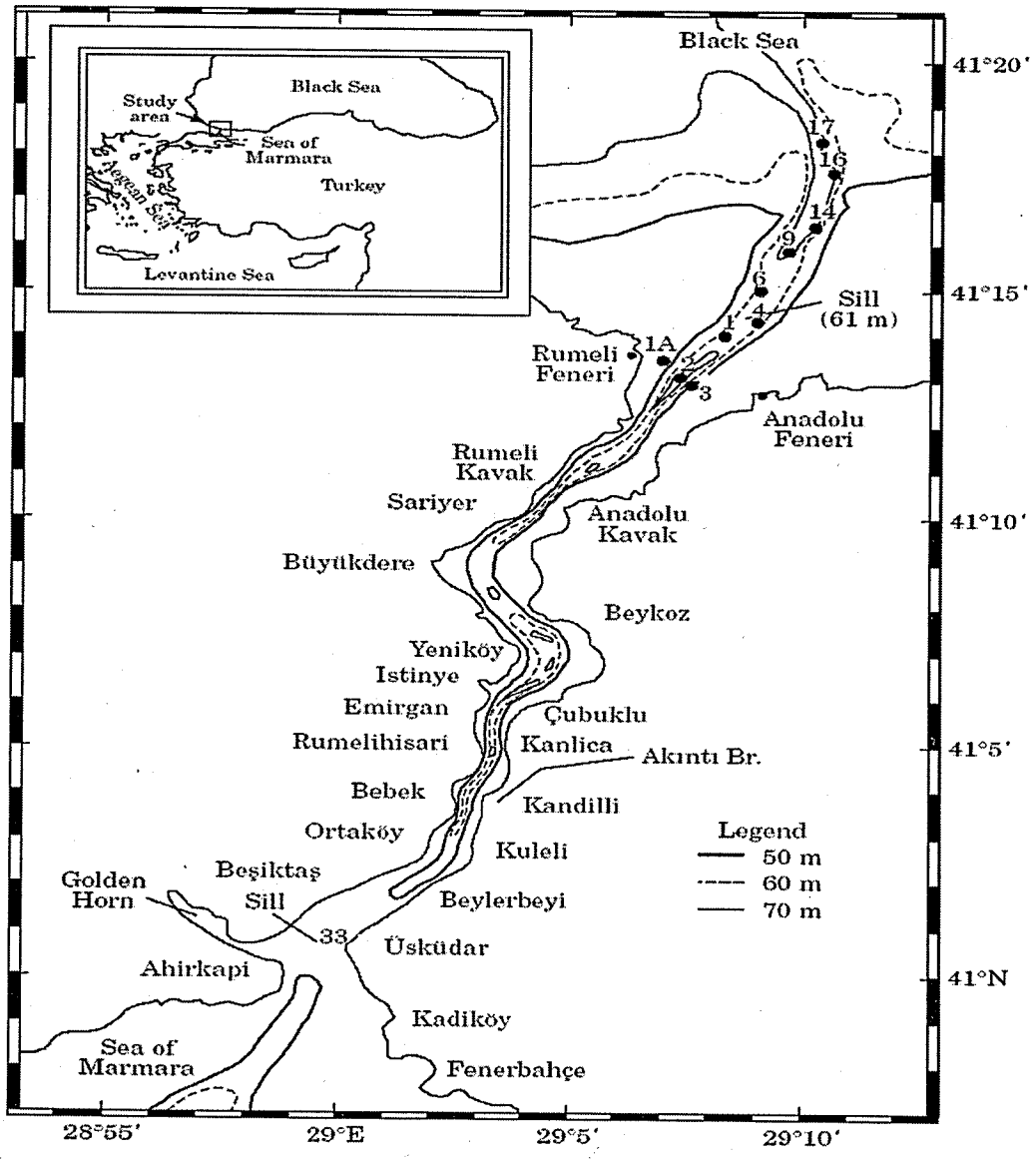

Figure 2.2. Bathymetry and location chart of the Strait (Yüce, 1996)

The bottom topography of the Bosphorus changes significantly along both the lateral and the longitudinal directions. The average depth is about 64.5 m and it tends to become deeper towards the northern sections where depths greater than 100 m can be observed.

There are two sills in the Bosphorus. One is located at about 3 km north of the southern tip of the strait and its depth is about 28 m. The other sill is located at about 4 km away from the northern entrance and its depth is about 50 m. Both sills play a significant role on the flow dynamics of the Bosphorus. However the effect of the sills is not included in the present study.

2.2. Oceanographic Characteristics

2.2.1. Circulatory Features

A detailed coverage of the oceanographic characteristics of the Bosphorus was given by Ünlüata and Oğuz (1983) and Tolmazin (1985). Only a brief account of these characteristics will therefore be presented here.

It is a well-known fact that two-layer stratification and an associated two-layer current system exists in the Bosphorus. Consequently, waters of Black Sea origin flow towards the Sea of Marmara along the surface on top of the denser Maramara waters flowing in the opposite direction.

The basic mechanism leading to such a two-layer current system is related to the difference in the sea surface elevations and densities of the adjacent basins located at both ends of the Bosphorus. The Black Sea possesses the characteristics of a dilution basin in which the average gain due to the precipitation and river run off exceeds losses through evaporation as compared to those observed in the Sea of Marmara. This fact results in a higher sea surface elevation on the Black Sea side and the associated horizontal pressure gradient drives a surface current in the southward direction through the Bosphorus.

On the other hand, the deeper section of the Sea of Marmara is occupied by denser Mediterranean waters as compared with those observed in the Black Sea. The resulting density gradient established along the Bosphorus reverses the sign of the horizontal pressure gradient at deeper levels and thereby induces a northward flowing bottom current along the Bosphorus.

The magnitude of velocities in each layer varies seasonally as well as with the distance along the Bosphorus, and is further affected significantly by the short term transient southerly and northerly wind episodes. The typical magnitudes of surface currents are about 40-50 cm/s on the northern part of the Bosphorus. They become stronger near the Marmara end and may reach up to about 250 cm/s (DAMOC Report, 1971: TNHO Map No: 2921 A, B).

During strong northerly winds, the surface currents increase further in magnitude and may attain values of about 100 cm/s and 350 cm/s respectively on the vicinity of the Black Sea end the Sea of Marmara ends of the Bosphorus (Black Sea Pilot, 1955). The southerly winds, on the other hand, weaken the surface currents to a considerable extent and may even change its direction leading to flow reversals observed frequently during winter months (Pektaş, 1953). Less is, however, known about the lower layer currents; magnitudes of up to 100 cm/s in the southern sections of the Bosphorus are reported by Moller (1928). Magnitudes in the range of 0-75 cm/s were measured near Çubuklu, located midway between the two ends of the strait, at about 60 m depth in 1965 (DAMOC Report, 1971).

The water exchange through the Bosphorus varies seasonally depending on the water balance of the adjacent basins. It is reported by the U.S. Navy Hydrographic Office (1967) that the flow rates in either direction vary between 3,000 – 30,000 m^3/s. The first estimates of the flow were given by Moller (1928). On the basis of available data, he estimated the amount of flow entering the Bosphorus from the Black Sea as being 12,600 m^3/s, whereas the lower layer flow rate was found to be 6,100 m^3/s. A more recent numerical study by Sümer and Bakioğlu (1981) proposes these values as 17,400 m^3/s and 7,900 m^3/s respectively.

In the Madericha and Konstantinov's study (2002), the calculated yearly mean level difference between seas and volumetric flow rate in the upper layer and bottom layer were Δh = 0.299 m, Q_1=13,089 $m^3\ s^{-1}$, Q_2=-6,459 $m^3\ s^{-1}$, respectively. As expressed in their study, it was difficult to directly compare the results of seasonal simulations with short-term measurement data that were given by Moller (1928) and Özsoy *et al.* (1996) because of synoptic scale variations of currents in time. Therefore in Figure 2.3 the volumetric flow

rates in the upper layer Q_1 and bottom layer Q_2 of Bosphorus were plotted against the net barotropic flow Q by Madericha and Konstantinov (2002). As seen in the figure the quasi-stationary hydraulic model with simple topography well describes in a quantitative sense the seasonal flow dynamics in the Strait with complicated topography and forcing. The high values of the observed flow rates are connected with the short time variability of the level difference along the strait, barometric pressure difference between the Black and Marmara seas and local winds (Ünlüata *et al.*, 1990; Özsoy *et al.*, 1996; Yüce, 1996).

The relation between seasonal Black Sea level deviation $\Delta\varsigma_b$ from the mean value and seasonal deviation ΔQ_f of the freshwater influx from the mean value is shown Figure 2.4. The variation of level lagged behind the freshwater influx with delay time of about 2 months. The computations were compared with the Black Sea data (Simonov and Altman, 1991) in Madericha and Konstantinov's study (2002). The discrepancies were explained by the sensitivity of the calculation to the Marmara Sea level that is averaged only over a short period of 3 years (Alpar and Yüce, 1998).

The relation between the seasonal components of the barotropic net flow and the fresh water influx into the sea is far from simple. At the same time the dependence of the volumetric flows in the upper and bottom layer on the level difference between the Black and Marmara seas is close to linear Figure 2.5.

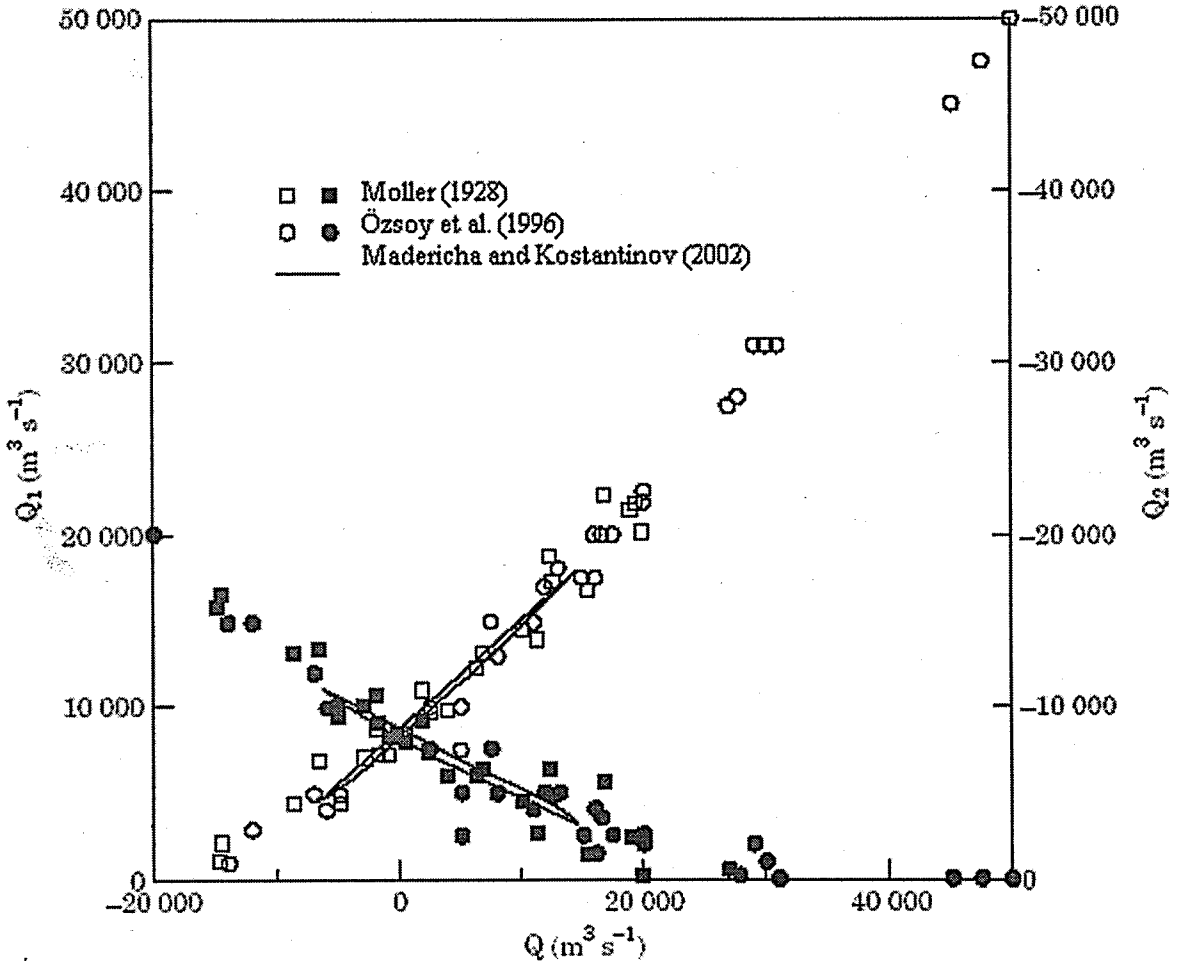

Figure 2.3. The volumetric flow rate in the upper layer Q_1 (open symbols) and bottom layer Q_2 (filled symbols) of the Bosphorus versus net flow Q (Madericha and Konstantinov, 2002)

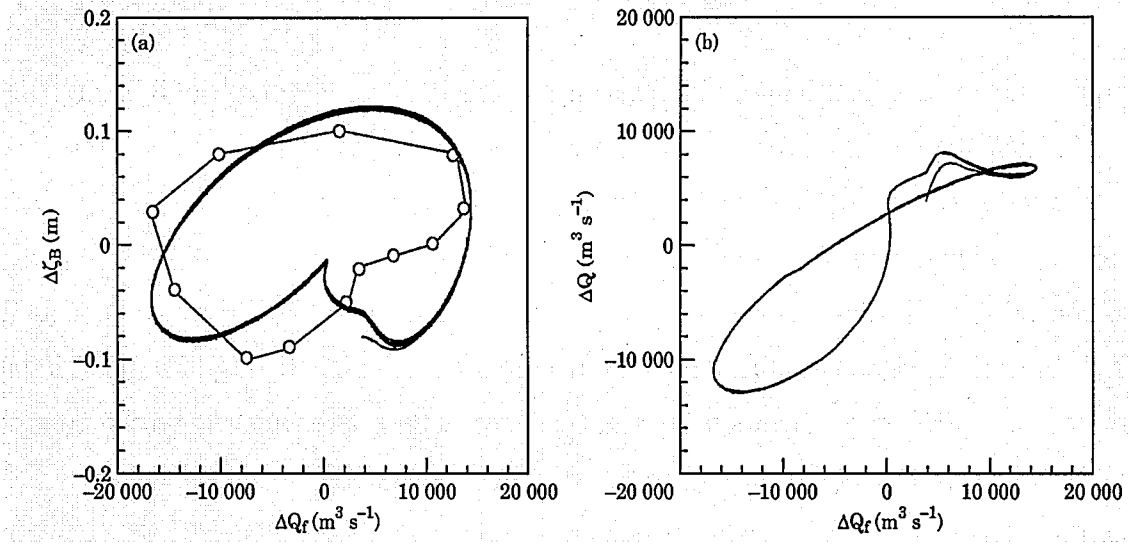

Figure 2.4. The Black Sea level deviation $\Delta\zeta_B$ from the mean value (a) and seasonal deviation of barotropic net flow ΔQ through the Bosphorus from the mean value (b) versus the deviation of freshwater influx to the sea ΔQ_f (Simonov and Altman, 1991)

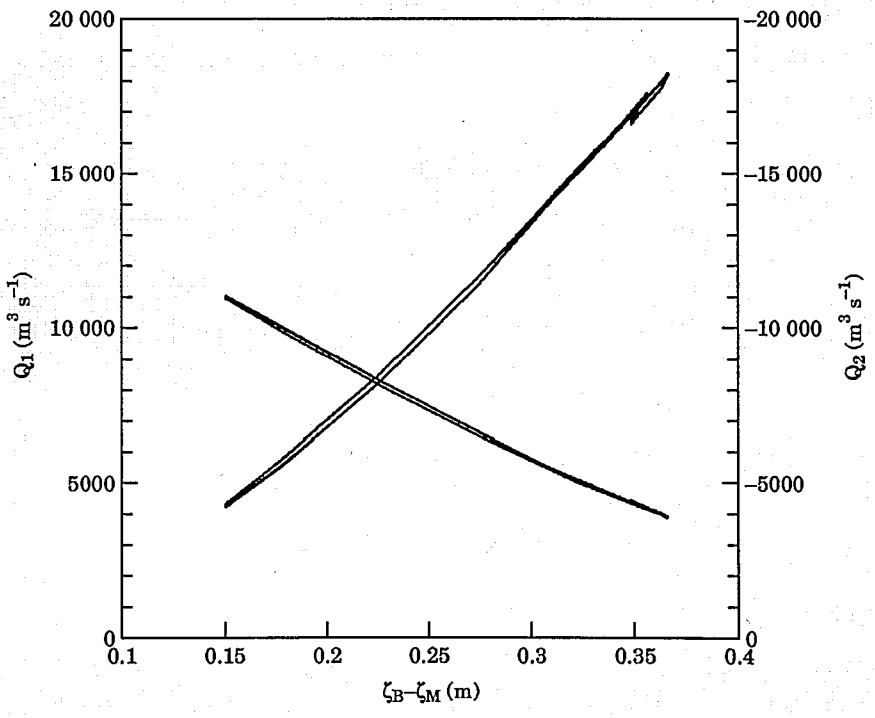

Figure 2.5. The calculated volumetric flow rates in the upper layer Q_1 and bottom layer Q_2 of strait versus the level difference between the Black and Marmara Seas (Madericha and Konstantinov, 2002)

2.2.2. Hydrographic Features

In addition to the currents of the Bosphorus, salinity and temperature characteristics also show seasonal and spatial variations throughout the year. While a typical salinity near the Black Sea end may be assumed to be about 17.5 parts per thousand (ppt), it decreases down to the values of 16.5-17 ppt during the summer season corresponding to the period of higher rate of surface inflow from the Black Sea. As the surface salinities do not show significant changes along the northern half of the Bosphorus, a considerable vertical mixing taking place near its southern end causes a 2-3 ppt increase in the surface salinities. On the other hand, the lower layer salinities near the Marmara entrance attain values of about 38-38.5 ppt and are further reduced to approximately 36.5 ppt as a result of mixing with surface waters by the time they reach the Black Sea end of the Bosphorus.

As far as temperature variations are concerned, the winter season is characterized by almost uniform, cold surface waters having temperatures of about $9-10°C$ above relatively warmer bottom waters of Mediterranean origin with temperature values in the range $14.5-15°C$. This two-layer structure in temperature, however, starts to change during the late spring and early summer months. Due to increased radiational heating, the upper parts of the surface waters become warmer than the rest of the water column. Consequently, a new temperature structure is formed with the surface layer consisting of warm surface waters and cold waters of the Black Sea underneath which are further separated by a sharp thermocline from the lower layer of Marmara waters. As the radiational heating intensifies and affects also the lower parts of the upper layer, all of the waters lying above the interface become eventually warmer than those in the lower layer and a temperature structure opposite to the one observed in winter months results along the Bosphorus during the late summer.

Moller's (1928) studies as well as those carried out by Bogdanova (1965), Günnerson and Özturgut (1974), Çeçen *et al.* (1981) reveal the existence of a sharp density transition between the surface and the bottom waters of the Bosphorus. The respective average densities of the upper and lower layers are 1013 and 1028 g/cm^3, implying a relative density difference of 0.014 g/cm^3. The measured interface is essentially linear along the Bosphorus. The typical interface slope estimated by Moller (1928) is 1.13m/km

which is higher than the 0.97 m/km slope estimated by Çeçen *et al.* (1981) and smaller than the DAMOC (1971) estimate of 1.6 m/km.

The thickness of the interface as well as the salinity, temperature, and pressure difference between the two layers varies along the strait. Salinity, temperature, and pressure difference affect the mixing characteristics and quantifying the density. As it is noted before, considerable mixing across the interface evidently occurs along the strait. The lack of reliable current data, however, prevents the computation of Richardson numbers (ratio of the stabilizing forces-due to stratification- to the de-stabilizing forces-due to the flow), and evaluation of the temporal and spatial mixing characteristics. It is worth pointing out also that lateral mixing resulting from meandering features of the strait is well evident in the data that collected for DAMOC (1971).

2.2.3. Interaction with Black Sea and the Marmara Sea

The existence of the sill 4 km north of the Bosphorus - Black Sea junction (BBJ) at a depth of 50 m plays a crucial role for the Mediterranean waters issuing from the Bosphorus. Ullyott and Ilgaz (1943; 1946); Ullyott (1953) claim the return of 75% of the Mediterranean waters back to the Bosphorus as a result of the blocking by the sill. Pektaş (1953; 1956) later proposed that the Ullyott-Ilgaz hypothesis should be partially valid for only the March-August period coinciding with the times of increased outflows from the Black Sea. Utilizing all the available data obtain for the BBJ region, Bogdanova (1961; 1969); Bogdanova and Stopanov (1974) and later Tolmazin (1985) show that the Mediterranean waters in fact enter into the Black Sea throughout the year along the bottom. They are not blocked by the sill, but flow over it and then turn northwestwards and eventually are entrained into the Black Sea waters.

Measurements reported in Çeçen *et al.* (1981); Bayazıt and Sümer (1982) show that a complete blockage may occur near BBJ at certain times of the year, corresponding to periods of high rate Black Sea inflow into the Bosphorus. They report such a blockage event in May 1981 about 3 km south of the Black Sea junction of the Bosphorus. The May 1981 blockage event is, however, the only case reported among the observations conducted up to now in the BBJ. It may, therefore, be considered that the Mediterranean waters enter

into the Black Sea continuously except at rare events such as the one observed in May 1981. However the role of southern winds was not stated in the reports.

Under calm weather conditions, the Black Sea waters emanating from the Bosphorus tend to spread asymmetrically in the region just south of the Marmara end of the strait. The surface currents first attach to the Anatolian coast and then curl around in the vicinity of the Prince Islands and form an anticyclonic grye. While most of flow then proceeds westwards, a branch of it flows towards the bay of İzmit. Evidence relating to the presence of such a flow structure is reported in detail by Ünlüata and Oğuz (1983).

2.3. Studies on Various Physical Quantities

2.3.1. Wind Drag Coefficient

Wind stress is generally proportional to wind speed squared with a drag coefficient which, in empirical formulas, is merely a function of wind speed. According to Neumann (1966), pure drift currents are bringing forth by the drag of the wind passing over homogenous water. Horizontal pressure gradients within the water do not exist. The driving force is the wind stress applied at the sea surface and frictional coupling between individual layers of the medium. According to Kowalik and Murty (1993) summarized wind drag coefficients, C_{10}, due to various researchers. Garratt (1977) analyzed available measured data and concluded that C_{10} under a neutral atmospheric stability depends linearly on the wind velocity. In the storm surge computations according to Henry and Heaps (1976), the wind drag coefficient is usually set as constant.

2.3.2. Bottom Drag coefficient

For the bottom stress, commonly two assumptions, linear friction which is mathematically simpler and quadratic friction which is physically more realistic are used. According to Wang (1990) the friction coefficient can in certain flow regimes be related to the Chezy coefficient or the Manning coefficient, however it generally depends on roughness and Reynolds number as given by the Colebrook-White formula stated by Daily and Harlemann (1996). According to Al-Rabeh and Günay (1992), the friction coefficient

should be computed locally using a fit based on local water depth and observed velocity. For bottom stress a drag coefficient, r, can also be used according to Kowalik and Murty (1993). r is a function of the bottom roughness and the properties of the bottom boundary layer as Komar (1976) has also stated. This coefficients magnitude is related to the averaged flow condition.

Table 2.1. Dimensions L, H, frictional parameters, f_b, and α for various straits (Zaremba *et al.*, 2003)

	L (km)	H(m)	f_b	$\alpha = f_b$ H/L	Source
Bab el Mandeb	160	172	0.012	11.2	Defant (1961)
	160	180	0.03	26.7	Assaf &Hecht (1974)
	160	180	0.012	10.7	Maderich & Efroimson (1990)
Bering Strait	100	50	0.002	4.0	Pratt (1986)
Bosphorus	30	60	0.0046	2.3	Defant (1961)
	30	60	0.03	15.0	Assaf &Hecht (1974)
	20	20	0.002	2.0	Pratt (1986)
	31	40	0.012	9.3	Maderich & Efroimson (1990)
	30	50	0.0046	2.8	Oğuz *et al.* (1990)
Burlington Ship Canal	0.84	9.5	0.0052	0.5	Dick & Marsalek (1973)
Dardanelles	60	70	0.012	10.3	Defant (1961),
	60	70	0.03	25.7	Assaf &Hecht (1974)
	65	55	0.0046	5.4	Oğuz et al. (1990)
Denmark Strait	500	500	0.002	2.0	Pratt (1986)
Ecuador Trench	300	300	0.002	2.0	Pratt (1986)
Gibraltar	60	300	0.012	2.4	Defant (1961)
	60	350	0.03	5.1	Assaf &Hecht (1974)
	20	200	0.002	0.2	Pratt (1986)
	50	300	0.012	2.0	Maderich & Efroimson (1990)
Iceland-Faroe Ridge	400	400	0.002	2.0	Pratt (1986)

Schijf and Schönfeld (1953), was first, who considered the effect of friction on two-layer flow by in their classic study of a salt wedge. Anati *et al.* (1977) investigated the relative importance of frictional and inertial forces in exchange flows in constant-width channels.

Anati *et al.* (1977) classified the dynamic length of the channel by the parameter f_b L/H, where f_b is the friction coefficient, L is the channel length, and H is the channel depth. In a short channel, f_b L/H < 1 and bottom friction can be neglected compared to inertial forces. In a long channel, f_b L/H > 1 and inertial forces can be neglected. In channels of marginal length, f_b L/H « 1, both terms need attention to take into consideration. Estimates of f_b L/H listed in Table 2.1 indicate that, in general, sea straits are either marginal or long.

3. THE MATHEMATICAL MODEL OF THE FLOW

3.1. Background

Although the Navier-Stokes equations are generally solved for determining the circulation in water bodies, most numerical models used for modeling of coastal waters and estuaries are based on SWE, obtained from the full three-dimensional hydrodynamical equations by averaging over the vertical coordinate.

Coriolis force is a consequence of relative accelerations generated due to noninternal nature of the rotating coordinate frame. Effect of the coriolis force is not significant in Bosphorus Strait since the strait is not a large scale water body and is not included in the two layer model.

Another such deviation from the conventional incompressible Navier-Stokes equations may be the inclusion of salinity effects, which introduce the density gradients in the domain. In the present study, density is assumed to be constant for each layer.

One further simplification from the fully 3D Navier-Stokes equations is the so called hydrostatic approximation. When the vertical motions are small, overwhelmed by gravitational forces, and vertical frictional forces are small, the fluid acts as though under static equilibrium as far as vertical motions are concerned. However, this approximation fails when large salinity gradients exist in the domain. On the other hand, hydrostatic approximation is generally accurate enough and applicable to handle numerically.

A review of such models with application of various numerical techniques is given by Liu and Leendertse (1978) who gave examples of the implicit finite difference method. In fact, the current work may be introduced as a successor of the thesis by Bozoklar (1990), in the respect that here, an efficient meshless numerical scheme based on RBFs are used in order to approximate the spatial derivatives of the equations derived from the model.

3.2. Governing Equations of the System

The governing equations of the proposed model are simplified version of the three dimensional hydrodynamics model derived from the Navier-Stokes equations. The specification of incompressibility and constant density decouples the dynamics. The SWEs developed may be adapted for use in modeling a flow system that has density stratification. The simplest of these is the two layer system which may be thought of as the first approximation to a full three dimensional model.

The flow of each layer will be governed by the SWE with appropriate boundary and matching conditions (in terms of normal and tangential stresses) at the interface of the layers. The two layer system is being driven by pressure gradients (atmospheric and hydrostatic imposed by the tilted free surface and interface) and the momentum transferred from the wind blowing over the free surface.

3.2.1. Three Dimensional Equations

The set of averaged equations of motion in rectangular system of coordinates by observing the presence of the Reynolds stresses or the eddy coefficient are:

$$\frac{Du}{Dt} - fv = -\frac{1}{\rho}\frac{\partial p}{\partial x} + A\nabla^2 u \tag{3.1}$$

$$\frac{Dv}{Dt} - fu = -\frac{1}{\rho}\frac{\partial p}{\partial y} + A\nabla^2 v \tag{3.2}$$

$$\frac{Dw}{Dt} = -\frac{1}{\rho}\frac{\partial p}{\partial z} + A\nabla^2 w \tag{3.3}$$

where u, v and w are the mean velocity components in x-,y- and z- directions, respectively, A is the eddy viscosity coefficient, p is the pressure and ρ is the density. The operator $\frac{D}{Dt}$ is the material derivative.

$$\frac{D}{Dt} = \frac{\partial}{\partial t} + u\frac{\partial}{\partial x} + v\frac{\partial}{\partial y} + w\frac{\partial}{\partial z} \tag{3.4}$$

In these equations, the Coriolis parameter,

$$f = 2\Omega \sin\Theta \tag{3.5}$$

is a function of the earth's angular velocity $\Omega = 7.29 * 10^{-5} s^{-1}$ and the latitude, Θ.

The two dimensional Laplace operator defined as,

$$\nabla^2 = \frac{\partial^2}{\partial x^2} + \frac{\partial^2}{\partial y^2} \tag{3.6}$$

$$\frac{\partial u}{\partial t} + u\frac{\partial u}{\partial x} + v\frac{\partial u}{\partial y} + w\frac{\partial u}{\partial z} - fv = -\frac{1}{\rho}\frac{\partial p}{\partial x} + A_z\frac{\partial^2 u}{\partial z^2} + A_h\nabla^2 u \tag{3.7}$$

$$\frac{\partial v}{\partial t} + u\frac{\partial v}{\partial x} + v\frac{\partial v}{\partial y} + w\frac{\partial v}{\partial z} + fu = -\frac{1}{\rho}\frac{\partial p}{\partial y} + A_z\frac{\partial^2 v}{\partial z^2} + A_h\nabla^2 v \tag{3.8}$$

$$\frac{\partial w}{\partial t} + u\frac{\partial w}{\partial x} + v\frac{\partial w}{\partial y} + w\frac{\partial w}{\partial z} + fu = -\frac{1}{\rho}\frac{\partial p}{\partial y} - g + A_z\frac{\partial^2 w}{\partial z^2} + A_h\nabla^2 w \tag{3.9}$$

where the parameters A_h and A_z are the horizontal and vertical eddy viscosity coefficients, respectively.

If the flow is considered to be predominantly horizontal and the vertical acceleration is small compared to the gravitational acceleration, such as in coastal and estuarine-flows, the equation of vertical motion can be reduced to the hydrostatic law.

$$-\frac{\partial p}{\partial z} - \gamma = 0 \tag{3.10}$$

Equation (3.10) indicates that the pressure variation in the vertical direction is hydrostatic. By integrating Equation (3.10), from any depth z to the free surface $z = \eta\ (\mathrm{x, y, t})$ for a fluid with density variations,

$$\int_z^\eta dp = -\int_z^\eta g(\rho_0 + \rho')dz \tag{3.11}$$

where ρ_0 is the density of the water and ρ' is the density fluctuation of the water.

$$\begin{aligned} p &= p_0 + p' \\ p' &= p_a - p_0 + g\int_z^0 \rho_0 dz + g\rho_0(\eta - z) + g\int_z^\eta \rho' dz \end{aligned} \tag{3.12}$$

where ρ_a is the atmospheric pressure. In Equation (3.12), by the integration of Equation (3.10) the unknown pressure variations as a sum of terms related to the atmospheric pressure p_a and hydrostatic pressure p_0 have been obtained.

Using the Boussinesq approximation which describes the way the density variation enter into the equation of motion, Equation (3.1) becomes

$$(\rho_0 + \rho')\left(\frac{Du}{Dt} - fv\right) = -\frac{\partial(p_0 + p')}{\partial x} + \frac{\partial}{\partial z}A_z\frac{\partial u}{\partial z} + A_h\nabla^2 u \tag{3.13}$$

or more simplified equation in the Boussinesq form can be written by neglecting variational terms,

$$\rho_0\left(\frac{Du}{Dt} - fv\right) = -\frac{\partial(p_0)}{\partial x} + \frac{\partial}{\partial z}A_z\frac{\partial u}{\partial z} + A_h\nabla^2 u \tag{3.14}$$

Combining Equations (3.12) and (3.14) with Boussinesq or hydrostatic approximation and using Equation (3.12), and applying similar conditions to the conditions of motion along y coordinate, the system of equations becomes,

$$\frac{Du}{Dt} - fv = -\frac{1}{\rho_0}\left(\frac{\partial p_a}{\partial x}\right) - g\frac{\partial \eta}{\partial x} - g\frac{\partial}{\partial x}\int_z^\eta \rho' dz + \frac{1}{\rho_0}\left(\frac{\partial}{\partial z}A_z\frac{\partial u}{\partial z} + A_h\nabla^2 u\right) \quad (3.15)$$

$$\frac{Dv}{Dt} + fu = -\frac{1}{\rho_0}\left(\frac{\partial p_a}{\partial y}\right) - g\frac{\partial \eta}{\partial y} - g\frac{\partial}{\partial y}\int_z^\eta \rho' dz + \frac{1}{\rho_0}\left(\frac{\partial}{\partial z}A_z\frac{\partial u}{\partial z} + A_h\nabla^2 u\right) \quad (3.16)$$

The SWEs are composed of the depth integrated horizontal components of the momentum equation and the continuity equation. Both the sea surface, $z = \eta\ (\mathrm{x, y, t})$, and the sea bottom, $z = -\mathrm{h}\ (\mathrm{x, y, t})$ may in general be functions of x, y and t. At both these locations kinematic surface conditions that assumes a fluid particle remains on the surface, must be satisfied and gives

$$w(\eta) = \frac{d\eta}{dt} = \frac{\partial \eta}{\partial t} + \frac{\partial \eta}{\partial x}\frac{\partial x}{\partial t} + \frac{\partial \eta}{\partial y}\frac{\partial y}{\partial t} = \frac{\partial \eta}{\partial t} + u\frac{\partial \eta}{\partial x} + v\frac{\partial \eta}{\partial y} \quad (3.17)$$

At the bottom, $z = -h(x, y, t)$, the kinematic bottom condition requires that the flow be parallel to the bottom. Equation (3.17) then becomes

$$w(-h) = -\frac{dh}{dt} = \frac{\partial}{\partial t}(-h) + \frac{\partial}{\partial x}(-h)\frac{\partial x}{\partial t} + \frac{\partial}{\partial y}(-h)\frac{\partial y}{\partial t} \quad (3.18)$$

$$= \frac{\partial}{\partial t}(-h) + u\frac{\partial}{\partial x}(-h) + v\frac{\partial}{\partial y}(-h) \quad (3.19)$$

The momentum conservation or the dynamic condition states that the forces acting on the fluid at the free surface is in equilibrium. As there is a steady flow assumption, differentiating the depth of water in time will give zero. Therefore the Equation (3.19) is rewritten

$$w(-h) = -u\frac{\partial}{\partial x}(h) - v\frac{\partial}{\partial y}(h) \quad (3.20)$$

At the bed, a no slip condition is applied. Due to viscous effects, the velocity of fluid is the velocity of the bed, assuming the velocity of bed zero, no slip boundary condition for viscous flow can be applied.

$$u = v = w = 0 \tag{3.21}$$

where $z = -h(x, y)$.

Integrating the Equation (3.15) term by term

$$\rho_0 \int_{-h}^{\eta} \frac{\partial}{\partial z}\left(A_z \frac{\partial u}{\partial z} \right) dz = \tau_x^s - \tau_x^b \tag{3.22}$$

$$\rho_0 \int_{-h}^{\eta} \frac{\partial}{\partial z}\left(A_z \frac{\partial v}{\partial z} \right) dz = \tau_y^s - \tau_y^b \tag{3.23}$$

where τ_x^b, τ_y^b is the bottom shear stresses, τ_x^s, τ_y^s is the wind induced surface shear stress in the x-direction and y- direction respectively. The components of the stress are defined as,

$$\rho_0 N_z \frac{\partial u}{\partial z} = \tau_x \quad \text{and} \quad \rho_0 N_z \frac{\partial v}{\partial z} = \tau_y \tag{3.24}$$

Applying Leibnitz rule (Appendix B) to the horizontal acceleration term in Equation (3.15),

$$\int_{-h}^{\eta} \frac{\partial u}{\partial t} dz = \frac{\partial}{\partial t} \int_{-h}^{\eta} u dz + u(-h) \frac{\partial}{\partial t}(-h) - u(\eta) \frac{\partial \eta}{\partial t} \tag{3.25}$$

where

$$u(-h) \frac{\partial}{\partial t}(-h) = 0 \tag{3.26}$$

and differentiating the depth of water in time is zero because steady flow assumption is adopted.

The convective horizontal acceleration term in Equation (3.15) transformed as,

$$\int_{-h}^{\eta} u\frac{\partial u}{\partial x}dz = \frac{\partial}{\partial x}\int_{-h}^{\eta} u^2 dz - \int_{-h}^{\eta} u\frac{\partial u}{\partial x}dz - u^2(\eta)\frac{\partial \eta}{\partial x} - u^2(-h)\frac{\partial(-h)}{\partial x} \tag{3.27}$$

$$\int_{-h}^{\eta} v\frac{\partial u}{\partial y}dz = \frac{\partial}{\partial y}\int_{-h}^{\eta} uvdz - \int_{-h}^{\eta} u\frac{\partial v}{\partial y}dz - uv(\eta)\frac{\partial \eta}{\partial y} - uv(-h)\frac{\partial(-h)}{\partial x} \tag{3.28}$$

and

$$\int_{-h}^{\eta} w\frac{\partial u}{\partial z}dz = wu\big|_{z=\eta} - wu\big|_{z=-h} - \int_{-h}^{\eta} u\frac{\partial w}{\partial z}dz \tag{3.29}$$

The combination of the Equations from (3.27) to (3.29) is,

$$-\left[u\left(\frac{\partial \eta}{\partial t} + u\frac{\partial \eta}{\partial x} + v\frac{\partial \eta}{\partial y}\right)\right]_{z=\eta} - \int_{-h}^{\eta} u\left(\frac{\partial u}{\partial x} + \frac{\partial v}{\partial y} + \frac{\partial w}{\partial z}\right)dz + wu\big|_{z=\eta} - wu\big|_{z=-h} \tag{3.30}$$

First term of Equation (3.30) is

$$-\left[u\left(\frac{\partial \eta}{\partial t} + u\frac{\partial \eta}{\partial x} + v\frac{\partial \eta}{\partial y}\right)\right]_{z=\eta} = -[uv]_{z=\eta} \tag{3.31}$$

and

$$\int_{-h}^{\eta} u\left(\frac{\partial u}{\partial x} + \frac{\partial v}{\partial y} + v\frac{\partial w}{\partial z}\right)dz = 0 \tag{3.32}$$

Solely the Equation (3.33) is the continuity equation.

$$\left(\frac{\partial u}{\partial x}+\frac{\partial v}{\partial y}+v\frac{\partial w}{\partial z}\right)=0 \tag{3.33}$$

The last term of the Equation (3.30) is,

$$-wu\big|_{z=-h}=0 \tag{3.34}$$

since the definition of the bottom boundary condition stated in Equation (3.21).

Combining Equations (3.25), (3.27), (3.28), (3.30), the Equation (3.15) become,

$$\begin{aligned}&\frac{\partial}{\partial t}\int_{-h}^{\eta}udz+\frac{\partial}{\partial x}\int_{-h}^{\eta}u^2dz+\frac{\partial}{\partial y}\int_{-h}^{\eta}uvdz-f\int_{-h}^{\eta}vdz=\\&\int_{-h}^{\eta}\frac{1}{\rho_0}\frac{\partial p_a}{dx}dz-\int_{-h}^{\eta}g\frac{\partial \eta}{dx}dz-\frac{g}{\rho_0}\int_{-h}^{\eta}\int_{z}^{\eta}\frac{\partial \rho'}{\partial x}dzdz\\&+\int_{-h}^{\eta}\frac{\partial}{dz}A_z\frac{\partial u}{\partial z}\partial z+\int_{-h}^{\eta}A_h\nabla^2udz\end{aligned} \tag{3.35}$$

where;

$$\int_{-h}^{\eta}\frac{1}{\rho_0}\frac{\partial p_a}{\partial x}dz=\frac{1}{\rho_0}\frac{\partial p_a}{\partial x}(h+\eta) \tag{3.36}$$

$$\int_{-h}^{\eta}g\frac{\partial \eta}{\partial x}dz=g\frac{\partial \eta}{\partial x}(h+\eta) \tag{3.37}$$

and

$$\int_{-h}^{\eta}\frac{\partial}{dz}\left(A_z\frac{\partial u}{\partial x}\right)dz=\frac{1}{\rho_0}\left(\tau_x^s-\tau_x^b\right) \tag{3.38}$$

Finally, the total depth is defined as,

$$d=h+\eta \tag{3.39}$$

and then Equation (3.35) turns to,

$$\frac{\partial}{\partial t}\int_{-h}^{\eta} u dz + \frac{\partial}{\partial x}\int_{-h}^{\eta} u^2 dz + \frac{\partial}{\partial y}\int_{-h}^{\eta} uv dz - f\int_{-h}^{\eta} v dz = \frac{d}{\rho_a}\frac{\partial p_a}{\partial x} + gd\frac{\partial \eta}{\partial x} - g\int_{-h}^{\eta}\int_{-h}^{\eta}\frac{\partial \rho'}{\partial x} dz dz + \frac{\left(\tau_x^s - \tau_x^b\right)}{\rho_0} + \int_{-h}^{\eta} A_h \nabla^2 u dz \tag{3.40}$$

Also, with similar applications Equation (3.16) can be written as,

$$\frac{\partial}{\partial t}\int_{-h}^{\eta} v dz + \frac{\partial}{\partial y}\int_{-h}^{\eta} v^2 dz + \frac{\partial}{\partial x}\int_{-h}^{\eta} uv dz + f\int_{-h}^{\eta} u dz = \frac{-h+\eta}{\rho_a}\frac{\partial p_a}{\partial y} - gd\frac{\partial \eta}{\partial y} - g\int_{-h}^{\eta}\int_{-h}^{\eta}\frac{\partial \rho'}{\partial y} dz dz + \frac{\left(\tau_y^s - \tau_y^b\right)}{\rho_0} + \int_{-h}^{\eta} A_h \nabla^2 v dz \tag{3.41}$$

Starting using Equations (3.40) and (3.41), applying the nonlinear and horizontal terms in Equation (3.40), and defining the depth averaged velocities as,

$$\hat{u} = \frac{1}{d}\int_{-h}^{\eta} u dz \text{ and } \hat{v} = \frac{1}{d}\int_{-h}^{\eta} v dz \tag{3.42}$$

where d is the total depth from the bed to the surface.

$$\frac{\partial}{\partial x}\int_{-h}^{\eta} u^2 dz + \frac{\partial}{\partial y}\int_{-h}^{\eta} uv dz \cong \frac{\partial}{\partial x}\hat{u}\hat{u}d + \frac{\partial}{\partial y}\hat{u}\hat{v}d \tag{3.43}$$

$$\int_{-h}^{\eta}\left(A_h \nabla^2 u\right) dz \cong dA_h \nabla^2 \hat{u} \tag{3.44}$$

SWEs are now presented as,

$$\frac{\partial}{\partial t}\left(\rho_0 \widehat{u}\right)+\frac{\partial}{\partial x}\left(\rho_0 \widehat{u}^2\right)+\frac{\partial}{\partial y}\left(\rho_0 \widehat{u}\widehat{v}\right)=-\frac{\partial p_a}{\partial x}-g\rho_0\frac{\partial \eta}{\partial x}+\rho_0 f\widehat{v}+\frac{\tau_x^s-\tau_x^b}{d}+\rho_0 A_h\nabla^2\widehat{u} \quad (3.45)$$

$$\frac{\partial}{\partial t}\left(\rho_0 \widehat{v}\right)+\frac{\partial}{\partial x}\left(\rho_0 \widehat{u}\widehat{v}\right)+\frac{\partial}{\partial y}\left(\rho_0 \widehat{v}^2\right)=-\frac{\partial p_a}{\partial y}-g\rho_0\frac{\partial \eta}{\partial y}-f\widehat{u}+\frac{\tau_y^s-\tau_y^b}{d}+\rho_0 A_h\nabla^2\widehat{u} \quad (3.46)$$

Above two equations are the depth averaged momentum equations representing SWEs in the Eulerian form along the x and y directions, respectively.

The depth averaged form of the continuity equation is obtained by integrating three dimensional continuity equation over depth using the Leibnitz Rule (Appendix B),

$$\int_{-h}^{\eta}\frac{\partial u}{\partial x}dz=\frac{\partial}{\partial x}\int_{-h}^{\eta}udz-u\frac{\partial \eta}{\partial x}\bigg|_{z=\eta}-u\frac{\partial h}{\partial x}\bigg|_{z=-h} \quad (3.47)$$

$$\int_{-h}^{\eta}\frac{\partial u}{\partial y}dz=\frac{\partial}{\partial y}\int_{-h}^{\eta}vdz-v\frac{\partial \eta}{\partial y}\bigg|_{z=\eta}-v\frac{\partial h}{\partial y}\bigg|_{z=-h} \quad (3.48)$$

$$\int_{-h}^{\eta}\frac{\partial w}{\partial z}dz=w|_{\eta}-w|_{-h} \quad (3.49)$$

Using the boundary conditions given in Equations (3.17), (3.19) and (3.20),

$$w|_{\eta}-w|_{-h}=\left(\frac{\partial \eta}{\partial t}+u\frac{\partial \eta}{\partial x}+v\frac{\partial \eta}{\partial y}\right)\bigg|_{z=\eta}+\left(u\frac{\partial h}{\partial x}+v\frac{\partial h}{\partial y}\right)\bigg|_{z=-h} \quad (3.50)$$

Inserting the terms in Equation (3.47), (3.48) and (3.49) into the continuity equation,

$$\frac{\partial}{\partial x}\int_{-h}^{\eta} u dz - u\frac{\partial \eta}{\partial x}\bigg|_{z=\eta} - u\frac{\partial h}{\partial x}\bigg|_{z=-h} +$$
$$\frac{\partial}{\partial y}\int_{-h}^{\eta} v dz - v\frac{\partial \eta}{\partial y}\bigg|_{z=\eta} - v\frac{\partial h}{\partial y}\bigg|_{z=-h} + \qquad (3.51)$$
$$\left(\frac{\partial \eta}{\partial t} + u\frac{\partial \eta}{\partial x} + v\frac{\partial \eta}{\partial y}\right)\bigg|_{z=\eta} + \left(u\frac{\partial h}{\partial x} + v\frac{\partial h}{\partial y}\right)\bigg|_{z=-h}$$

Rewriting Equation (3.51),

$$\frac{\partial}{\partial x}\int_{-h}^{\eta} u dz + \frac{\partial}{\partial y}\int_{-h}^{\eta} v dz + \frac{\partial \eta}{\partial t}\bigg|_{z=\eta} - u\frac{\partial \eta}{\partial x}\bigg|_{z=\eta} + u\frac{\partial \eta}{\partial x}\bigg|_{z=\eta} - u\frac{\partial h}{\partial x}\bigg|_{z=-h} + u\frac{\partial h}{\partial x}\bigg|_{z=-h}$$
$$-v\frac{\partial \eta}{\partial y}\bigg|_{z=\eta} + v\frac{\partial \eta}{\partial y}\bigg|_{z=\eta} - v\frac{\partial h}{\partial y}\bigg|_{z=-h} + v\frac{\partial h}{\partial y}\bigg|_{z=-h} = 0 \qquad (3.52)$$

Simplifying Equation (3.52),

$$\frac{\partial}{\partial x}\int_{-h}^{\eta} u dz + \frac{\partial}{\partial y}\int_{-h}^{\eta} v dz + \frac{\partial \eta}{\partial t}\bigg|_{z=\eta} = 0 \qquad (3.53)$$

and integrating Equation (3.53) yields,

$$\frac{\partial \eta}{\partial t} + d\frac{\partial \hat{u}}{\partial x} + d\frac{\partial \hat{v}}{\partial y} = 0 \qquad (3.54)$$

which is the depth averaged form of the continuity Equation.

Thus, the depth averaged two dimensional momentum and the continuity equations are obtained.

$$\frac{\partial}{\partial t}\left(\rho_0 \hat{u}\right) + \frac{\partial}{\partial x}\left(\rho_0 \hat{u}^2\right) + \frac{\partial}{\partial y}\left(\rho_0 \hat{u}\hat{v}\right) = -\frac{\partial p_a}{\partial x} - g\rho_0\frac{\partial \eta}{\partial x} + \rho_0 f\hat{v} + \frac{\tau_x^s - \tau_x^b}{d} + \rho_0 A_h \nabla^2 \hat{u} \qquad (3.55)$$

$$\frac{\partial}{\partial t}\left(\rho_0 \hat{v}\right)+\frac{\partial}{\partial x}\left(\rho_0 \hat{u}\hat{v}\right)+\frac{\partial}{\partial y}\left(\rho_0 \hat{v}^2\right)=-\frac{\partial p_a}{\partial y}-g\rho_0\frac{\partial \eta}{\partial y}-f\hat{u}+\frac{\tau_y^s-\tau_y^b}{d}+\rho_0 A_h\nabla^2\hat{u} \quad (3.56)$$

$$\frac{\partial\left(\hat{u}d\right)}{\partial x}+\frac{\partial\left(\hat{v}d\right)}{\partial y}=0 \quad (3.57)$$

3.2.2. Theoretical Development of Stratified Flow

Fluid motions in a gravitational field which are originated or influenced by variations in density within the fluid are characterized by the term stratified flow (two-layer flow). The density differences are therefore due to temperature gradients and variations in solute concentrations. The SWE developed in section 3.2.1. may be adapted for use in modeling a flow system that has density stratification.

Starting from one layer, for ρ is constant and with the vertical coordinate z located at the still water level

$$\frac{\partial u}{\partial t}+u\frac{\partial u}{\partial x}+v\frac{\partial u}{\partial y}-fv=-\frac{1}{\rho_0}\frac{\partial p_a}{\partial x}-g\frac{\partial \eta}{\partial x}+\frac{\tau_s^x-\tau_b^x}{\rho d}+N_h\nabla_h^2 u \quad (3.58)$$

$$\frac{\partial v}{\partial t}+u\frac{\partial u}{\partial x}+v\frac{\partial u}{\partial y}-fu=-\frac{1}{\rho_0}\frac{\partial p_a}{\partial y}-g\frac{\partial \eta}{\partial y}+\frac{\tau_s^y-\tau_b^y}{\rho d}+N_h\nabla_h^2 v \quad (3.59)$$

$$\frac{\partial d}{\partial t}+\frac{\partial}{\partial x}(ud)+\frac{\partial}{\partial y}(vd)=0 \quad (3.60)$$

where $N_h = A_h / \rho$.

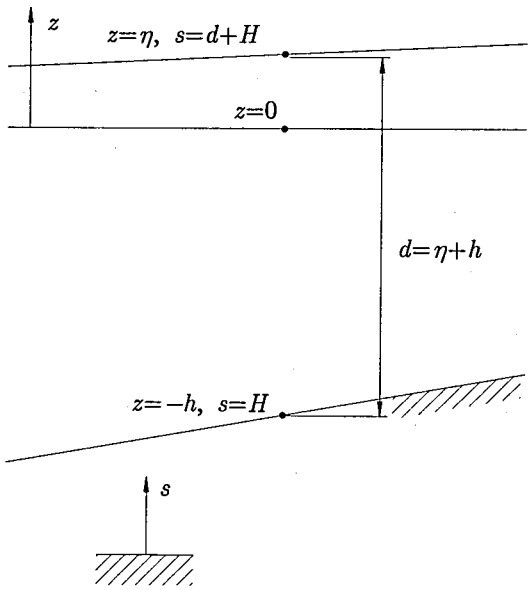

Figure 3.1. A typical vertical cross section and definitions of basic parameters

With the vertical coordinates located below the bottom, as shown in the Figure 3.1 above, one can rewrite the equations in terms of the variation of the total flow depth d. to this end,

$$z=\eta \rightarrow s=d+H$$
$$\frac{\partial \eta}{\partial x}=\frac{\partial d}{\partial x}+\frac{\partial H}{\partial x}, \frac{\partial \eta}{\partial y}=\frac{\partial d}{\partial y}+\frac{\partial H}{\partial y} \tag{3.61}$$

Defining, $S_0^x=-\frac{\partial H}{\partial x}$ and $S_0^y=-\frac{\partial H}{\partial y}$ where is bottom slope in the x and y directions, respectively. H is the elevation from the datum plane to the bed,

$$\frac{\partial \eta}{\partial x}=\frac{\partial d}{\partial x}-S_0^x, \frac{\partial \eta}{\partial y}=\frac{\partial d}{\partial y}-S_0^y \tag{3.62}$$

and Equation (3.61) yields

$$\frac{\partial u}{\partial t}+u\frac{\partial u}{\partial x}+v\frac{\partial u}{\partial y}-fv=-\frac{1}{\rho}\frac{\partial p_a}{\partial x}-g\frac{\partial d}{\partial x}+gS_0^x+\frac{\tau_s^x-\tau_b^x}{\rho d}+N_h\nabla_h^2 u \tag{3.63}$$

$$\frac{\partial v}{\partial t}+u\frac{\partial u}{\partial x}+v\frac{\partial u}{\partial y}+fu=-\frac{1}{\rho}\frac{\partial p_a}{\partial y}-g\frac{\partial d}{\partial y}+gS_0^y+\frac{\tau_s^y-\tau_b^y}{\rho d}+N_h\nabla_h^2 v \tag{3.64}$$

$$\frac{\partial d}{\partial t}+\frac{\partial}{\partial x}(ud)+\frac{\partial}{\partial y}(vd)=0 \tag{3.65}$$

When two reservoirs filled with liquids of different densities are connected with a channel, a two directional flow occurs in the channel. The liquid from the low density reservoir flows into the high density reservoir through an upper layer and the liquid from the high density reservoir flows in the opposite direction through a bottom layer. In emphasizing thin similarity with familiar stratified flow, represents an important simplification in analysis which is very often useful in rapidly estimating orders of magnitude for velocities and depths.

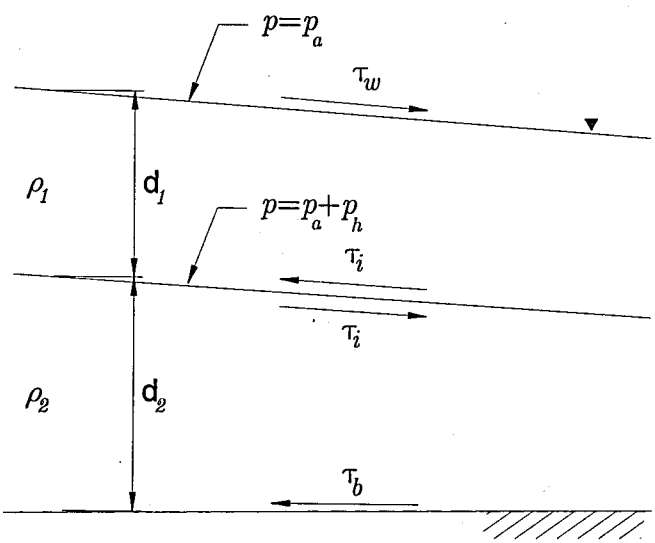

Figure 3.2. Vertical cross section of a two layer flow and definitions of basic parameters

The simplest of a flow system that has density stratification is the two layer system which may be thought of as the first approximation to a full three dimensional model. The flow of each layer will be governed by the SWE with appropriate boundary and matching conditions (in terms of normal and tangential stresses) at the interface of the layers. The

two layer system shown above is being driven by pressure gradients (atmospheric and hydrostatic imposed by the tilted free surface and interface) and the momentum transferred from the wind blowing over the free surface. In the developments that follow, we will make use of the SWE with the vertical coordinate placed below the bottom.

For the upper layer, in view of the single layer system, the bottom of the upper layer is now located at the interface, that is at $s = H + d_2$ and the flow resistance at this location is provided by the interfacial shear, τ_i with these points in mind, one can modify the SWE to read,

$$\frac{Du_1}{Dt} - fv_1 = -\frac{1}{\rho_1}\frac{\partial \rho_a}{\partial x} - g\frac{\partial (d_1 + d_2)}{\partial x} + gS_o^x + \frac{\tau_w^x - \tau_i^x}{\rho_1 d_1} + N_h \nabla_h^2 u_1 \tag{3.66}$$

$$\frac{Dv_1}{Dt} + fu_1 = -\frac{1}{\rho_1}\frac{\partial \rho_a}{\partial_y} - g\frac{\partial (d_1 + d_2)}{\partial y} + gS_o^y + \frac{\tau_w^x - \tau_i^x}{\rho_1 d_1} + N_h \nabla_h^2 u_1 \tag{3.67}$$

$$\frac{\partial \mathrm{d}_1}{\partial \mathrm{t}} + \frac{\partial}{\partial x}(u_1 d_1) + \frac{\partial}{\partial y}(v_1 d_1) = 0 \tag{3.68}$$

where D/Dt stands for the material derivative.

For the lower layer, the matching condition of the normal stresses at the interface introduces the horizontal gradients of the hydrostatic pressure of the upper layer $\rho_1 g \nabla d_1$, into the equations.

$$\frac{Du_2}{Dt} - fv_2 = -\frac{1}{\rho_2}\frac{\partial \rho_a}{\partial x} - -g\frac{\partial d_2}{\partial x} - g\frac{\rho_1}{\rho 2}\frac{\partial d_1}{\partial x} + gS_o^x + \frac{\tau_i^x - \tau_b^x}{\rho_2 d_2} + N_h \nabla_h^2 u_2 \tag{3.69}$$

$$\frac{Dv_2}{Dt} + fu_2 = -\frac{1}{\rho_2}\frac{\partial \rho_a}{\partial y} - g\frac{\partial d_2}{\partial y} + g\frac{\rho_1}{\rho_2}\frac{\partial d_1}{\partial y} + gS_o^y + \frac{\tau_i^y - \tau_b^y}{\rho_2 d_2} + N_h \nabla_h^2 u_2 \tag{3.70}$$

$$\frac{\partial \mathrm{d}_2}{\partial \mathrm{t}}+\frac{\partial}{\partial x}(u_2 d_2)+\frac{\partial}{\partial y}(v_2 d_2)=0 \tag{3.71}$$

where subscript index 1 denotes the quantities for the upper layer and index 2 denotes the quantities for the upper layer. Hence, the momentum equations and the continuity equation can be summarized in conservation forms.

In the presented study, applying the same analogy stated in Appendix C to the two dimensional, two layer SWE (for constant width) is obtained for one dimension.

$$u_1 \frac{\partial u_1}{\partial x}=-g\frac{\partial (d_1+d_2)}{\partial x}+gS_0^x+\frac{\tau_w^x-\tau_i^x}{\rho_1 d_1} \tag{3.72}$$

$$\frac{\partial (u_1 d_1)}{\partial x}=0 \tag{3.73}$$

$$u_2 \frac{\partial u_2}{\partial x}=-g\frac{\partial d_2}{\partial x}-g\frac{\rho_1}{\rho_2}\frac{\partial d_1}{\partial x}+gS_0^x+\frac{\tau_i^x-\tau_b^x}{\rho_2 d_2} \tag{3.74}$$

$$\frac{\partial (u_2 d_2)}{\partial x}=0 \tag{3.75}$$

3.2.3. Bottom Shear Stress

The bottom shear stress is the shear stress on the bed of the Strait. A quadratic shear formulation is commonly adopted for the bottom shear stress. This formulation is expressed as,

$$\tau_x^b=\rho_2 r|V_t|u \text{ and } \tau_y^b=\rho_2 r|V_t|v \tag{3.76}$$

where ρ_2 is the lower layer density. The magnitude of the fluid velocity is

$$|V_t| = \sqrt{u^2 + v^2} \tag{3.77}$$

The bottom drag coefficient, r, is a function of the bottom roughness and the properties of the bottom boundary layer (Komar, 1976) and is usually taken in the rang of 2-4 10^{-3}

Another form for the bottom shear stress is,

$$\tau_x^b = \frac{\rho_2 g}{C^2}|V_t|u \text{ and } \tau_y^b = \frac{\rho_2 g}{C^2}|V_t|v \tag{3.78}$$

where C is the Chezy coefficient.

Gerritsen and Bijlsma (1988) suggest a depth dependent form for C

$$C = \begin{cases} 65, h \le 40m \\ h + 25, 40 < h \le 65m \\ 90, h > 65m \end{cases} \tag{3.79}$$

Komar's (1976) r will be used in the present study, in the value of 0.003

3.2.4. Interfacial Shear Stress

The interfacial shear stress is the shear stress between heavier saline lower layer and the less saline upper layer Thus, the momentum transfer from the upper layer to lower layer can be achieved by the interfacial shear stress,

$$\tau_i = \overline{\rho} k (u_1 - u_2)|(u_1 - u_2)| \tag{3.80}$$

where $\overline{\rho} = (\rho_1 + \rho_2)/2$ is the average density and k is the interfacial friction coefficient. For the purpose of this present study interfacial coefficient was taken as 0.0007 after Sümer and Bakioğlu (1981).

3.2.5. Wind Shear Stress

The wind shear stress, τ_b, is usually expressed through a quadratic form containing a resistance coefficient called wind drag coefficient, C_{10}, the air density, ρ_a and the wind velocity, $W=(W_x,W_y)$. In a depth averaged model, the surface wind stress appears as body force as the can be no distinction of vertical position.

$$\tau_x^w = C_{10}\rho_a|W|W_x \text{ and } \tau_y^w = C_{10}\rho_a|W|W_y \tag{3.81}$$

where $|W|$, the wind speeed is

$$|W| = \sqrt{W_x^2 + W_y^2} \tag{3.82}$$

and $\rho_a = 1.2\,\text{kg/m}^3$.

The value of C_{10} is based on wind velocity 10m above the surface. C_{10} depicts the resistance of the underlying surface. For flow over water, the sea surface roughness can vary with the wind speed. A brief summary of a variety of values or formulations is below:

Neuman (1952) suggests using a value of 0.9 for all wind speeds. Heaps (1965) suggested a relationship where C_{10} is based on wind speed,

$$C_{10} = 0.565\ 10^{-3} \quad \text{W<5m/s} \tag{3.83}$$

$$C_{10} = (-0.12 + 0.137W)*10^{-3} \quad \text{5<W<19.22 m/s} \tag{3.84}$$

$$C_{10} = 0.565\ 10^{-3} \quad \text{W>5 m/s} \tag{3.85}$$

Ekman (1905) reported in Neumann and Pierson (1966) suggested the factor as 2.6 for all wind speeds. Garratt (1977) analyzed measured data and concluded that C_{10} under a neutral atmospheric stability depends linearly on the wind velocity as

$$C_{10} = (0.75 + 0.067 * 10^{-2} w) * 10^{-3} \ , \ C_{10} = 2.7 \times 10^{-3} \tag{3.86}$$

where the wind velocity is expressed in centimeters per second.

In this study, Garrat (1977)'s C_{10} will be used.

4. THE NUMERICAL MODEL OF THE FLOW

4.1. Background

Mathematical models have been widely used to predict the hydrodynamics and transport processes of real life problems. Modeling real life problems usually involves solving a set of governing differential equations subject to realistic boundary conditions. To reflect the real physical characteristics, a three-dimensional model is usually needed to obtain an accurate approximation. However, this usually means the development of a complex code and is demanding in terms of computer resources when dealing with large-scale problems. A compromise is to use a system, which converts a three dimensional problem into a number of related two or one dimensional problems by splitting the domain into different horizontal and vertical layers. Each layer consists of its own distinct properties and the flow rate across adjacent layers.

However, as domain or boundary meshing is required the accuracy of the solutions is affected by the quality of the mesh. On the other hand, recent improvements in the development of meshless methods have caused interest in applying these methods to solve linear and non-linear engineering problems. Some examples of meshless methods are the meshless local Petrov-Galerkin and local boundary integral equations methods by Atluri (Atluri *et al.*, 1999; Atluri and Zhu, 2000). This chapter discusses a truly meshless algorithm based on RBFs for solving steady PDEs derived from SWEs.

RBF approximation was initially devised for scattered geographical data interpolation by Hardy (1971). He introduced a class of RBFs called multiquadric functions (MQ). A review of several types of RBFs for scattered data interpolation was presented by Franke (1982). Franke and Schaback (1998) showed that MQ have the best performance in terms of accuracy among the methods tested. An intensive study on the theory of the RBFs approximation had been presented by Powell (1992).

Kansa (1900a; 1990b; 1992) refined the Hardy's MQ approximation method for solving elliptic, parabolic and hyperbolic PDEs problems over irregular regions. A number

of experiments of the method had been carried out and applied to solve a various scientific and engineering problems over the last decade; however most of these applications deal with hypothetical examples. Recently some attempts of the RBFs method have been made successfully to solve more complex initial-boundary time-dependent PDEs problems for real-life applications. The good prospect for the RBFs method attracts attention of more researchers in developing the theory of RBFs as well as applying in solving PDEs.

4.2. RBF Interpolation and Collocation Method

There are an infinite number of possible RBFs. Denoting r by the Euclidean distance between any pair of points in the domain Ω, some of the more commonly employed RBFs are:

$$
\begin{aligned}
&\phi(r) = r^m \log(r) && m^{th} \text{ Order spline} \\
&\phi(r) = -r^\beta, j \in (0,2) && \text{Power spline} \\
&\phi(r) = \sqrt{r^2 + c^2} && \text{Hardy's multiquadric} \\
&\phi(r) = 1/\sqrt{r^2 + c^2} && \text{Inverse multiquadric} \\
&\phi(r) = e^{-cr} && \text{Exponential spline} \\
&\phi(r) = e^{-cr^2} && \text{Gaussian spline} \\
&\phi(r) = e^{-cr} K_\nu(cr) && \text{Matern spline} \\
&\phi(r) = (1-r)^m_{+p(r)} && \text{Compactly supported spline}
\end{aligned}
\tag{4.1}
$$

Here K_ν is the modified Bessel function of order ν, and p(r) is a polynomial of the compactly supported spline (CS-RBF) (Wendland, 1995).

The idea of RBFs is establishing linear combinations of translates of one function $\phi(r)$ of one real variable which is centered at "data centre" and approximating an unknown function by

$$
s(x) = \sum_{k=1}^{n} \lambda_k \phi\left(\|x - x_k\|\right) + p(x) \tag{4.2}
$$

where p is an appended polynomial of degree m-1 or less. The data centers, x_k can be chosen arbitrarily in the domain of interest, hence creating a truly meshfree method.

The interpolation problem is to find λ_k and p(·) such that the interpolant s(x) passes through all given data, $s(x_i) = f_i$. In matrix form, it becomes

$$\begin{bmatrix} A_\phi & \mathrm{P} \\ \mathrm{P}^{\mathrm{T}} & 0 \end{bmatrix} \begin{bmatrix} \lambda \\ \gamma \end{bmatrix} = \begin{bmatrix} \mathrm{f} \\ 0 \end{bmatrix} \tag{4.3}$$

where $(A_\phi)_{ij} = \phi(x_i - x_j), P_{ij} = p_j(x_i), j = 1,...,N$ and the set $\{p_j\}$. RBF requires a distinct set of data points, and a RBF requires any set of data points that is not co-linear in order to guarantee an invertible matrix system.

According to Hardy (1990), one of the most powerful methods is the RBF method based on MQ basis function given as,

$$\phi(r) = \sqrt{r^2 + c^2} \tag{4.4}$$

To specify a MQ basis, one must specify the centers x_j and the MQ shape parameter c or c_j. Most authors use the collocation points as centers for the MQ. Fornberg *et al.*. (2002) showed some observations of different data centers and collocation points placements near boundary. Too large or too small shape parameters c_j make the MQ basis too flat or too peaked, respectively, and should both be avoided. Hardy (1971) suggested a constant shape parameter c=0.815 times mean(d_j), where d_j is the distance from the j^{th} point to its nearest neighbor. Moody and Darken (1989) suggested a simple varied shape parameters $c_j = \theta d_j$, where $\theta > 0$ is a constant factor. Other shape parameters were employed by Kansa *et al.* (1990a; 1990b; 1992). Hon *et al.* (1997; 1999) uses c=4 times mean (d_j). Wang and Liu (2002) studied the effect of shape parameters on the numerical accuracy of MQ.

The history of using RBF in solving PDEs is relatively short. Kansa (1990a; 1990b; Kansa and Hon, 2000) pioneered the use of RBF for the solving numerical solution of the Navier-Stokes equations of flow. Applications of RBF arise commonly in various ordinary differential equations and PDEs. To name a few, they include initial value problem (Hon *et al.*, 1997), nonlinear Burgers' equation (Hon and Mao, 1998), operator splitting-RBF (Balakrishnan *et al.*, 2002), boundary layer problems (Hon *et al.*, 1999), surface wind field approximation (Hickernell and Hon, 1998), biphasic and triphasic models of mixtures (Hon *et al.*, 1997; 1999), and the SWE (Hon *et al.*, 1999; Wong *et al.*, 2002).

To introduce RBF collocation methods, we consider a boundary value problem given in the form

$$\begin{aligned} Lu &= f(x) \text{ in } \Omega \subset \mathbb{R}^{\mathrm{d}} \\ Bu &= \mathrm{g}\ (\mathrm{x}) \text{ on } \partial\Omega \end{aligned} \tag{4.5}$$

where d is the dimension, $\partial\Omega$ denotes the boundary of the domain, Ω, L is the differential operator that operates on the interior, and B is an operator that specifies the boundary conditions of the type of Dirichlet, Neumann or mixed. Both f and g are given functions mapping on $\mathbb{R}^d \to \mathbb{R}$.

There is more than sufficient evidence that RBFs, especially MQ-RBFs, offer many computational advantages over traditional methods. Some of the advantages of RBFs are their truly mesh-free nature and their very high order rates of convergence; see Golberg *et al.* (1996), Fedoseyev *et al.* (2002). One of the disadvantages of RBF is the problem of ill-conditioned large systems of equations. However, finite differences, finite elements, and finite volumes also suffer from ill-conditioning when dimension of the system becomes very large.

4.3. Numerical Formulation

The steady, two layer, one dimension governing Equations 3.67-3.69 of the present study are,

$$u_1 \frac{\partial u_1}{\partial x} = -g \frac{\partial (d_1 + d_2)}{\partial x} + gS_0^x + \frac{\tau_w^x - \tau_i^x}{\rho_1 d_1} \tag{4.6}$$

$$\frac{\partial (u_1 d_1)}{\partial x} = 0 \tag{4.7}$$

$$u_2 \frac{\partial u_2}{\partial x} = -g \frac{\partial d_2}{\partial x} - g \frac{\rho_1}{\rho_2} \frac{\partial d_1}{\partial x} + gS_0^x + \frac{\tau_i^x - \tau_b^x}{\rho_2 d_2} \tag{4.8}$$

$$\frac{\partial (u_2 d_2)}{\partial x} = 0 \tag{4.9}$$

Given a parameter ϕ at a node i specified in a domain Ω, one can present its value using RBF-MQ or RBF-4th order spline (4thOS) as such,

$$r = \sqrt{(x_i - x_j)^2} \tag{4.10}$$

Table 4.1. System matrix and its derivatives

	RBF-MQ	RBF-4thOS
F	$\sqrt{r^2 + c^2}$	$r^4 \ln r$
F_x	$\frac{(x_i - x_j)}{f}$	$(x - x_j) r^2 (2 \ln r + 1) \frac{(x_i - x_j)}{f}$

$$\{u_1\} = [F]\{\alpha^{u_1}\} \tag{4.11}$$

$$\{u_2\} = [F]\{\alpha^{u_2}\} \tag{4.12}$$

$$\{d_1\} = [F]\{\alpha^{d_1}\} \tag{4.13}$$

$$\{d_2\} = [F]\{\alpha^{d_2}\} \tag{4.14}$$

where an entry of u_1, u_2, d_1 and d_2 denotes the upper and lower layer velocities and depths at a collocation point, respectively. F is the system matrix with its ij^{th} component defined by the relationship given in Table 4.1. depending on the type of the RBF, and their derivatives are given as,

$$\frac{\partial\{u_1\}}{\partial x} = [F^x]\{\alpha^{u_1}\} \tag{4.15}$$

$$\frac{\partial\{d_1\}}{\partial x} = [F^x]\{\alpha^{d_1}\} \tag{4.16}$$

$$\frac{\partial\{u_2\}}{\partial x} = [F^x]\{\alpha^{u_2}\} \tag{4.17}$$

$$\frac{\partial\{d_2\}}{\partial x} = [F^x]\{\alpha^{d_2}\} \tag{4.18}$$

Similarly, F^x is the system matrix with its ij^{th} component defined by the relationship given in Table 4.1. Upper layer momentum Equation (4.6) becomes,

$$\{\alpha^{d_1}\} = [F^x]^{-1}\left[\frac{1}{g}[U_1][F^x]\{\alpha^{u_1}\} - [F^x]\{\alpha^{d_2}\} + \{S_0^x\} + \frac{1}{\rho_1 g}\left\{\frac{\tau_w^x - \tau_i^x}{d_1'}\right\}\right] \tag{4.19}$$

where U_1 is the matrix containing u_1 on its main diagonal and zero elsewhere The wind shear stress Equation (4.20) and interface shear stress Equation (4.21) terms can be demonstrated as,

$$\tau_w^x = C_{10}\rho_a w^2 \tag{4.20}$$

$$\tau_i^x = \overline{\rho} k [F]\left[(\alpha^{u1} - \alpha^{u2})\left|\alpha^{u1} - \alpha^{u2}\right|\right] \tag{4.21}$$

and at the first node the boundary condition Equation (4.22) is used.

$$d_1(1) = F_{1j}\alpha_j^d \; j = 1,..,n \tag{4.22}$$

The upper layer continuity equation discritised as,

$$\left\{[D_1]\left[F^x\right]+\left[D_1^x\right][F]\right\}\left\{\alpha^{u_1}\right\} = \{0\} \tag{4.23}$$

$$u_1(n) = F_{nj}\alpha_j^d \; j = 1,..,n \tag{4.24}$$

where D_1 and D_1^x are the matrices containing d_1 and $\partial d_1/\partial x$ on its main diagonal and zero elsewhere, respectively. At the last node the boundary condition Equation (4.24) is used.

Similar approach can be applied to the lower layer of the stratified flow,

$$\left\{\alpha^{d_2}\right\} = \left[F^x\right]^{-1}\left[\frac{1}{g}[U_2]\left[F^x\right]\left\{\alpha^{u_2}\right\} - \frac{\rho_1}{\rho_2}\left[F^x\right]\left\{\alpha^{d_1}\right\} + \left\{S_0^x\right\} + \frac{1}{\rho_2 g}\left\{\frac{\tau_i^x - \tau_b^x}{d_2'}\right\}\right] \tag{4.25}$$

where U_2 is the matrix containing u_1 on its main diagonal and zero elsewhere The interface shear stress Equation (4.26) and the bottom shear stress Equation (4.27) terms can be demonstrated as,

$$\tau_i^x = \overline{\rho} k\left[F\right]\left[(\alpha^{u1} - \alpha^{u2})\left|\alpha^{u1} - \alpha^{u2}\right|\right] \tag{4.26}$$

$$\tau_b^x = \rho_2 r\left[\left[F\right]\alpha^{u2}\right]^2 \tag{4.27}$$

and at the last node the boundary condition Equation (4.28) is used as,

$$d_2(n) = F_{nj}\alpha_j^d \; j = 1,..,n \tag{4.28}$$

The lower layer continuity equation discritised as,

$$\left\{[D_2][F^x]+[D_2^x][F]\right\}\left\{\alpha^{u_2}\right\}=\{0\} \tag{4.29}$$

$$u_2(1)=F_{1j}\alpha_j^d \; j=1,..,n \tag{4.30}$$

where D_2 and D_2^x are the matrices containing d_2 and $\partial d_2/\partial x$ on its main diagonal and zero elsewhere, respectively. At the first node the boundary condition Equation (4.30) is used.

4.4. Boundary Conditions

In the present study, the boundary conditions are expressions of the same physical principals in the set of governing equations such as no slip boundary condition and kinematic and dynamic boundary conditions which are briefly explained and used in section 3.2.1.

The upper layer boundary condition for the first node is the upper layer thickness and for the last node the upper laver velocity Equations (4.22) and (4.24). The lower layer boundary condition for the first node is the lower layer velocity and for the last node the lower layer thickness Equations (4.28) and (4.30).

Initial conditions of the depths and velocities are evaluated by conducted previous studies in order to start the successive iteration.

4.5. Solution Strategy and Convergence

The upper layer momentum equation clearly determines the upper layer thickness. The only way to determine the upper layer velocity is by continuity equation, which infect will be used in the lower layer equations. The lower layer momentum equation clearly determines the lower layer thickness. Similarly, lower layer velocities computed by using lower layer continuity equation.

In the present study, in order to solve the layer velocities and thicknesses, an iterative solution strategy is needed because of the non-linearity in the momentum equations. The algorithm starts with an initial guess of velocities and thicknesses. The discretised momentum equation is solved to find new upper layer thicknesses in all nodes of domain. Using the new quantities, new upper layer velocities computed by the continuity equation. Successively the same algorithm applied to the lower layer discretised equations. Updating the iteratively improved quantities, solution process computed until the convergence criteria satisfied.

In fact there is not an exact value of convergence criteria; the convergence of the process constructed with the difference of the new and pre-iterated discharge values. In the test runs, the model has taken minimum two and maximum five iterations to converge.

If the node number is selected too large or too small, this may cause oscillatory or divergent iterative solutions. However, the system cannot suffer from ill-conditioning if the node number is higher than to some extent.

5. DISCUSSION OF THE RESULTS

The main purpose of this study was to develop a model which could simulate and predict currents and the variation of layer thicknesses within the Istanbul Strait, results of the model were compared with those of Sümer and Bakioğlu (1981) and of Madericha and Konstantinov (2002).

To facilitate comparisons with Sümer and Bakioğlu (1981), the wind stress term was neglected and similar boundary conditions were defined. Since there are four PDEs to be solved four boundary conditions were defined. The thicknesses of both layers at the two ends and the velocities of both layers at the two ends the Bosphorus Strait were used as boundary conditions.

As mentioned before, the strait has a length of 31.25 km so in the computations; it is divided into 25 cross-sectional areas of 1,250 m apart. For discharge computations the average width of the Bosphorus was taken as 907 m and the depth of the water column was taken as 64.5 m. Several cases were run to calibrate the model. In the studies regarding the Bosphorus Strait, the sea level difference between the two ends of the strait is given within the range of 0.15-0.40 meters, in these simulations, similarly, those values were taken as 0.15, 0.20, 0.25, 0.30, 0.33, 0.35 and 0.40 m, respectively.

In the simulation runs, the sea level differences decreased the discharge values of the upper layer also decreased as expected. The lower layer discharge values, however, increased with decreased sea level differences. In both studies this trend was similar. The interface obtained for the average decline in the surface elevation between the two ends of the Bosphorus, $\Delta h = 33$ cm, is illustrated in Figure 5.9 and Figure 5.10 The agreement between the present finding and the DAMOC (1971) data appears to be fairly good as the slope of the interface concerns.

In the simulation runs, the bottom drag coefficient was 0.003 which gave the reasonable accordance with the studies. Comparison of the discharge values (for different sea level differences) of this present study and of Sümer and Bakioğlu (1981) are shown in

Table 5.1. where average discharge values of the computations are presented. In Madericha and Konstantinov (2002) study, there is a shifting as seen in Figure 5.15 and Figure 5.16 due to the discharges of different cross sections in their numerical model. For that reason the two models cannot be compared by error norms. Errors involved, however, are given as the relative L_2 error norm (Shu *et al.*., 2004), which defined as

$$\frac{\sqrt{\sum_{i=1}^{N}\left|Q_{computed}-Q_{S\&B}\right|^2}}{\sqrt{\sum_{i=1}^{N}\left|Q_{S\&B}\right|^2}} \tag{5.1}$$

From Table 5.2, it can be seen that the error percentage of the lower layer increases with increasing sea level difference due to the fact that upper layer converges faster than the lower layer as the boundary conditions concerns. In the tables Q_1 is the discharge of the upper layer, while Q_2 represents the lower layer flow rate. Both values are given in m^3/s. The sea level difference is denoted by Δh in meters. Although over predicting values of the layer discharges the values of this study were found within the maximum and minimum values as reported in U.S. Navy Oceanographic Office (1967) as stated in Chapter 2.

Despite the uncertainties involved in the numerical values of the various input quantities due to insufficient data (particularly that in the decline in surface elevation between the two ends of the Bosphorus Strait) and also the assumption in connection with the shape of the interface. The results seem to be satisfactory when compared with the available information. In summary, the hydrodynamic model has been tested with Sümer and Bakioğlu's (1981) study and Madericha and Konstantinov (2002). It can be concluded that the results are relatively correct and reasonable.

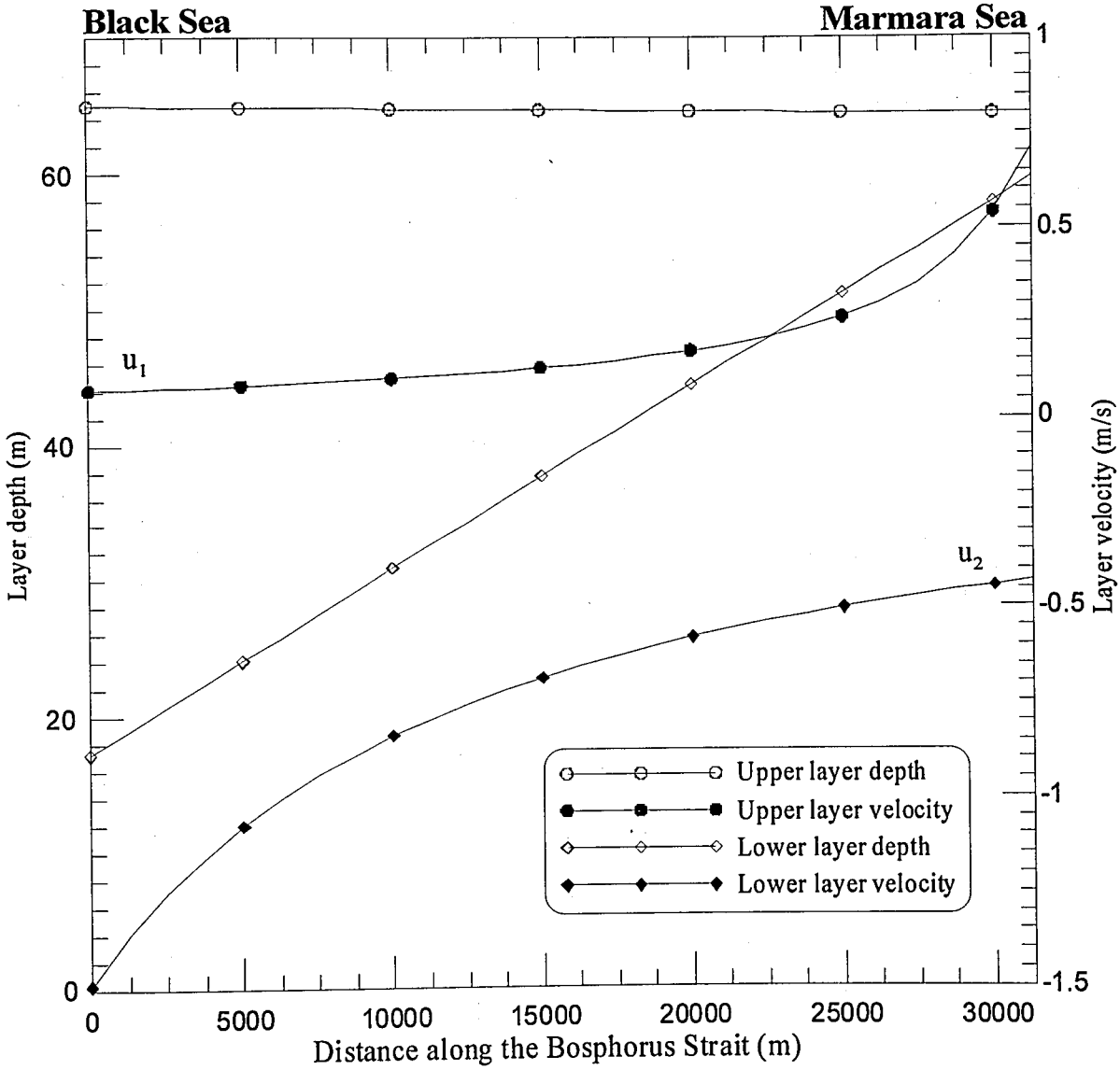

Figure 5.1. Flow velocities and layer thicknesses for a free surface level of 0.15 m between the Black Sea and Marmara Sea boundaries of the Bosphorus by using MQ (c=5000)

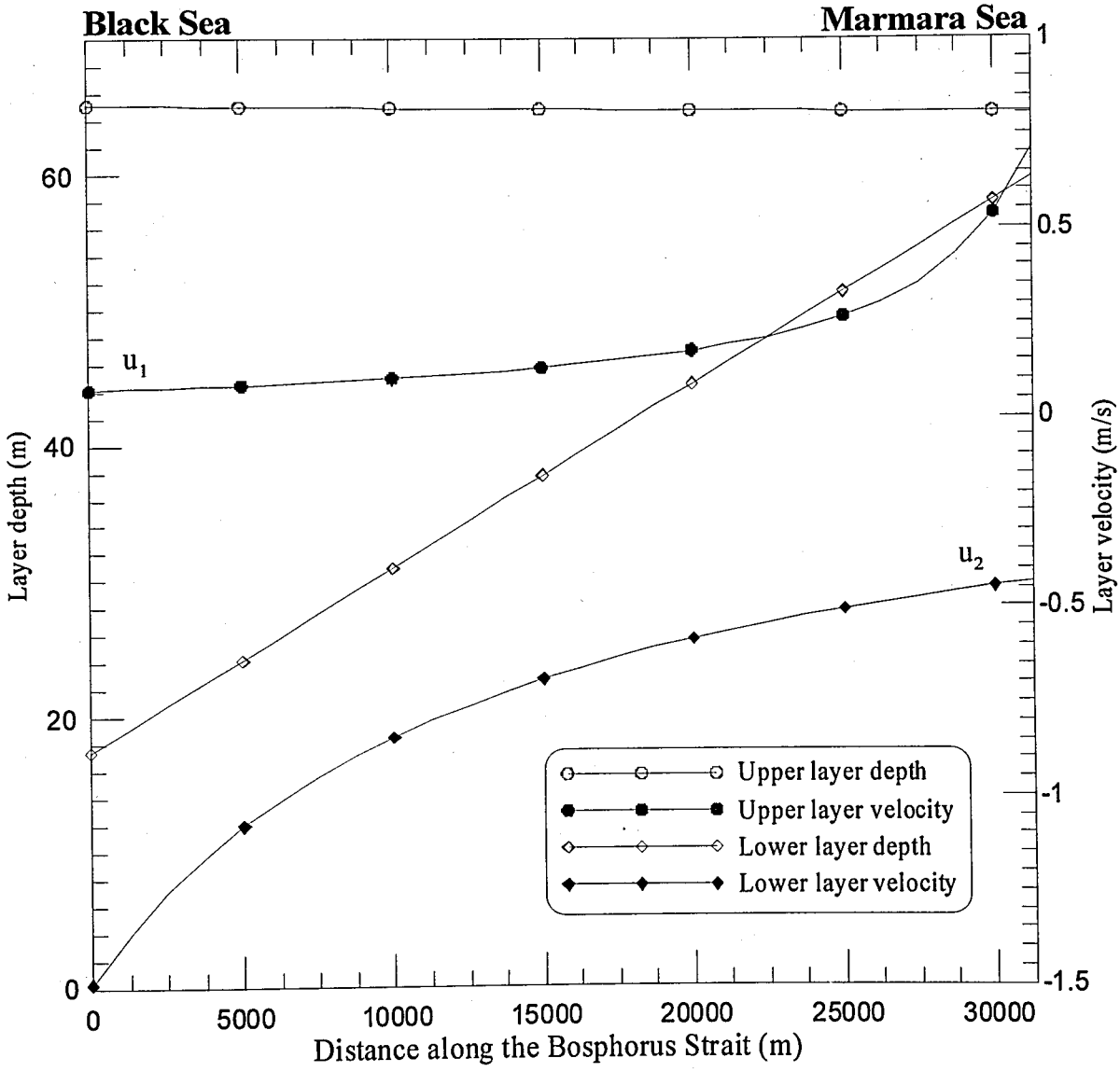

Figure 5.2. Flow velocities and layer thicknesses for a free surface level of 0.15 m between the Black Sea and Marmara Sea boundaries of the Bosphorus by 4^{th}OS

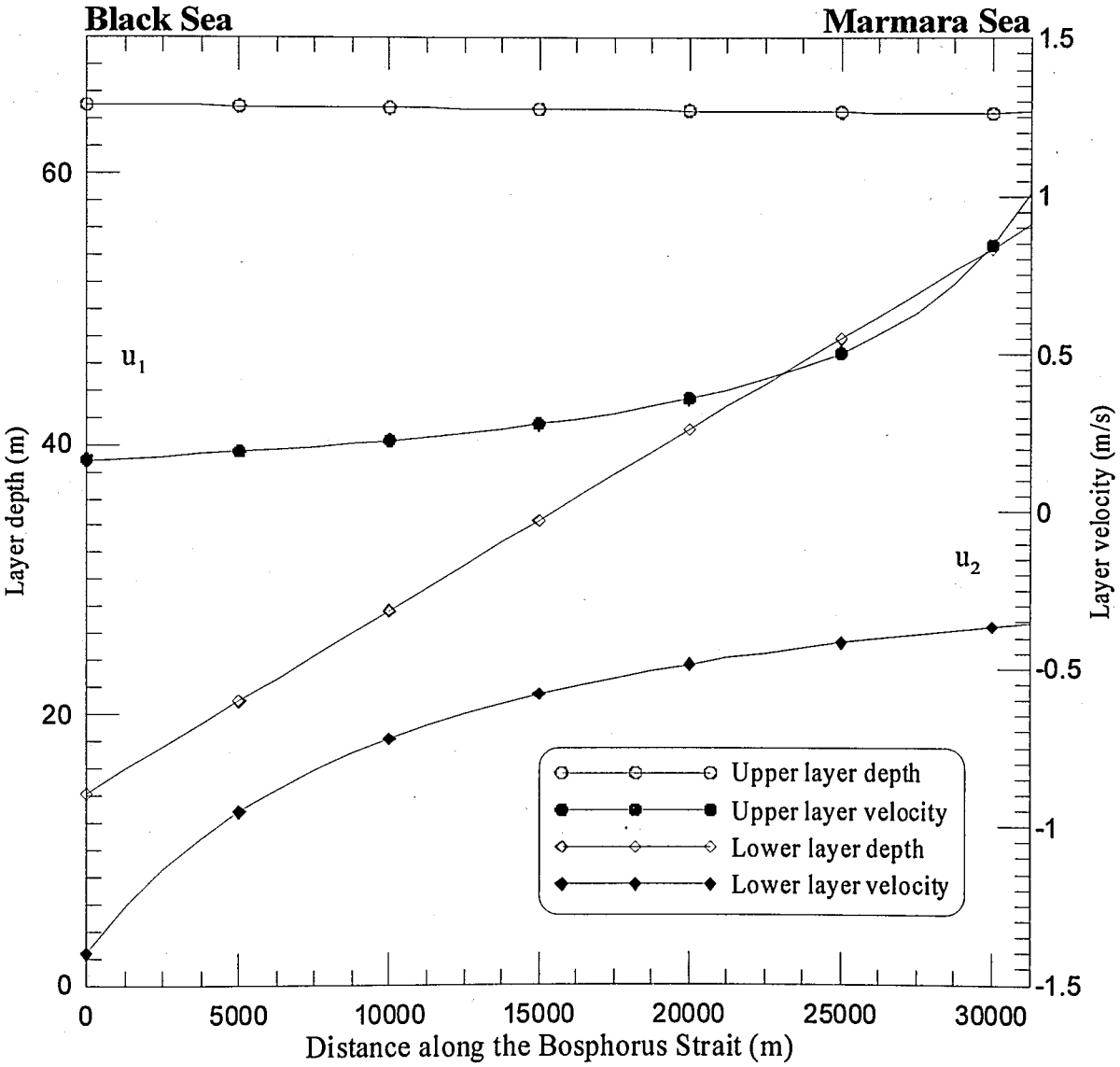

Figure 5.3. Flow velocities and layer thicknesses for a free surface level of 0.2 m between the Black Sea and Marmara Sea boundaries of the Bosphorus by using MQ (c=5000)

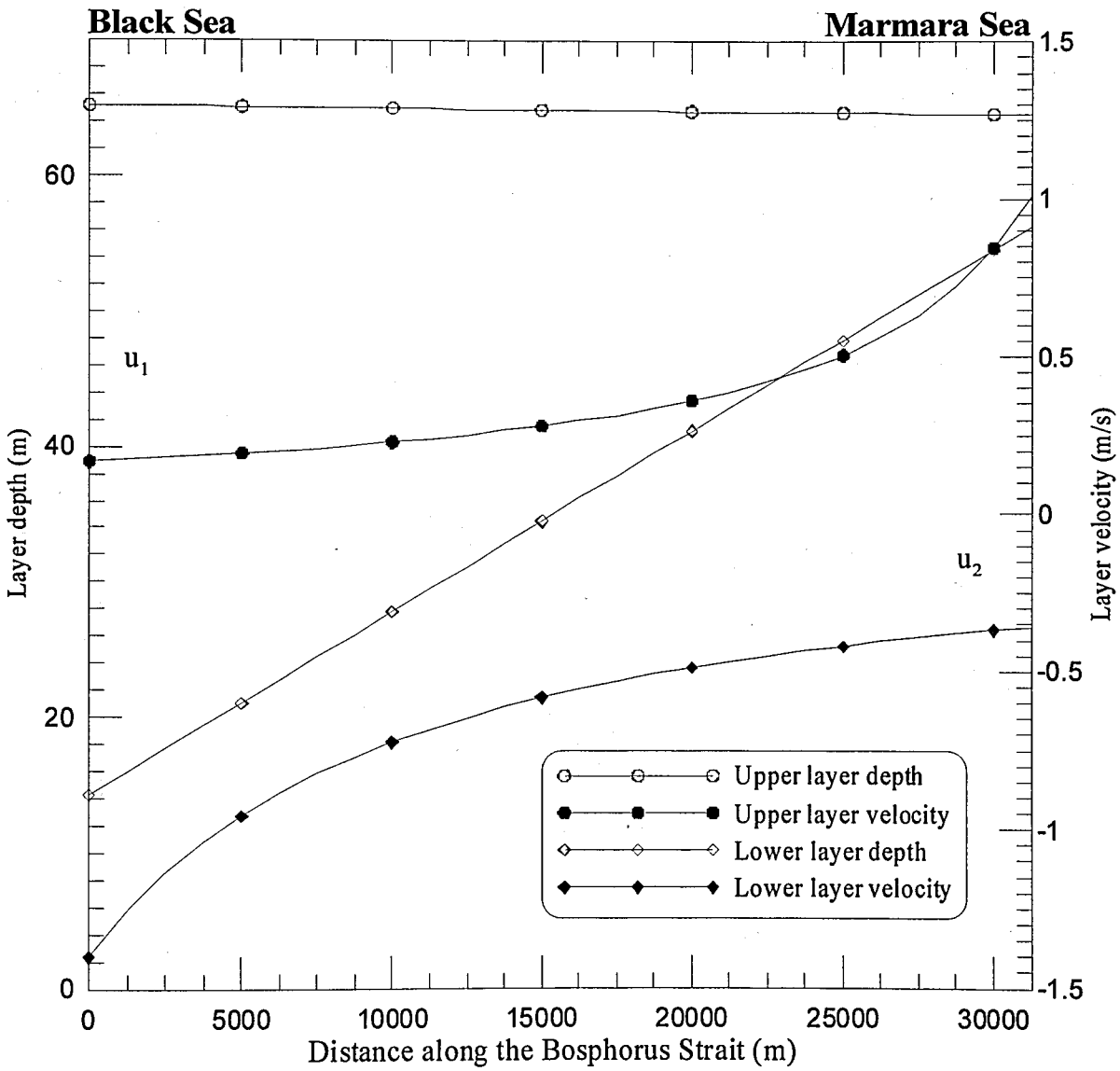

Figure 5.4. Flow velocities and layer thicknesses for a free surface level of 0.2 m between the Black Sea and Marmara Sea boundaries of the Bosphorus by 4thOS

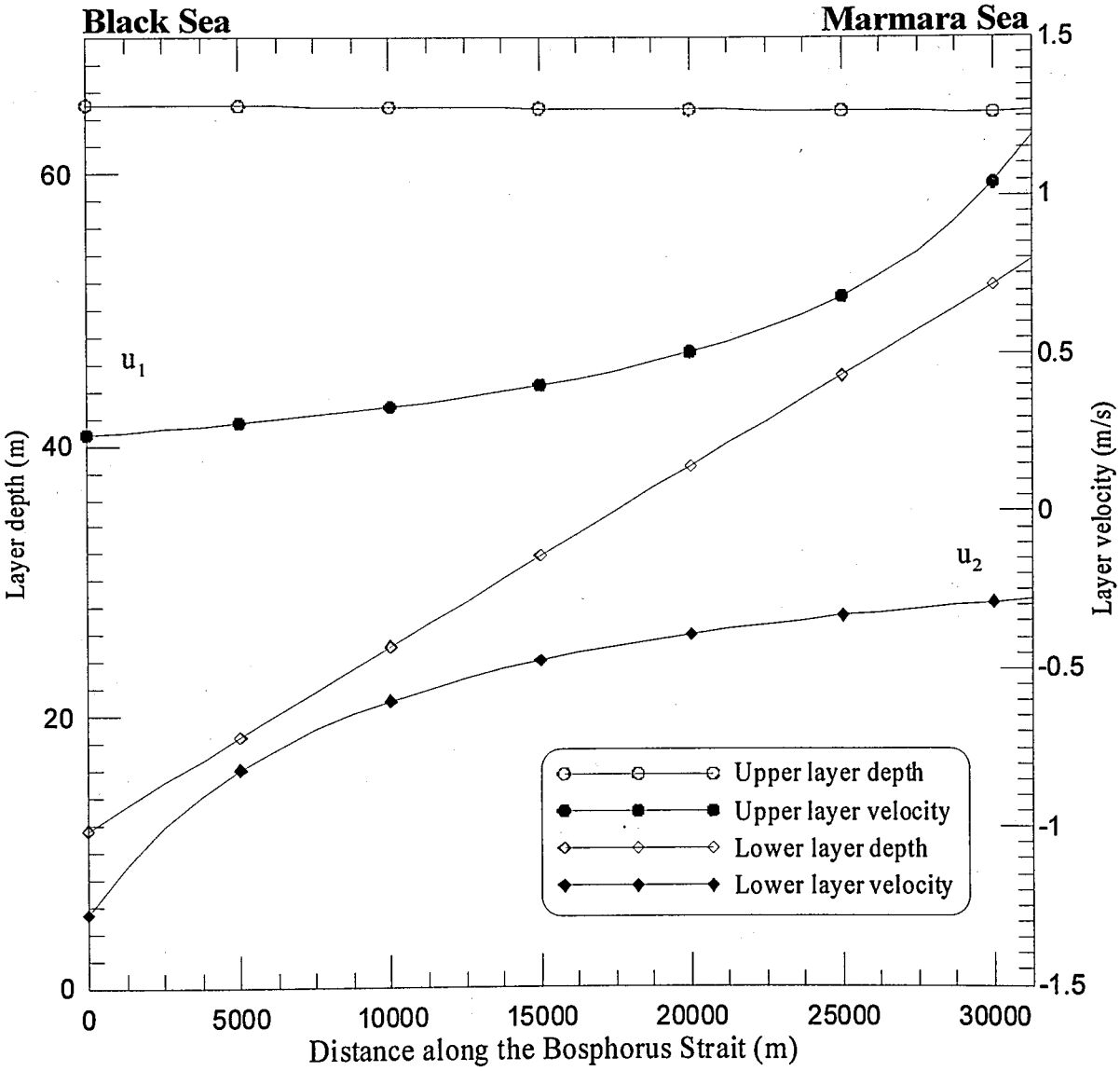

Figure 5.5. Flow velocities and layer thicknesses for a free surface level of 0.25 m between the Black Sea and Marmara Sea boundaries of the Bosphorus by using MQ (c=5000)

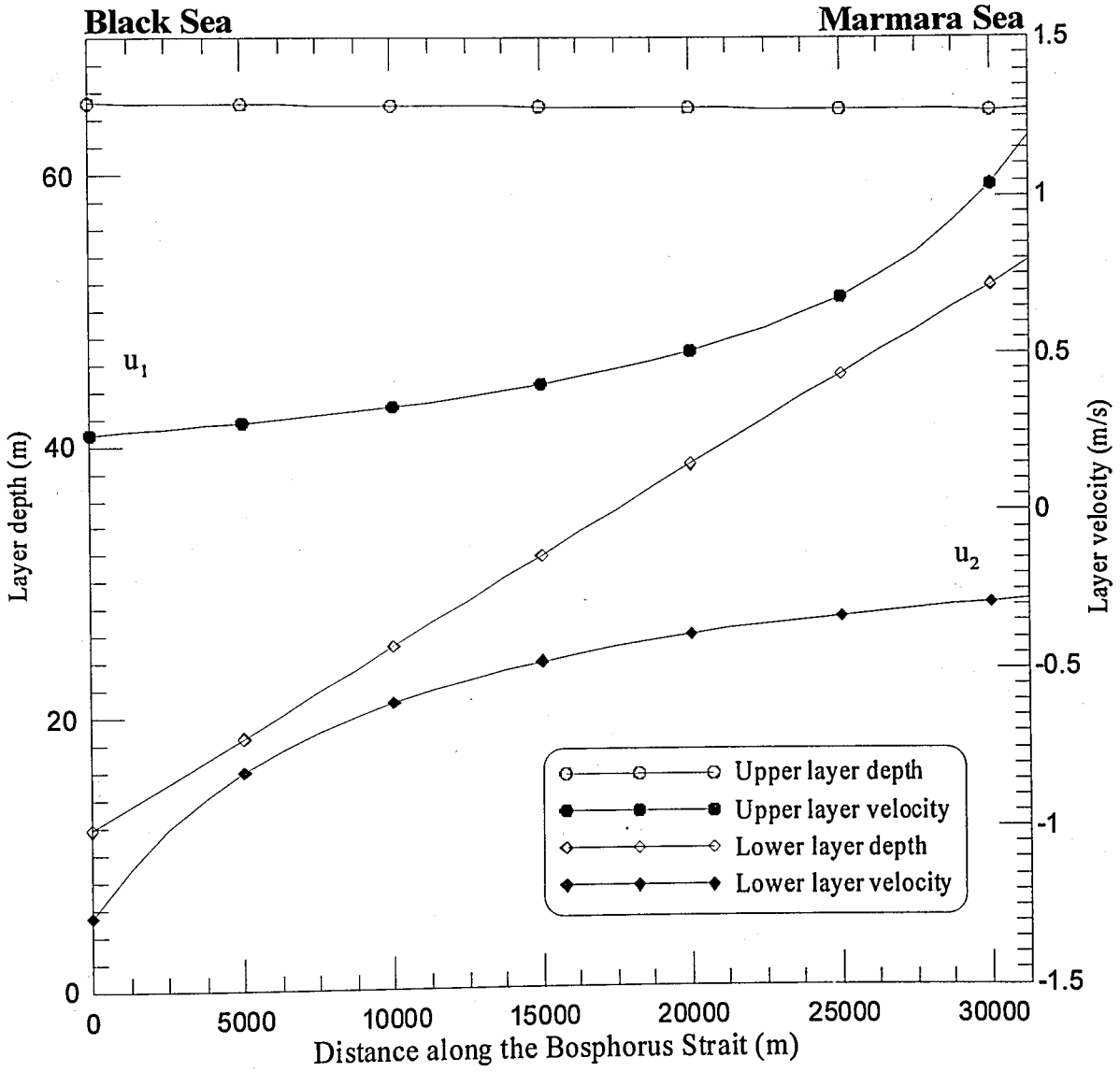

Figure 5.6. Flow velocities and layer thicknesses for a free surface level of 0.25 m between the Black Sea and Marmara Sea boundaries of the Bosphorus by 4^{th}OS

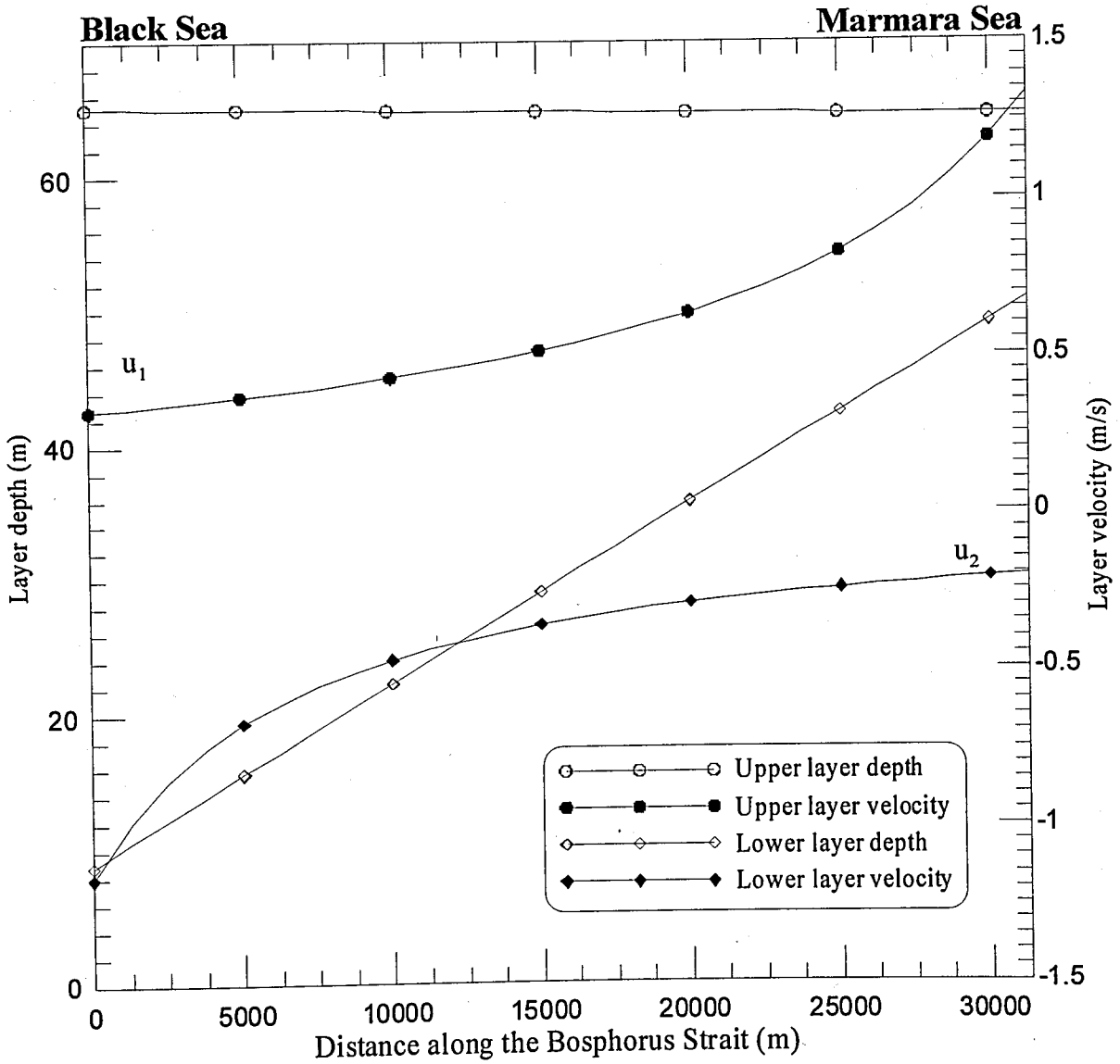

Figure 5.7. Flow velocities and layer thicknesses for a free surface level of 0.3 m between the Black Sea and Marmara Sea boundaries of the Bosphorus by using MQ (c=5000)

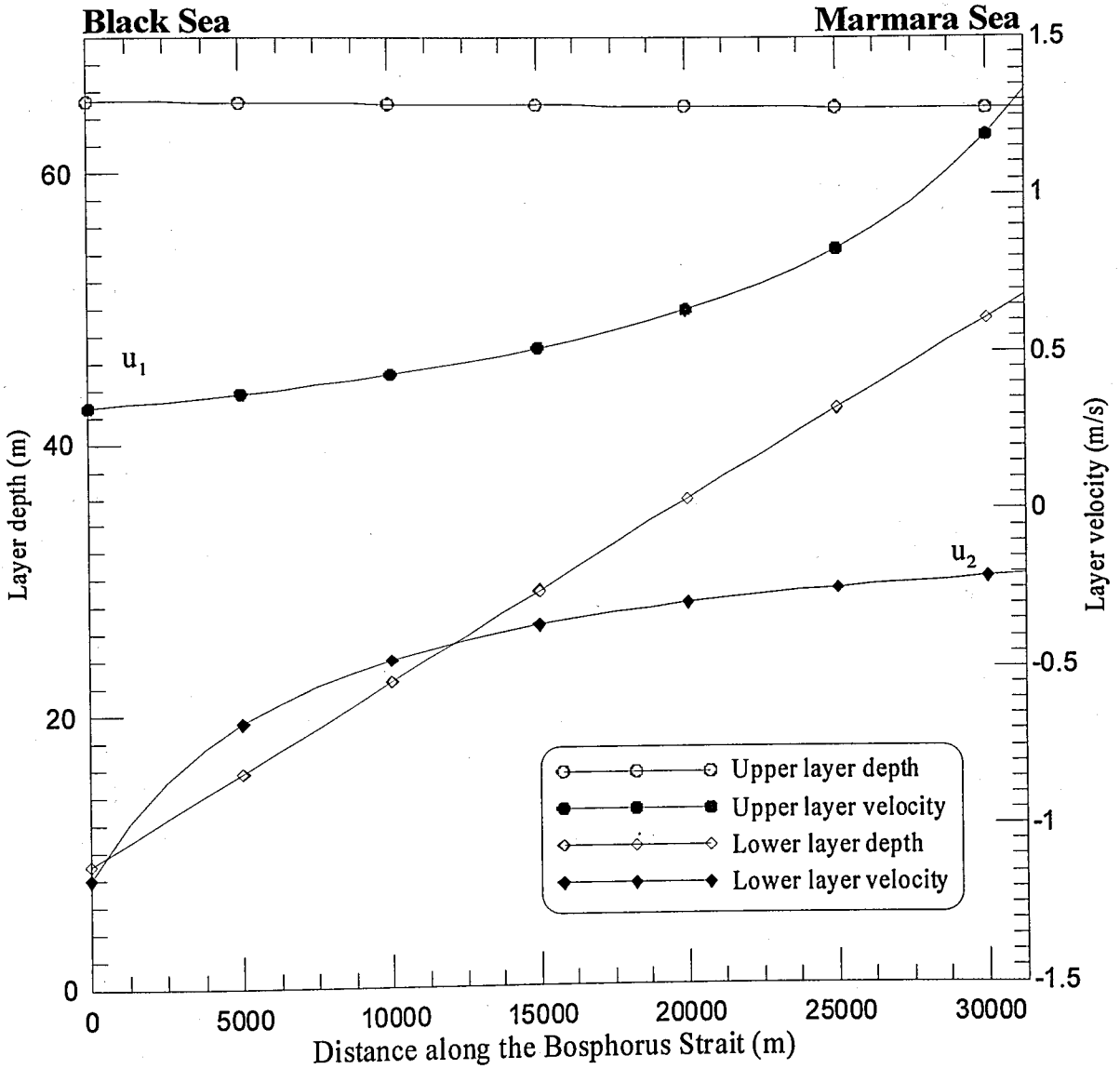

Figure 5.8. Flow velocities and layer thicknesses for a free surface level of 0.3 m between the Black Sea and Marmara Sea boundaries of the Bosphorus by 4thOS

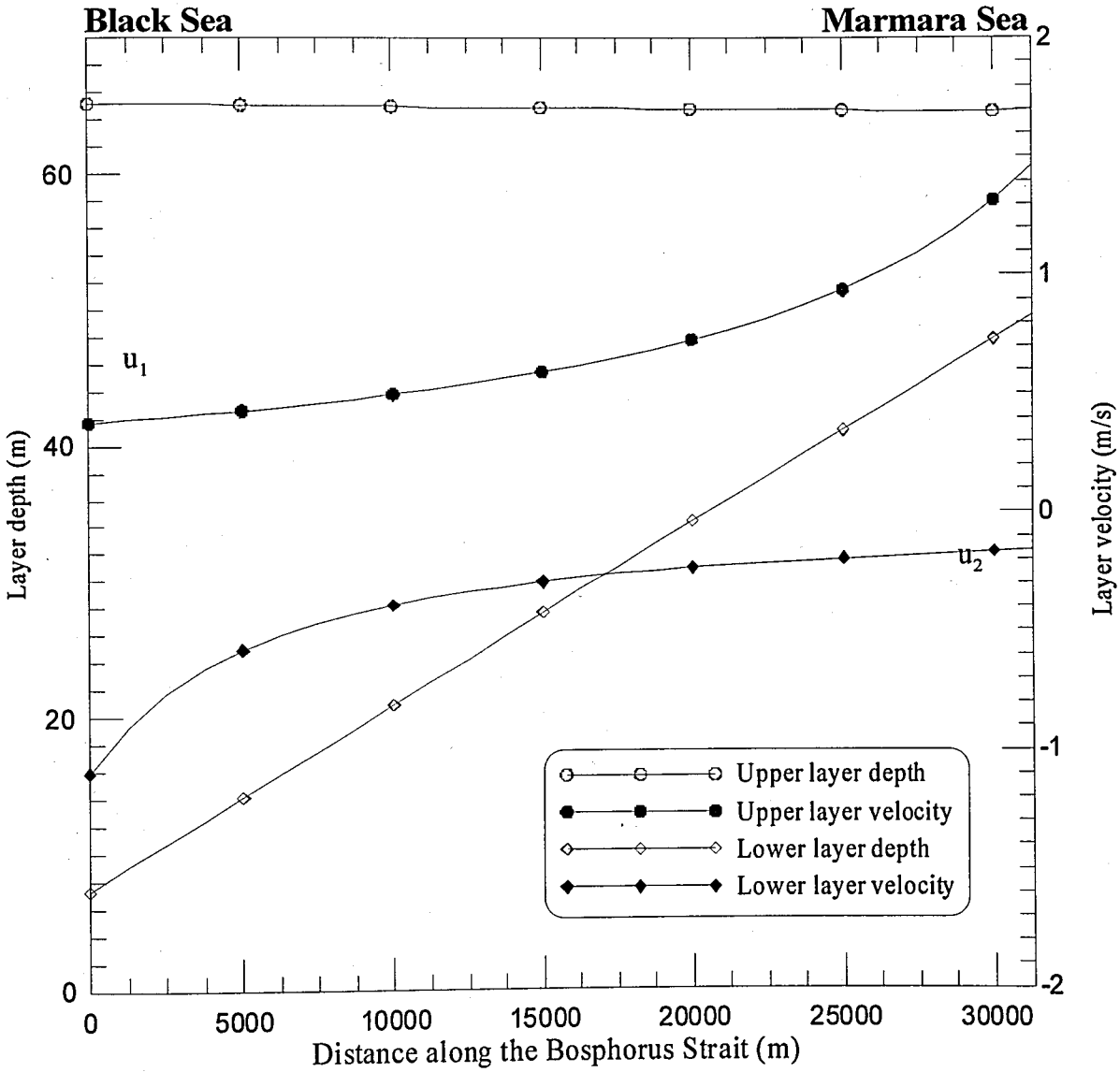

Figure 5.9. Flow velocities and layer thicknesses for a free surface level of 0.33 m between the Black Sea and Marmara Sea boundaries of the Bosphorus by using MQ (c=5000)

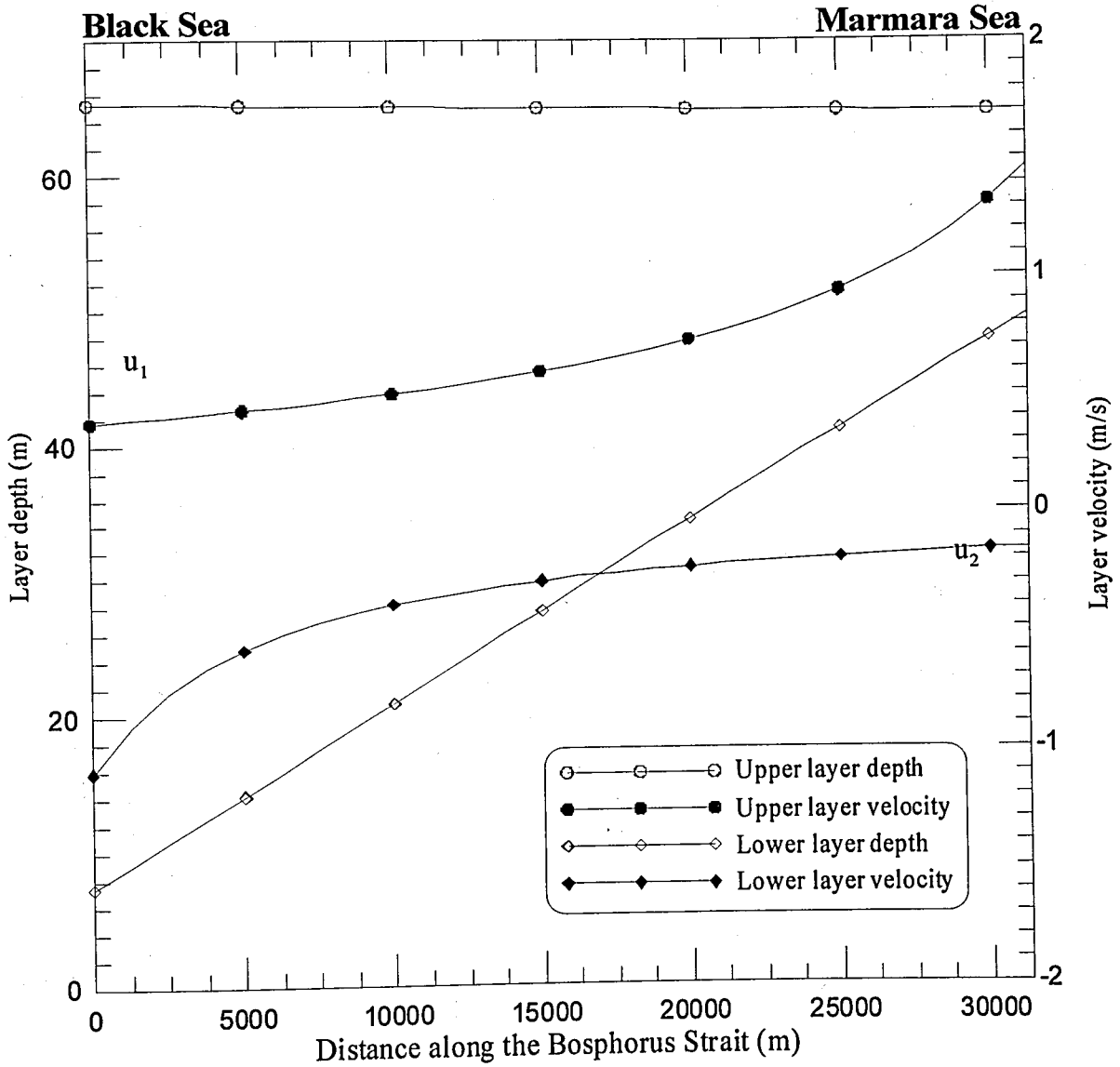

Figure 5.10. Flow velocities and layer thicknesses for a free surface level of 0.33 m between the Black Sea and Marmara Sea boundaries of the Bosphorus by 4thOS

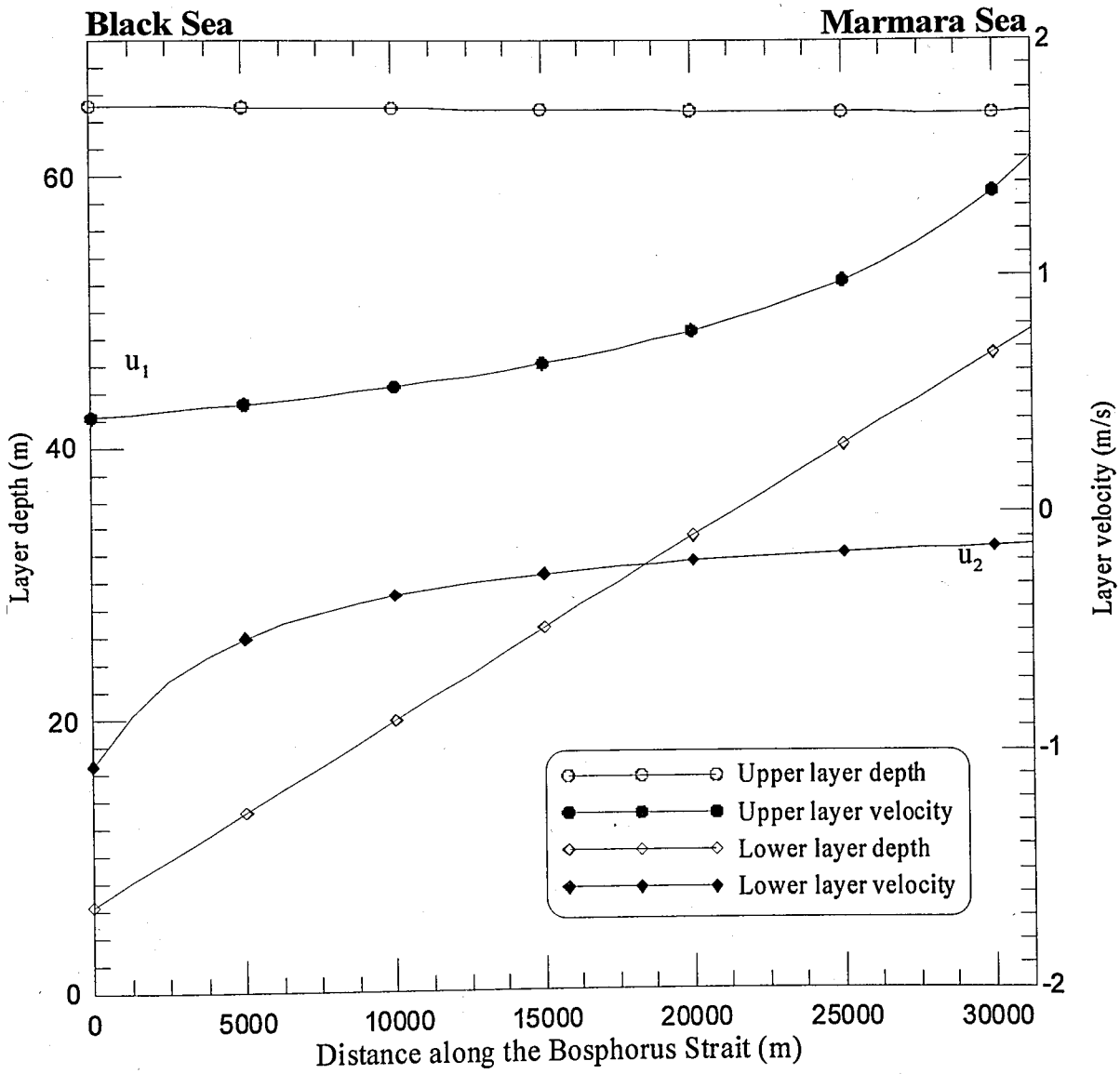

Figure 5.11. Flow velocities and layer thicknesses for a free surface level of 0.35 m between the Black Sea and Marmara Sea boundaries of the Bosphorus by using MQ (c=5000)

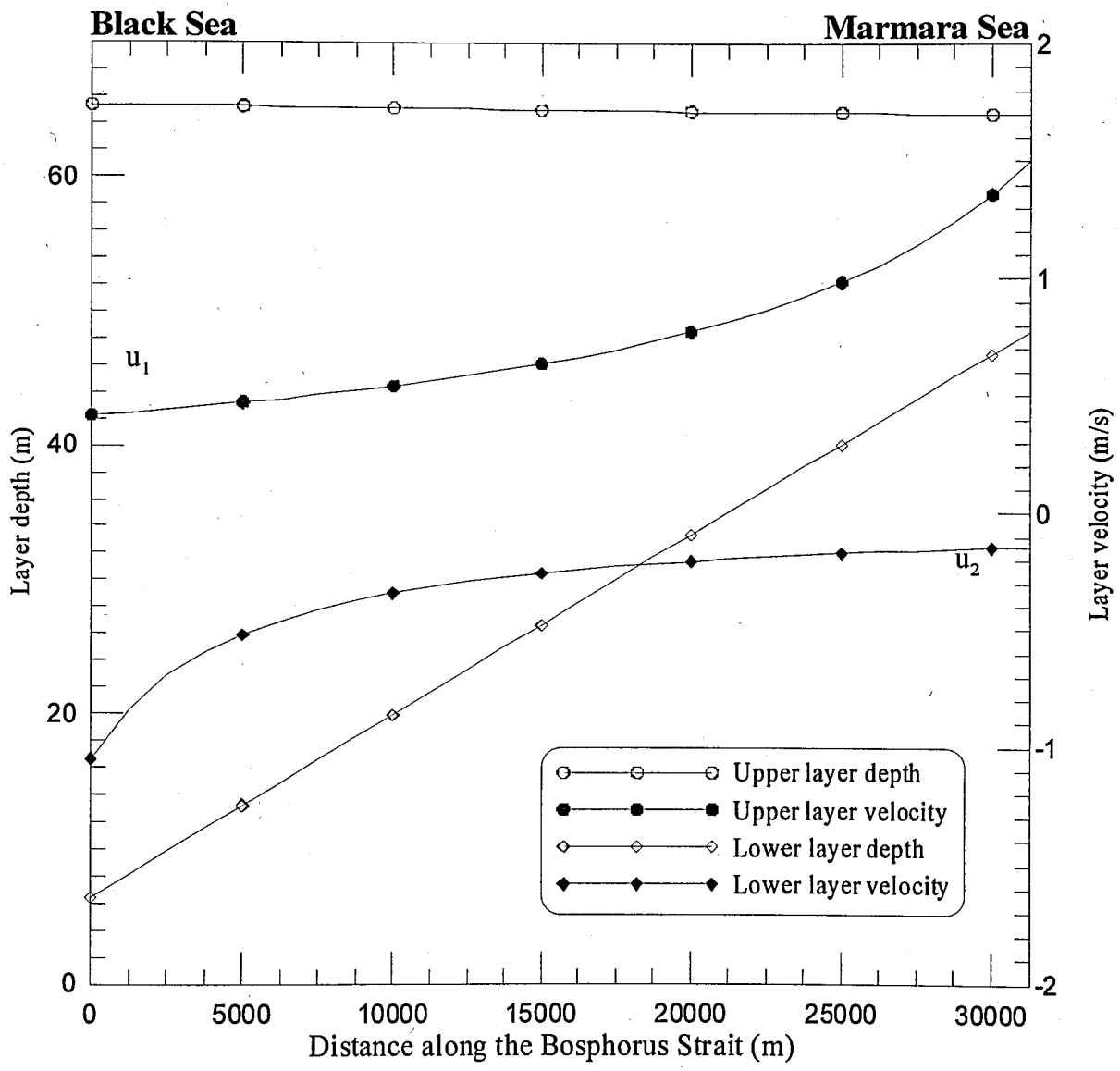

Figure 5.12. Flow velocities and layer thicknesses for a free surface level of 0.35 m between the Black Sea and Marmara Sea boundaries of the Bosphorus by 4thOS

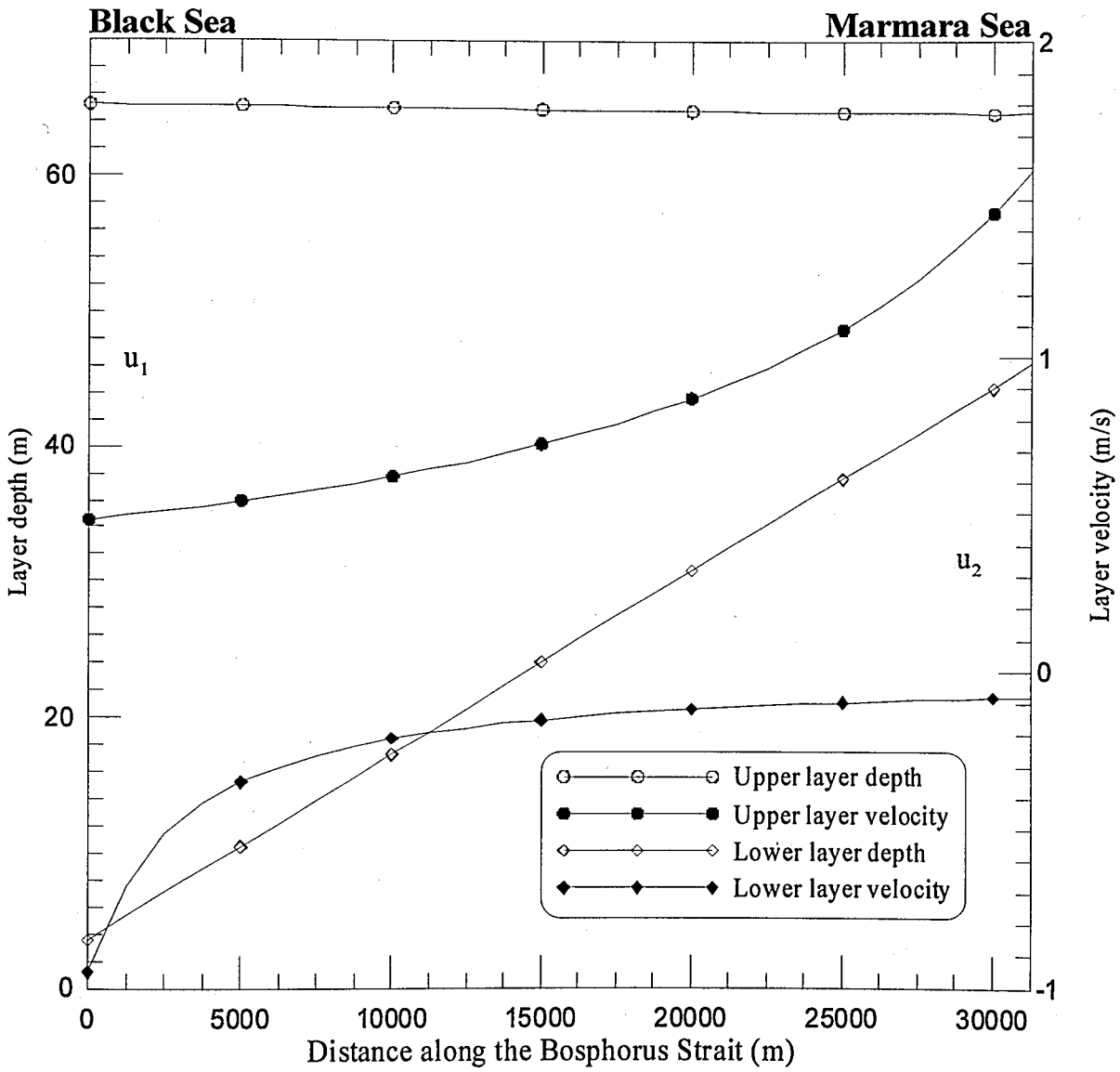

Figure 5.13. Flow velocities and layer thicknesses for a free surface level of 0.40 m between the Black Sea and Marmara Sea boundaries of the Bosphorus by using MQ (c=5000)

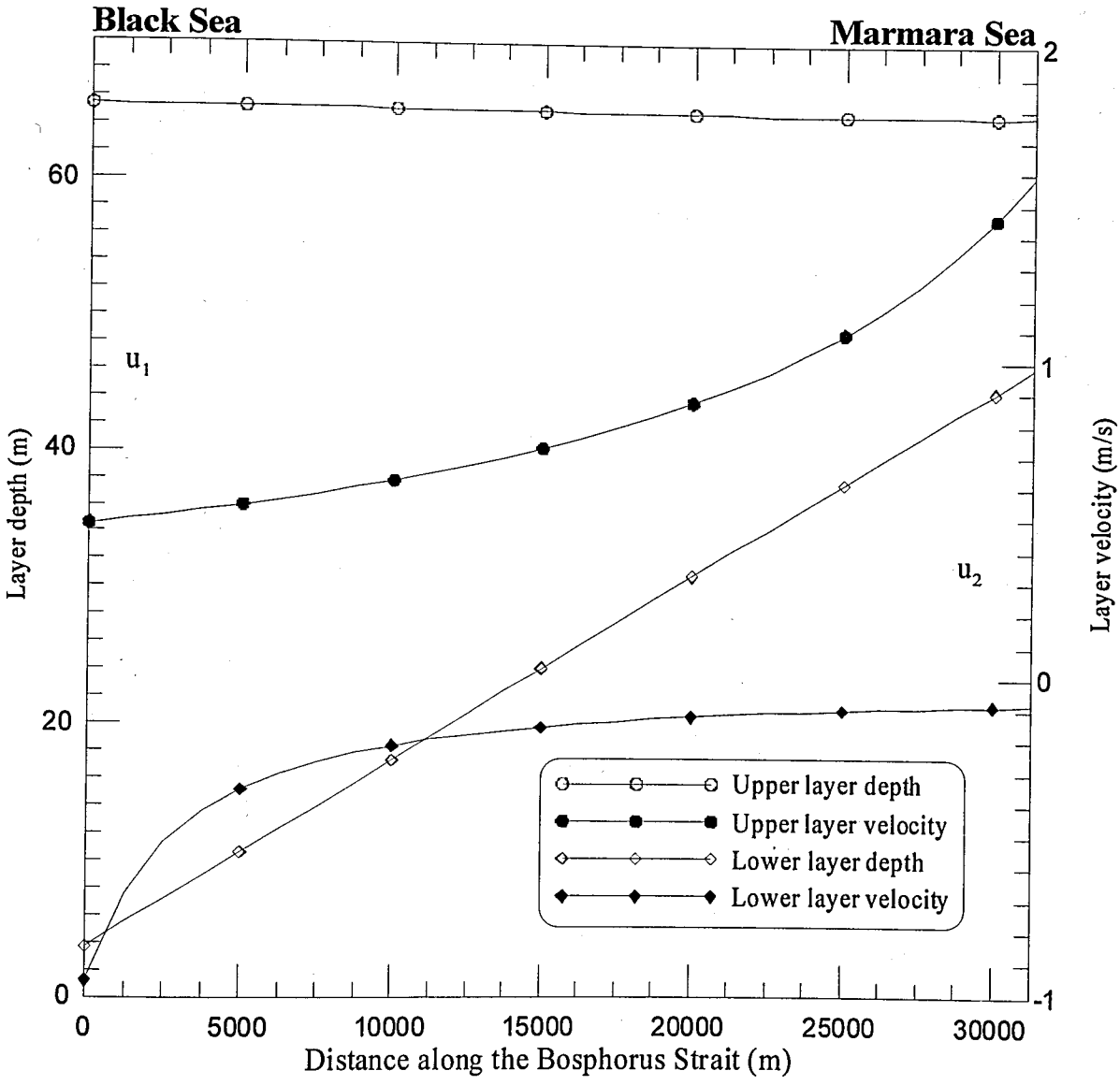

Figure 5.14. Flow velocities and layer thicknesses for a free surface level of 0.40 m between the Black Sea and Marmara Sea boundaries of the Bosphorus by 4^{th}OS

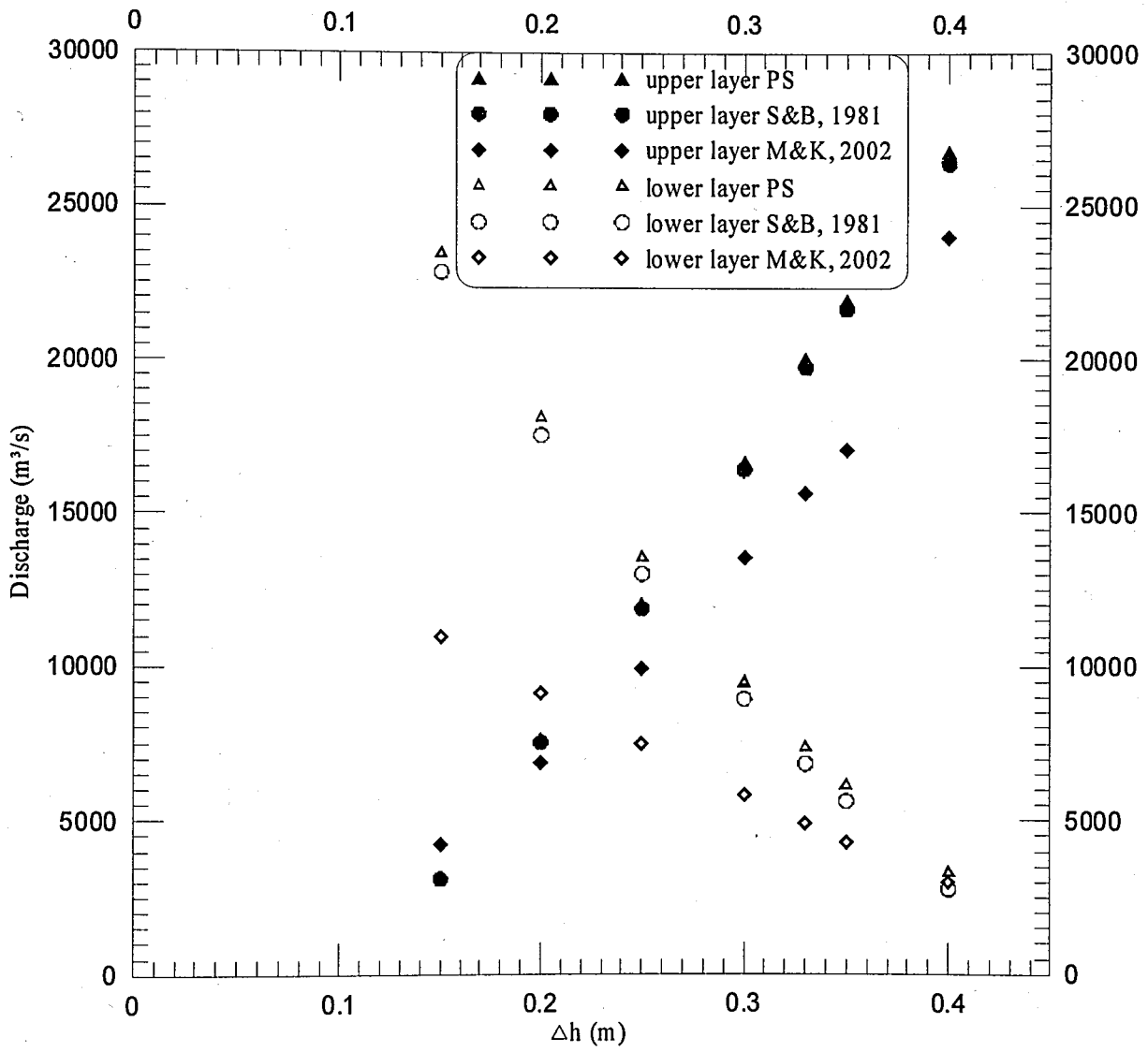

Figure 5.15. Calculated discharge by RBF-MQ versus surface elevation

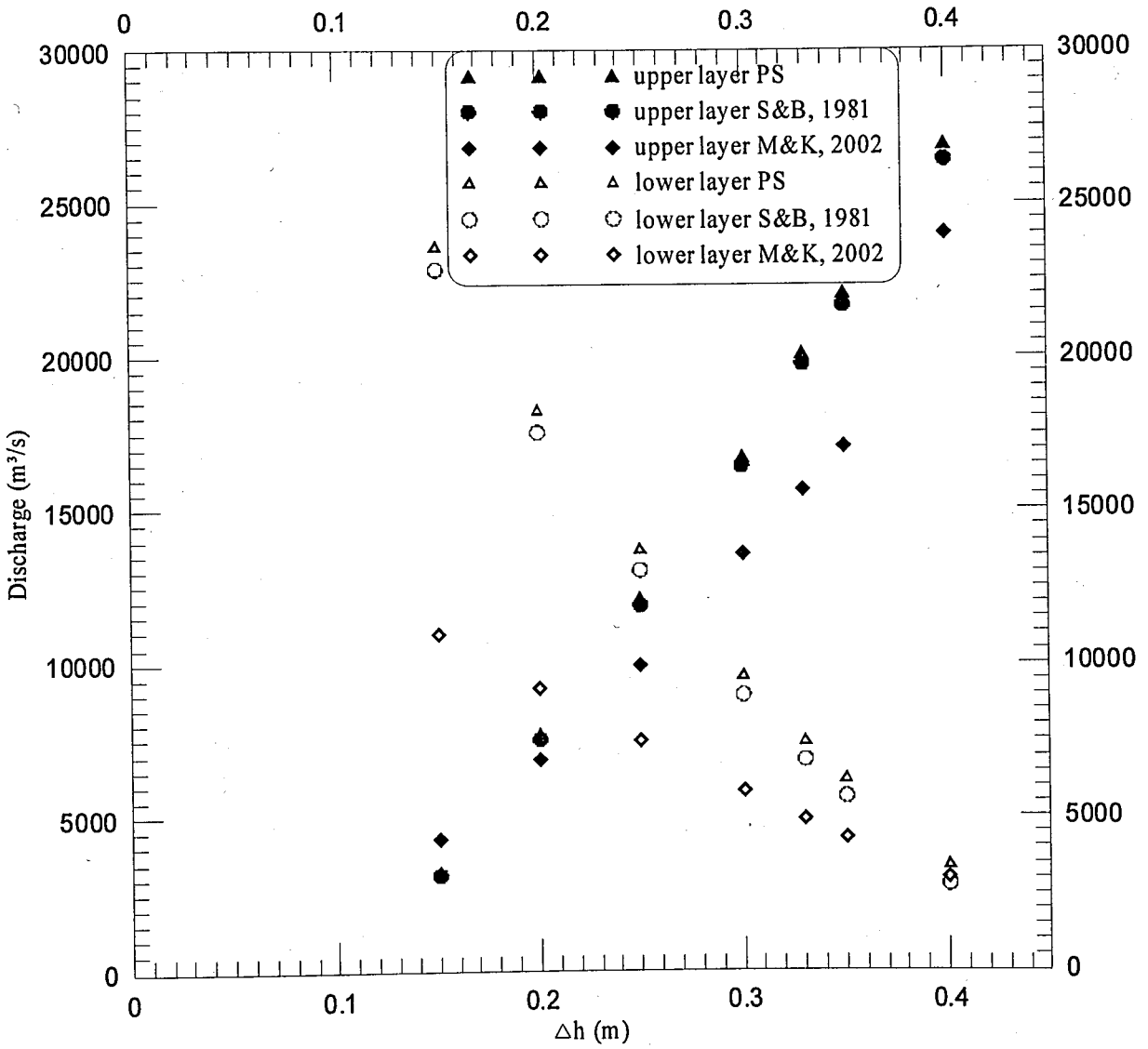

Figure 5.16. Calculated discharge by RBF-4thOS versus surface elevation

Table 5.1. Comparison of discharges with previous studies

F(x)	(m)	Present Study (m^3/s)		Sümer & Bakioğlu (1981) (m^3/s)		Madericha & Konstantinov (2002) (m^3/s)	
RBF	Δh	$AvgQ_1$	$AvgQ_2$	Q_1	Q_2	Q_1	Q_2
MQ	0.15	3180	23444	3091	22839	4247	10987
4^{th}OS	0.15	3214	23582	3091	22839	4247	10987
MQ	0.20	7635	18108	7512	17523	6860	9160
4^{th}OS	0.20	7684	18226	7512	17523	6860	9160
MQ	0.25	12047	13561	11873	13016	9933	7477
4^{th}OS	0.25	12110	13659	11873	13016	9933	7477
MQ	0.30	16644	9470	16406	8943	13540	5797
4^{th}OS	0.30	16720	9551	16406	8943	13540	5797
MQ	0.33	20024	7340	19731	6822	15623	4883
4^{th}OS	0.33	20111	7413	19731	6822	15623	4883
MQ	0.35	21953	6133	21632	5619	17076	4297
4^{th}OS	0.35	22046	6201	21632	5619	17076	4297
MQ	0.40	26789	3289	26391	2757	23996	3012
4^{th}OS	0.40	26894	3348	26391	2757	23996	3012

Table 5.2. Relative error norm L_2 (Equation 5.1) of the upper and lower layer flow rates

RBF TYPE	Δh (m)	L_2 Norm Upper Layer	L_2 Norm Lower Layer
MQ	0.15	2.94	2.65
4^{th}OS	0.15	4.01	3.25
MQ	0.20	1.66	3.34
4^{th}OS	0.20	2.30	4.01
MQ	0.25	1.48	4.19
4^{th}OS	0.25	2.00	4.94
MQ	0.30	1.45	5.90
4^{th}OS	0.30	1.91	6.80
MQ	0.33	1.48	7.63
4^{th}OS	0.33	1.92	8.67
MQ	0.35	1.49	9.18
4^{th}OS	0.35	1.91	10.37
MQ	0.40	1.51	19.35
4^{th}OS	0.40	1.91	21.45

6. CONCLUSIONS

In this study, a two- layer model is adopted; the dynamic equations are integrated to determine the flow rates and depths, with particular application to the Bosphorus Strait. The model takes into consideration the wind stress on the surface because of its short-term character. It neglects the side-wall effects as it assumes very large aspect ratios (e.g. the latter is about 1:30 for the Bosphorus). Results of the model were compared with those of Sümer and Bakioğlu (1981).

The model has been solved for the Bosphorus with the assumption that the interface has a linear shape. The interface obtained appeared to be in fairly good agreement with the DAMOC data (1971) and in accordance with Sümer and Bakioğlu's study (1981). Thus relatively realistic results have been obtained in the simulations.

Pointing out the considerable influence of the decline in surface elevation between the two ends of the strait, h, upon the flow is of importance. This implies that changes in h throughout the year (depending on various effects such as wind, runoff, pressure etc.) will result in drastic changes in the two-layer current system. In this connection, one poses the following questions:

- How long is the surface elevation present to maintain the presence of the decline?
- How does the two-layer system respond to changes in h, and how long does is take for the two-layer system to reach a new state of equilibrium?
- How does the latter period of time compare with the time duration during which h is persistent?

Time-dependent solutions are needed to answer these questions, which, in author's opinion, are of great importance as to the dynamics of sea straits.

Moreover, the two-layer currents in opposite directions create secondary currents flowing vertically. Therefore for the development of the present study, starting with a reasonable intermediate state 2D, 2-layer model than steady state assumption by a 3D

model should be more realistic. Since in three-dimensional modeling, there are no limitations and the full momentum and continuity equations are solved. This greatly improves the computed results quantitatively and qualitatively. But this additional dimension requires a very long additional computational time and space. Thus the philosophy of this study is bring to a more elaborate, advanced, living model in the future that can be updated and modified.

In order to develop the present study, the physical quantities such as wind drag coefficient, bottom drag coefficient and interfacial drag coefficient should be measured or calculated from field or laboratory experiments. The absence of long term salinity, temperature, wind and current data, also unavoidably prevent to make qualitative and quantitative testes in the Strait where is very important for militarily purposes. For that reason, regular monitoring data can be publicly accessible to industry and academic environment.

Significant importance must also be given to hydrodynamic modeling as a highly invaluable tool to preserve and protect water bodies from effects of urban and industrial developments.

APPENDIX A: CHORONOLOGICAL REVIEW OF THE OCEANOGRAPHIC INVESTIGATIONS OF THE TURKISH STRAITS

The straits being the only passage between the Mediterranean and the Black sea, and forming a bridge between Europe and the Near East has attracted the scientists to investigate the conditions of the area. The biggest emphasis was given to the geological evolution of the straits. But the oceanographic features and the exchange of water, including the current systems of the area became also very important for oversea transportation and military purposes. Thus, a growing interest for scientific investigations dated back to as early as 1861.

In 1681, the first written evidence of the existence of the two-directional currents of the Bosphorus and a description of the undercurrent was given in Count Marsilli's letters to Queen Christina of Sweden. Count Marsilli thought that a counter current was physically essential under the existing upper current forces. Further, he made observations on the changes of the water level in the Sea of Marmara and on the surface currents of the Bosphorus. In order to back his physically sound two directional current theory for the straits, he prepared a chart showing the current systems in the Bosphorus with a main surface current towards the Sea of Marmara and the eddy currents in some of the bays such as the Galata – Ortaköy Bay, off Üsküdar and Anadolu Kavak Bay. The theory of Count Marsilli was regarded for a long time as being doubtful. Only after two hundred years from Marsilli's work new interest were directed to his undercurrent theory (Marsilli, 1861).

In 1870, Captain Spratt started to investigate the hydrography of the Bosphorus with current-anchors and also measured the salinity. He came to the conclusion that no undercurrent can exist in the strait and that the observed heavy and saline water in the deeper parts of the Bosphorus can only be transported by strong wind driven surface water from the Aegean towards the Black Sea in autumn and winter periods (Spratt, 1870).

In 1872, British Admiral Wharton on board the vessel Shear Water performed careful drogue studies, density measurements (with aerometer) and temperature readings (with reversing thermometers.). He studied the hydrographic conditions of the Bosphorus at two cross-sections and those of the Dardanelles at three cross-sections.

In contrast to the statements of Captain Spratt, Admiral Wharton came to the conclusion that an undercurrent existed below the surface current layer all the way from Aegean to the Black Sea and that the velocity and strength of this undercurrent was dependent on the velocity of the surface current. According to his findings, the interface between these two opposite currents at the northern end (Black Sea entrance) was at 37 m and at the southern end of the Bosphorus (Marmara) at 18 m. But that the interface (thermo-halocline) between the Black Sea and Marmara water layers was recorded at 48 and 27 m. His measurements in August 1872 indicated a temperature minima (thermocline) of between 35 m and 47 m. At the same time he measured at the surface and at a depth of 60 m. This condition forming the thermocline was absent in October 1872. His observations showed that the velocity of the surface current was ranging from 125 cm / s. to 225 cm/s. depending on the site of the measurement. For the lower current, the measured velocities were ranging from 13 to 55 cm/s. In the Dardanelles off Gelibolu, the current interface was found at 33 m and at the Aegean end of the strait it ranged from 16 to 22 m. The interface of the Black Sea and Mediterranean water layers was between 18-36 m. He also recorded that the extraordinarily variable current velocities at the surface were on the average 75 cm/s. with a maximum of 150 cm/s and the undercurrent with a maximum velocity of 40 cm/s. He related the wind forces to the sea level changes, reaching 70 cm over the average water level and he pointed out to the prolongation of the lunar tides which may cause an elevation of 10 cm at the surface. He also pointed out the importance of the winds, their direction and speed to the surface flow from the Black Sea. But he ignored the effect of the density differences between the Black Sea and Mediterranean (Wharton, 1886).

In 1881, Makaroff from the Russian Navy carried out winter hydrographic investigations in the Turkish Straits on board the Russian ship Taman.

In order to solve the problem of the undercurrent, he performed approximately 1000 current readings and 4000 temperature and density measurements. Without prior knowledge of previous studies in the area, he came to the same conclusion as Marsilli and Wharton. He proved trough careful temperature and density measurements that the water column in the straits consisted of two layers, with an interface inclining towards the Black Sea. His findings should be regarded as a qualitative picture of the hydrographic conditions in the straits. His results may be summarized as follows:

- A two directional current system, with an upper and undercurrent is present in the straits.
- The strength of these currents depends on the density differences between the two layers and to the water level conditions in the Black Sea and the Sea of Marmara.
- The interface between these two layers consists of a water layer with a large gradient of density and is motionless. He recorded the depth of this layer as being 42.1 m at Büyükdere, 49.4 m at Rumelihisar, 34.8 m at Anadoluhisar, 25.6 m at Arnavutköy, and 20.1 m at Sarayburnu located at the southern end of the strait.
- The depth of the interface was dependent on the water level changes in the Black Sea and also on the wind forces.

Makaroff's current measurements indicate different characteristics for the upper and the undercurrents. The undercurrent flows following the density gradient and is affected by the configuration of the sea bed, but not always filling completely the narrow channel. The velocity of this flow shows in cross-sections some differences like those in different parts of a river. The maximum velocities were obtained approximately 5.5 m below the current interface, ranging from 0.6 to 1.1 m/s. By hourly current measurements, he recorded some periodic fluctuations in the velocities of the surface current. Like the undercurrent the surface current flowing in the opposite direction did not fill all the surface area of the channel, giving way to eddies in the bays along the strait. The maximum velocity of the surface current was just at the surface with an average of 1 m/s. Deviations from this average were observed at different locations and the maximum was observed at Arnavutköy with 1.9 m/s. Off Büyükdere, the current ran at only 0.35 m/s. Based on his current and density measurements, he estimated the water budget of the Black Sea and the extent of the exchange of water between two seas. He estimated a level difference of 0.52

m between the Black Sea and the Marmara Sea. Taking the calculated average velocities of the upper (0.78 m/s.) and the undercurrent (0.63 m/s.) he estimated the Black Sea outflow 9990 m^3/s. and the inflow amounting to 5400 m^3/s. The difference of the out and the inflow amounting to 4590 m^3/s. gives the runoff from the rivers and precipitation minus the evaporation. He stated that this difference may change from year to year and/or seasonally depending on the meteorological conditions of the area, as well as on the density of the water mass (Makaroff, 1885).

In 1884, Magnaghi started his observations on board the ship Washington with a magnetic current meter and established 6 stations in the Dardanelles and 7 stations in the Bosphorus. He recorded velocities and the directions of the current at different depths. At the same time, he made temperature readings in order to locate the position of the interface between the two layers. He found the current interface at the northern end at 45 m and at the southern end at 15 m. He observed also that the velocity of the surface current was increasing from 30 cm/s due to shallowing of the upper current depth. At the same time the undercurrent velocity was decreasing towards the Black Sea from 84 cm/s to 42 cm/s. In the Dardanelles the current interface was recorded at Nağra Burnu at 8 m depth and the Aegean Sea at 12 m. In the Dardanelles the surface velocities were ranging from 100 to 130 cm/s. and the undercurrent velocities from 10 to 55 cm/s (Magnaghi, 1894).

In 1886, Gueydon on board the ship Petrel performed some current velocity and direction measurements along with some temperature and density readings at different depths and locations. His investigations led Gueydon to the conclusion that the volume of the undercurrent was much greater compared with that of the surface flow from the Black Sea (at least during the period of his observations). Although his conclusions are not acceptable, the data collected by him, by some very simple methods fits fairly well into the overall picture of the Bosphorus hydrography. He located the boundary between the currents at 15-18 m and another current interface between 30-45 m. During his 48 hour velocity measurement off Tophane in March 1886, he was able to track some fluctuations in the undercurrent velocities 9 m above the bottom. During his 48 hour velocity measurement off Tophane in March 1886 he was able to track some fluctuations on the undercurrent velocities 9 m below the bottom (Gueydon, 1886).

In 1892, Wolf and Luksch on board the ship Pola carried out temperature, salinity and current measurements in the Dardanelles. They located the thermohaline interface at 12 m depth. During their eight day observations, they tried to prove the effects of the winds on the distribution of temperature and salinity at the surface layers (Lulksch and Wolf, 1892).

In 1894, Natterer on board the ship Taurus made chemically oriented oceanographic observations at 42 stations, located on N-S profiles of the Sea of Marmara with two additional stations in the Dardanelles. The standard depths for sampling were 0.5, 10, 50 and 100 m. He measured important variables of the Sea of Marmara water like temperature, salinity, dissolved oxygen and CO_2 but was not able to trace the actual location of the thermohaline interface with his standard depths. Temperature readings were obtained by deep-sea thermometers, salinity by calculations from the aerometer density readings, dissolved oxygen and CO_2 by titrations. In May 1894, he recorded temperatures of the upper layers of the Sea of Marmara ranging from $10°C$ to $12°C$. The salinities were higher than those of the Bosphorus during the same period and he attributed this salinity elevation to the mixing processes between two water masses, rather than the evaporation in the Marmara. The temperatures recorded at the lower water layer were ranging from $14.1°C$ to $14.6°C$. The vertical mixing of these two layers was attributed to the bottom relief of the Sea of Marmara. During his investigations he frequently observed "lenses" of water with higher salinity than the surrounding water. The distribution of the dissolved gases such as O_2 and CO_2 also proved the vertical mixing. No H_2S was detected and the O_2 content below 50 m was 50% of the surface concentrations. His work may be considered as the first mile-stone for the discovery of the chemistry of the Straits (Natterer, 1894).

In 1894, Spindler began his investigations on board the Turkish ship Selanik in the Sea of Marmara. One of his aims was to complete the bathymetric charting of the area, started earlier by Admiral Wharton. He estimated the average depth of the Sea of Marmara to be 289 m. To investigate the temperature and salinity distributions of the sea, he utilized a total of 61 hydrographic stations of which 52 were located in the Sea of Marmara, 8 in the Dardanelles and one station in the Bosphorus. He distinguished the following four

different layers with different hydrographic features in the Bosphprus and the Dardanelles Strait:

- A homohaline (25.5 ppt S) and homotherm (19.5°C) surface layers with a thickness of 11 m.
- Below this "cover" from 11 to 25 m depth a layer with a temperature decrease of 2°C and salinity increase of 10 ppt S.
- A deeper layer extending from 25 to 200 m depth with a temperature of 15°C and 38.1 ppt S.
- A deep layer below 200 m down to the bottom (1400 m) a homothermic (14.2°C) and homohaline (38.4 ppt S) deep water layer.

The water carried by the surface current from the Black Sea with 18.1 ppt S and the water carried by the undercurrent from the Mediterranean with 38.8 ppt S and the rate of their mixing play a role on the formation of these four layers. But the characteristics of these two different waters are already changed before they enter into the Marmara proper by intensive mixing in the channels. The interface between the upper and undercurrents located in the Sea of Marmara was on average at 13 to 14 m depth. At the Aegean entrance of the Dardanelles at 11-18.6 m. and at the entrance to the Sea of Marmara 12 to 16.5 m. In the Bosphorus it was located at 14 m. Current velocities in the Sea of Marmara, between the Princes Islands were 0.25 m/s. and in the bays across the prince Islands were 0.03 m/s. Spindler also tried to estimate the water exchange trough the Bosphorus and calculated the outflow as 14500 m^3/s (Spindler, 1894).

In August of 1910, Nielsen on board the ship Thor carried out investigations at a number of stations in the Straits and the Black Sea. He observed, at the Black Sea entrance of the Bosphorus, a homohaline (17.5 ppt) and homotherm (24°C) upper layer with a thickness of 17.5 m. Below this "cover layer" a transition zone both for salinity and temperature was present on which a temperature minimum of 7.3°C was recorded at 85 m. Approaching the Bosphorus entrance, a rapid rise of this temperature minimum layer up to 40 m depth was observed. For this layer the salinity was 19 ppt, below this thermocline both the temperature and salinity rose to 15.32°C and 36 ppt S. In the Bosphorus, the interface between the upper and the undercurrent was detected at 30-40 m at the northern

end, and at 20-25 m at the southern end. In the Sea of Marmara, the salinity distribution down to 10-15 m was almost constant around 22 ppt S. Below this layer, an increase of salinity was observed rising up to 37.5 ppt. The temperature in the upper layer was decreasing and reached its maximum of 16 to 16.5°C at 30 m depth. Below 600 m the temperature was constant at 14.15°C. From these observations it was concluded, that the deep basin of the Sea of Marmara was filled with heavier "winter water" of the Mediterranean and the relatively lighter "summer water" from the Mediterranean was above this water mass. Measurements of dissolved oxygen provided support for this assumption, because the oxygen concentration in the deeper layer was higher than that of the summer water layer. During this expedition a six-hourly observation on the fluctuation of the current interface based on temperature and salinity measurements was performed. No correlation was detected with the tidal oscillations and fluctuation of the current. On the surface strong fluctuations of the current velocity and formation of eddy currents were observed (Nielsen, 1912).

In 1917, Merz on board the yacht Adelgunde began his investigations of the hydrograhpy of the Bosphorus and the Dardanelles. The surface investigation was made at two different times. The first trip was in September/October 1917 and the second from May to July 1918. His investigations included the following observations:

- Depth soundings at 300 points.
- Metrological observations and analysis of the data collected from the meteorological stations (barometric pressure and wind).
- Clorinity measurement by Mohr titrimetry, salinity calculations from the clorinity data using Knudsen's tables and seawater temperature readings were done.
- Current measurements were done by Ekman magnetic currentmeters.
- Studies on the Morphology and Geology of the straits were done.

Merz carried out his measurements at 18 cross sections in the Bosphorus and 16 cross sections in the Dardanelles with a great number of hydrographic stations along the coasts of the straits. In total he used 310 stations with 2067 current measurements, 723 temprature readings and 623 water samples for clorinity titrations. Because of the death of

Merz, Moeller analyzed the hydrographic data compiled and came to the following conclusions:

- The distance for the travel of the water mass carried by the upper and undercurrent, described by the early researchers, is approximately 300 km. Taking the average velocities of these streams the time for the travel of the upper current is ½ months and the undercurrent 2 ¼ months.
- The hydrographic structure of the Black Sea and the Aegean leads to a characteristic stratification of the water layer along the straits. Below the low-saline "cover layer", a water mass with high salinity exists and the two are separated by a sharp halocline, mostly accompanied by a sharp thermocline. This thermohaline interface is at 100-150 m in the Black Sea and at the northern entrance of the Bosphorus it rises to 50 m. In the channel this rise is more pronounced and reaches a value of 15-20 m at the South end. Its depth changes only at the cross section Nağra in the Dardanelles where it rises to 10 m depth. Affected mainly by the water level changes in the Black Sea, the yearly changes in the position of the interface are very slight. Under the conditions of high water level in the spring the interface in the straits is deeper. A difference of 2.7 m water level was recorded in September/October 1917.
- Depth of the current interface was rising from north to south. The depth of the current interface at the north end of the Bosphorus was detected 7 m above the thermohaline interface and at the south end 4 m below it. In the Dardanelles, at the north end the current interface was 0.5 m above and at the south end 6 m below the thermohaline interface. This indicated that in the northern parts of the channels a portion of the under water mass flowed back with the upper current. This phenomenon is attributed to the vertical distribution of the water pressure, peculiar to this typical stratification.
- The surface water salinities at the north entrance of the Bosphorus were 16-18 ppt and at the south end of the Dardanelles 26-28 ppt. The gain of salt in the Bosphorus is 2 ppt, in the Sea of Marmara 5 ppt and in the Dardanelles 3 ppt. These figures indicate that no great exchange between the upper-and lower layers can be expected. The vertical distribution of the temperature may also be considered as a proof of this statement. In the summer period a thermal stratification is found at the upper water mass. A sharp thermocline as a minimum temperature layer may be followed from

the Black Sea to the South end of the Dardanelles. In contrary the upper water layer in winter period is homotherm. The salt content of the deeper water entering the Sea of Marmara, up to the south entrance of the Bosphorus is almost constant. In the Bosphorus due to the intensive mixing, the salt content drops by 3-5 ppt, i.e. to a level of 33-35 ppt. The salinity of the deep water layer entering the Black Sea decreases to 22-25 ppt as it leaves the Bosphorus. The density of the deep water entering Dardanelles is 1029 g/cm^{3}and decreases to 1024 g/cm^{3}by the time it reaches the Black Sea.

- The upper current with an average velocity of 40-50 cm/s flows as a shallow band through the Bosphorus and the Dardanelles. Its velocity increases at the south ends of the both channels reaching values of up to 150 cm/s. The decrease in the vertical distribution of the upper current velocity is slow at the north ends and extraordinarily rapid at the south ends of both channels. The interface between the currents is 2-10 m thick in the Bosphorus and 2-7 m in the Dardanelles. The velocity of the current within the interface does not approach zero, but is in the average 8 cm/s in the Dardanelles and 14 cm/s in the Bosphorus. The turning of the current directions at the transition zone is caused by a diversion of the upper current toward the coast as a cross-circulation. As it is seen in the northern parts of the Bosphorus and in the northern and southern parts of the Dardanelles, wherever the surface current approaches the European coast the current direction solemnly against, from SW to NE, and wherever it approaches the Asiatic coast, as seen in the southern parts of the Bosphorus it solemnly turns. In the narrow parts of the channels these rules are not valid. In the Bosphorus the current interface is 10 m thick and instead of a simple turning of the direction from one side to the other, a back and forth swinging is happened.
- The undercurrent following the topography of the channel more strictly than the upper current. The undercurrent is not always flowing under the upper current. They follow mostly different pathways in the channel. Because of the presence of a mixing-zone between the two currents, the minimum velocity of the undercurrent is detected on the average at 8 m below the thermohaline boundary surface in the Bosphorus, and at 16 m below in the Dardanelles.

- The current systems in the channels are subject to different types of fluctuations; yearly periodic fluctuations due to the sea level changes, periodic fluctuations due to the tidal forces, fluctuations due to the self-swinging of the stratified water mass.
- The effect of winds and air pressure changes to the currents are also discussed in details.

The observations of Merz and the evaluation of the results by Moeller is another milestone for the discovery of the hydrography of the straits (Merz, 1921; 1928).

Ullyott and Pektaş (1952) evaluated the data, collected from 1944 to 1952, on the yearly temperature and salinity cycles in the straits. They noticed that the winter conditions in the straits were especially important. Their observations had shown that there was a large difference between the water leaving the Sea of Marmara in the summer and in the winter. The winter salinity values were about 6 ppt higher than in summer, indicating a degree of mixing more than 100 0/0 greater during the winter than in summer. They stated that, as long as the surface waters of the Sea of Marmara were at a high temperature, the outflow past Çanakkale was of relatively low salinity (23-24 ppt), but as soon as the surface water began to cool down, the salinity began to rise. The increase of salinity was accompanied by a drop in temperature. At the beginning of April, with the first sign of warming, the salinity drop became noticeable. This decrease of salinity can be followed until the summer conditions attained, the end of June. They concluded from the density differences that the salinity of the Marmara out flow depends on the stability or instability of the discontinuity layer, separating the upper and lower water of the Sea. In the Bosphorus, in the Sea of Marmara and in the Dardanelles a process of mixing occurs between the upper and the lower waters trough the discontinuity layer. The dominant factor governing the hydrographic events in the straits is the stability of the discontinuity layer.

Pektaş (1953), in his study of the Bosphorus undercurrent and mixing of water gives together with a review of the previous studies a presentation of his observations made in the period 1951-1954. His conclusions are based on observations spread over a relatively long time span, covering all seasons of the year. He was able to track the monthly and yearly variations on the hydrographic conditions and current behavior. His conclusions may be summarized as follows:

- The connection between the Aegean and the Sea of Marmara forms the first stage of the link between the Mediterranean and the Black Sea and allows, during all seasons, both the layers to flow without any obstruction. Therefore in every season in the depths of the Sea of Marmara, the typical Mediterranean water is found. This is the indication of the presence of a normal open sea – basin connection.
- The salinity stratification in the Sea of Marmara is subject to seasonal variations. The thickness of the surface layer in the Sea of Marmara formed by mixing of the Black Sea waters, is in June at its greatest and in November at its lowest level. One of the most important factors affecting the behavior of the Bosphorus undercurrent is the difference of surface elevation between the Black Sea and the Sea of Marmara.
- Connection between the Sea of Marmara and the Bosphorus is restricted by the so called "Southern Sill", extending between Sarayburnu and Üsküdar. The sill plays an important role on the water exchange. Water entering over the southern sill into the deeper channel of the Bosphorus meets the surface current flowing from the Black Sea and is forced to return back to the Sea of Marmara. This is one of the most important factors controlling the flow of the Mediterranean water into the Black Sea basin.
- Meteorological changes and any variations in the water budget of the Black Sea are the main factors governing the water exchange through the Bosphorus.
- Some evidence supporting the hypothesis set by Ullyott and Ilgaz regarding the "return flow of the deeper water mass" was found during the surveys under some special occasions but not always. Therefore, it was suggested that this return flow should not be overemphasized.
- In the narrowest part of the Bosphorus, due to the speed of the surface current, some locations of low pressure were formed where upwelling of the deep water may be observed.

During his observations Pektaş found evidence that due to the changes of the salinity stratification of the surface water and the seasonal fluctuations of the surface currents, the undercurrent does not reach the Black Sea basin during a period of six months (March to August), but during the other half of the year (August to March) it passes over the "Northern sill" of the Bosphorus into the Black Sea (Pektaş, 1954).

Pektaş (1956), in his work on the "Hydrographical Peculiarities of the Seas Surrounding Turkey" states that the exit of the deep current from the Bosphorus is possible when the surface level of the Black Sea is low, but not when it is high. As a consequence, the mass of water contained in the Bosphorus is not of the same origin everywhere and during every season. Stratification can often be detected, with an upper most layer of pure Black Sea water, a lowest most layer of pure Marmara water and a mixture of the two as in the intermediate layer. During the winter and the spring it is not rare that the northern part of the Bosphorus consists of Black Sea water only.

Uyguner (1957) in his work on the Nitrite ($NO_2 - N$) concentrations of the waters of the Bosphorus, Dardanelles and off Trabzon, gives an account of his observations performed during April 1955 to January 1956. He studied horizontal and vertical distribution of nitrite and its yearly variations. He found a maximum of 7 mg/m³ in the surface waters of the Bosphorus; however he recorded 3.3 mg/m³ at 70 m depth. In the Dardanelles at the surface layers the maximum concentration recorded was 2.3 mg/m³ and in the deepwater it was 8 mg/m³.

In 1962, Artuz on board the R/S "ARAR" measured, at 57 hydrographic stations covering the Sea of Marmara, the temperature distribution in the different layers together with salinity and dissolved oxygen measurements. Monthly measurements were performed at these stations. The largest seasonal variation of the temperature was found at the surface layer (0-0.5 m) with a mean value of $14.9°C$. At greater depths, the variation decreased and reached a minimum of $0.1°C$ at 200 m. The temperature data collected on these surveys was used to explain the fluctuations on the abundance of pelagic fishes in the Sea of Marmara (Artuz, 1962).

In 1967, DAMOC (which is a consortium of consultant companies) investigations for the Master Plan for the marine outfalls for Istanbul Metropolitan area has been performed for World Health Organization (WHO)supported by United Nations Development Programme (UNDP). Physical and chemical oceanographic data collected by the Turkish Navy Hydrographic Office are presented in the documents of this work. The observations were conducted during the period September 1967 to February 1968. Measurements performed during this program are collected under the titles Temperature Measurement,

Salinity, Dissolved Oxygen, Transparency, Current Measurements, Sea Level Measurements, Biological Observations, Trace Metal Analyses and Meteorological Observations (DAMOC, 1971).

Çeçen *et al.* (1981) carried out investigations on the hydrographic conditions of the Bosphorus in order to determine the water mass transport of the undercurrent. In their final report submitted to Turkish National Science foundation (TUBITAK), the basic mechanism of the two layer current in the Bosphorus is explained as originating from the differences of the hydrographical conditions of the Sea of Marmara and the Black Sea.

During joint surveys together with the Turkish Navy Hydrographic and Oceanographic Office, salinity and temperature profiles were determined in the Bosphorus throughout 1980. Interface profiles based on these observations revealed that the slope of the interface is large in the winter and especially in the spring, whereas it is smaller in the summer and fall. A blockage of Marmara water occurs in the spring at the northern parts of the Bosphorus. In the report, the possibility of the construction of a mathematical model for the Bosphorus current system is discussed. Bayazıt and Sümer (1982) carried out some additional measurements in order to explain the properties of the two-layered flow and have submitted a report as an addendum to the first report. In their report, the results of the measurements performed along four vertical cross-sections of the Bosphorus near the Black Sea entrance are presented. The evaluation of these measurements has shown that the lower layer which enters from the Marmara does not always reach this section. It was concluded that flow in the lower layer could not reach the Black Sea basin in the spring when the discharge entering the Bosphorus from the Black Sea takes large values due to the increase of the runoff volumes. In this report, a two-layer model taking both the interfacial and bottom friction into account has been adopted. Their results appear to be in fair agreement with the available field data.

APPENDIX B: DIFFERENTIATION OF INTEGRALS CONTAINING A PARAMETER; LEIBNITZ'S RULE

The integral

$$I(\beta)=\int_{a(\beta)}^{b(\beta)} f(x,\beta)dx \tag{B.1}$$

has a function of the parameter β which is not a function of x, solely a dummy integration variable.

$$I'(\beta)=\frac{d}{d\beta}\int_{a(\beta)}^{b(\beta)} f(x,\beta)\,dx \tag{B.2}$$

In principle, evaluating the integral and then taking $d/d\alpha$ have to be done; in practice, however, inverting the order of integration and differentiation can be advantageous. The difference quotient is,

$$\frac{I(\beta+\Delta\beta)-I(\beta)}{\Delta\beta}=\frac{1}{\Delta\beta}\left\{\int_{a+\Delta a}^{b+\Delta b} f(x,\beta+\Delta\beta)\,dx-\int_{\alpha}^{b} f(x,\beta)\,dx\right\} \tag{B.3}$$

$$=\int_{a}^{b}\frac{f(x,\beta+\Delta\beta)-f(x,\beta)}{\Delta\beta}\,dx+\frac{1}{\Delta\beta}\int_{b}^{b+\Delta b} f(x,\beta+\Delta\beta)\,dx-\frac{1}{\Delta\beta}\int_{a}^{a+\Delta a} f(x,\alpha+\Delta\alpha)\,dx \tag{B.4}$$

$$\approx\int_{\alpha}^{b}\frac{f(x,\beta+\Delta\beta)-f(x,\beta)}{\Delta\beta}\,dx+f(b,\beta+\Delta\beta)\,\frac{\Delta b}{\Delta\beta}-f(a,\beta+\Delta\beta)\,\frac{\Delta\alpha}{\Delta\beta} \tag{B.5}$$

A Continuous function, f, is constant over the infinitesimal intervals from $b\le x\le b+\Delta b$ to $a\le x\le a+\Delta a$. Formally, letting $\Delta\alpha\to 0$, the Leibnitz rule is obtained as;

$$I'(\beta)=\int_{\alpha(\beta)}^{b(\beta)}\frac{\partial f(x,\beta)}{\partial\beta}\,dx+f\left[b(\beta),\beta\right]\frac{db}{d\beta}-f\left[a(\beta),\beta\right]\frac{da}{d\beta} \qquad (B.6)$$

Equation (B.1) is valid if $\partial f/\partial\beta$ be continuous in the rectangular x, and the derivatives $\partial f/\partial\beta$, $\partial b/\partial\beta$ and $\partial a/\partial\beta$ all exist.

APPENDIX C: WIDTH INTEGRATION OF SHALLOW WATER EQUATIONS

Assuming the steady flow, neglecting the Colioris force and pressure variations, Equation (3.58) becomes,

$$\int_{A(x)}^{B(x)} \left(\underbrace{u\frac{\partial u}{\partial x}}_{1} + \underbrace{v\frac{\partial u}{\partial y}}_{2} \right) dy = \int_{A(x)}^{B(x)} \left(\underbrace{-g\frac{\partial \eta}{\partial x}}_{3} + \underbrace{\frac{\tau_s^x - \tau_b^x}{\rho d}}_{4} + \underbrace{N_h \nabla_h^2 u}_{5} \right) dy \tag{C.1}$$

and the continuity equation becomes,

$$\int_{A(x)}^{B(x)} \left(\underbrace{\frac{\partial}{\partial x}(ud)}_{6} + \underbrace{\frac{\partial}{\partial y}(vd)}_{7} \right) dy = 0 \tag{C.2}$$

By definition

$$\int_{A(x)}^{B(x)} u dy = \bar{u} b \tag{C.3}$$

where b is the width at that cross section and the integral limits are the coordinates of the opposite sides. Bar denotes the width averaged quantities.

$$\int_{A(x)}^{B(x)} u^2 dy = \varepsilon \bar{u}^2 b \tag{C.4}$$

where ε is the kinetic energy factor taken as 1.05 for turbulent flows.

$$\int_{A(x)}^{B(x)} \eta dy = \bar{\eta} b \tag{C.5}$$

$$\int_{A(x)}^{B(x)} ddy = Db \tag{C.6}$$

where D denotes the total depth

For determining the equations used in the box model have been width integrated term by term as follows;

First term,

$$\int_{A(x)}^{B(x)} \left(u \frac{\partial u}{\partial x} \right) dy = \frac{\partial}{\partial x} \int_{A(x)}^{B(x)} u^2 dy - u(B) \frac{\partial B}{\partial x} + u(A) \frac{\partial A}{\partial x} = \frac{\partial}{\partial x} \left(\varepsilon \bar{u}^2 b \right) \tag{C.7}$$

Second term is

$$\int_{A(x)}^{B(x)} \left(v \frac{\partial u}{\partial y} \right) dy = \frac{\partial}{\partial y} \int_{A(x)}^{B(x)} uv dy - v(B) \frac{\partial B}{\partial y} + v(A) \frac{\partial A}{\partial y} = \frac{\partial}{\partial y} \int_{A(x)}^{B(x)} (uv) dy \cong 0 \tag{C.8}$$

and τ_{xy} lateral mixing is approximated as zero.

Third term is

$$-g \int_{A(x)}^{B(x)} \frac{\partial \eta}{\partial x} dy = -g \left(\frac{\partial}{\partial x} \int_{A(x)}^{B(x)} \eta dy \underbrace{- \eta(B) \frac{\partial B}{\partial x} + \eta(A) \frac{\partial A}{\partial x}}_{-\bar{\eta} \frac{\partial}{\partial x}(B-A)} \right) = -g \left(\frac{\partial (\bar{\eta} b)}{\partial x} - \bar{\eta} \frac{\partial b}{\partial x} \right) \tag{C.9}$$

Fourth term is

$$\int_{A(x)}^{B(x)}\left(\frac{\tau_s^x-\tau_b^x}{gd}\right)dy=\frac{\tau_s^x-\tau_b^x}{gD(x)}b(x) \tag{C.10}$$

Fifth term is

$$N_h\int_{A(x)}^{B(x)}\left(\underbrace{\frac{\partial^2 u}{\partial x^2}}_{a}+\underbrace{\frac{\partial^2 u}{\partial y^2}}_{b}\right)dy=N_h\left(\frac{\partial^2(b\bar{u})}{\partial x^2}+\frac{1}{\mu}\left[|\tau_A|+|\tau_B|\right]\right)$$

$$a=\int_{A(x)}^{B(x)}\frac{\partial^2 u}{\partial x^2}dy=\frac{\partial}{\partial x}\int_{A(x)}^{B(x)}\frac{\partial u}{\partial x}dy-\left.\frac{\partial u}{\partial x}\right|_B\frac{\partial B}{\partial x}+\left.\frac{\partial u}{\partial x}\right|_A\frac{\partial A}{\partial x}=\frac{\partial^2\left(\bar{u}b\right)}{\partial x^2} \tag{C.11}$$

$$b=\int_{A(x)}^{B(x)}\frac{\partial^2 u}{\partial y^2}dy=\left.\frac{\partial u}{\partial y}\right|_A^B=\frac{1}{\mu}\left[|\tau_A|+|\tau_B|\right]\cong 0$$

Lateral boundary shear stresses can be approximated as zero since model does not take the sides effects into consideration. No slip condition applied.

Sixth term is

$$\int_{A(x)}^{B(x)}\frac{\partial}{\partial x}(ud)dy=\frac{\partial}{\partial x}\int_{A(x)}^{B(x)}dudy-ud(B)\frac{\partial B}{\partial x}+ud(A)\frac{\partial A}{\partial x}=\frac{\partial(\bar{u}Db)}{\partial x} \tag{C.12}$$

Seventh term is

$$\int_{A(x)}^{B(x)}\frac{\partial}{\partial y}(vd)dy=vd\Big|_A^B=0 \tag{C.13}$$

Collecting all the terms and rearranging them the with integrated one dimensional equations for the box model the momentum equation becomes

$$\frac{\partial}{\partial x}\left(\varepsilon\bar{u}^2 b\right)=-g\left[\frac{\partial\left(\bar{\eta}b\right)}{\partial x}-\bar{\eta}\frac{\partial b}{\partial x}\right]+\frac{\tau_s^x-\tau_b^x}{gD(x)}b(x)+N_h\left(\frac{\partial^2(b\bar{u})}{\partial x^2}\right) \tag{C.14}$$

and the continuity equation becomes

$$\frac{\partial(\bar{u}Db)}{\partial x} = 0 \tag{C.15}$$

REFERENCES

Alpar, B. and H. Yüce, 1998, "Sea Level Variations and Their Interactions between the Black Sea and the Aegean Sea", *Estuarine, Coastal and Shelf Science*, Vol. 46, pp. 609–619.

Al- Rabeh, A. H. and N. Günay, 1992, "On the Application of a Hydrodynamic Model for a Limited Sea Area", *Coastal Engineering*, Vol. 17, pp. 173-194, Elsevier Science Publishers, Amsterdam.

Anati, D., G. Assaf and R. Thompson, 1977, "Laboratory Models of Sea Straits", *J. Fluid Mech.* Vol. 81, pp. 341-351.

Armi, L. and D. M. Farmer, 1988, "The Flow of Mediterranean Water Through the Strait of Gibraltar", *Progr. Oceanogr.*, Vol. 21, pp. 1-105.

Artuz, I., 1962, "Some Observations on the Yearly Temperature Variation in the Different Layers of the Manmara Sea", *Hidrobiologi*, Univ. of Istanbul, Seri B, Vol. VI, Fasc. 1-2, Istanbul.

Assaf, G. and A. Hecht, 1974, "Sea Straits: A Dynamical Model", *Deep-Sea Res.* Vol. 21, pp. 947-958.

Atluri, S. N. and T. Zhu, 2000, "New Concepts in Meshless Methods", *Int. J. Numerical Methods in Engineering*, Vol. 47, pp. 537-556.

Atluri, S. N., H. G. Kim and J. Y. Cho, 1999, "A Critical Assessment of the Truly Meshless Local Petrov-Galerkin (MLPG), and Local Boundary Integral Equation (LBIE) Methods", *Computational Mechanics*, Vol. 24, pp. 348-372.

Balakrishnan, K., R. Sureshkumar, and P. A. Ramachandran, 2002, "An Operator Splitting-Radial Basis Function Method for the Solution of Transient Nonlinear

Poisson Problems", *Computers and Mathematics with Applications,* Vol. 43, pp. 289-304.

Bayazıt, M. ve M. Sümer, 1982, "*Istanbul Boğazının Osinografik ve Hidrolik Etudu – 2*", ITU, TÜBİTAK Rapor No. 28.

Black Sea Pilot, 1955, Hydrographic Department of the Admiralty, Her Majesty's Service Office, London, England.

Bogdanova, A. K. and V. N. Stopanov, 1974, "Hydrodynamic Estimate of the Blocking Conditions of the Lower-Bosphorus Current", *Oceanology*, Vol. 14, pp. 37-40.

Bogdanova, A. K., 1961, "Raspredeleni Sredzemnomozkikh Vod v chenommore", Okeanologiya 1, No. 6, pp. 983-991; Engl. Trans., 1963, "The distribution of Nediterranean Waters in the Black Sea", *Deep Sea-Research*, Vol. 10, pp. 665-672.

Bogdanova, A. K., 1965, "Seasonal Fluctuation in the Inflow and Distrubution of the Mediterranean Waters in the Black Sea, in "*Basic Features of the Geological Structure of the Hydrologic Regime and Biology of the Mediterranean Sea,*" Ed. by L. M. Fain, Academy of Science, USSR, Moscow, Engl. Trans., 1969 Instutute of Modern Languages, Washington, DC (AD686001).

Bogdanova, A. K., 1969, "Hydrology of the Bosphorus and the pre-Bosphorus Area of the Black Sea", in "*Water Exchange through the Bosphorus and its Effect upon the Hydrology and Biology of the Black Sea,*", Naukova Dumka Press, Kiev, pp. 5-121.

Bozoklar, U., 1990, *A Hydrodynamic-Numerical Model for the Bosphorus*, M.S. Thesis, Boğaziçi University.

Çeçen, K., M. Bayazıt, M. Sümer, S. Güçler, M. Doğusal and H. Yüce, 1981, "*Istanbul Boğazinin Osinografik ve Hidrolojik Etudu-I, Tubitak Sulama Tesisleri*", Kesin Rapor No. 24, pp. 165, Istanbul Technical University.

Daily, J. W. and D. R. F. Harleman, 1996, *Fluid Dynamic*, Addison-Wesley.

DAMOC Report, 1971, "*Master Plan and Feasibility Report for Water Supply and Sewerage for the Istanbul Region*," Vol III, (A report prepared for the World Health Organization and United Nations Development Programme by Daniel, Mann, Johnson and Mendenball, Los Angles, California USA).

Defant, A., 1961, *Physical Oceanography,* Vol. 1, Pergamon.

Dick, T., and J. Marsalek, 1973, "Exchange Flow between Lake Ontario and Hamilton Harbour", *Environment Canada Inland Waters Directorate,* Scientific Series No. 36.

Ekman, V. W., 1905, "On the Influence of the Earth's Rotation on the Ocean Currents", *Astronomy and Physics*, Vol. 2, No. 11, pp. 1-53.

Fedoseyev, I., M. J. Friedman, and E. J. Kansa, 2002, "Improved Multiquadric Method For Elliptic Partial Differential Equations Via PDE Collocation On The Boundary", *Computer and Mathematics with Applications*, Vol. 43, No. 3, pp. 439-455.

Fornberg B., T. A. Driscoll, G. Wright and R. Charles, 2002, "Observations on the Behavior of Radial Basis Functions Near Boundaries", *Comput. Math. Appl.*, Vol. 43, pp. 473-490.

Franke, C., 1982, "Scattered Data Interpolation: Tests of Some Methods", *AMS Mathematics of Computation Journal*, Vol. 38, No. 157, pp. 181-200.

Franke, C. and R. Schaback, 1998, "Solving Partial Differential Equations by Collocation Using Radial Basis Functions", *Appl. Math. Comput.*, Vol. 93, pp. 73-82.

Garratt, J. R., 1977, "Reviev of Drag Coefficients over Ocean and Continents", *Monthly Weather Review*, Vol. 7, No. 105, pp. 915-929.

Gerritesen, H. and A. C. Biljlsma, 1988, "Modelling of Tidal and Wind Driven Flow: The Doutch Continental Shelf Model", in Schrefler and Zienkiewicz (Eds.), *Computer Modelling in Ocean Engineering*, No. 398, pp. 331-338, Rotherdam, Belkema.

Golberg, M. A., C. S. Chen and S. R. Karur, 1996, "Improve Multiquadric Interpolation for Partial Differential Equations", *Engineering Analysis with Boundary Elements,* Vol. 18, pp. 9-17.

Gregg, M. and E. Özsoy, 2002, "Flow, Water Mass Changes, and Hydraulics in the Bosphorus", *J. Geophys. Res.,* Vol. 107, No. 3, pp. 329-359.

Gueydon, de A., 1886, "Determination des Courrants Sousmarine", *Rev. Marit. et Col.*, Paris, Vol. 91, pp. 338-347.

Günnerson, C. G. and E. Özturgut, 1974, "*The Bosphorus and the Black Sea Geology, Chemistry and Biology*" Memoir No. 20, The American Assoc. of Petroleum Geologists, pp. 99-113.

Hamblin, P. and G. Lawrence, 1990, "Exchange flows between Hamilton Harbour and Lake Ontario", in *Proc. 1st Biennial Environmental Specialty Conference, CSCE,* pp. 140-148.

Hardy, R. L., 1971, "Multiquadric Equations of Topography and Other Irregular Surfaces", *J. Geophys. Res.*, Vol. 176, No. 3, pp. 1905-1915.

Hardy, R. L., 1990, "Theory and Applications of the Multiquadric-Biharmonic Method", *Comput. Math. Applic.*, Vol. 19, pp. 163-208.

Henry, R. F. and N. S. Heaps, 1976, "Development of a Three-Dimentional Numerical Model of the Irish Sea", *International Marine Construction,* Vol. 167, pp. 147-162.

Hickernell, F. J. and Y. C. Hon, 1998, "Radial Basis Function Approximation of The Surface Wind Field From Scattered Data", *Appl. Sci. Comput.*, Vol. 4, pp. 221-247.

Hon Y. C. and X. Z. Mao, 1998, "An Efficient Numerical Scheme For Burgers' Equation", *Appl. Math. Comput.*, Vol. 95, pp. 37-50.

Hon, Y. C., M. W. Lu, W. M. Xue and Y. M. Zhu, 1997, "Multiquadric Method for the Numerical Solution of a Biphasic Mixture Model", *Applied Math and Computation*, Vol. 88, pp. 153-175.

Hon, Y. C., K. F. Cheung, X. Z. Mao and E. J. Kansa, 1999, "A Multiquadric Solution for Shallow Water Equation", *ASCE J. of Hydraulic Engineering*, Vol. 125, No. 5, pp. 524-533.

Kansa, E. J., 1990a, "Multiquadrics; A Scattered Data Approximation Scheme with Applications to Computational Fluid Dynamics: I. Surface Approximations and Partial Derivative Estimates", *Comput. Math. Applic.*, Vol. 19, No. 8, pp. 127-145.

Kansa, E. J., 1990b, "Multiquadrics; A scattered Data Approximation Scheme with Applications to Computational Fluid Dynamics: II. Solutions to Parabolic, Hyperbolic, and Elliptic Partial Differential Equations", *Comput. Math. Applic.*, Vol. 19, No. 9, pp. 147-161.

Kansa, E. J., 1992, "A Strictly Conservative Spatial Approximation Scheme for the Governing Engineering and Physics Equations over Irregular Regions and Homogeneously Scattered Nodes", *Comput. Math. Applic.*, Vol. 24, No. 5, pp. 169-190.

Kansa, E. J. and Y. C. Hon, 2000, "Circumventing the Ill-Conditioning Problem with Multiquadric Radial Basis Functions: Applications to Elliptic Partial Differential Equations," *Comput. Math. Applic,* Vol. 39, No.7, pp. 123-137.

Komar, P. D., 1976, "Boundary Layer Flow under Steady Unidirectional Currents", *Marine Sediment Transport*, Vol. 28, pp. 91-106, John Wiley and Sons, Newyork.

Kowalik, Z. and T. S. Murty, 1993, *Numerical Modeling of Ocean Dynamics*, World Scientific Publishing, Singapore.

Liu, S. K. and J. J. Leendertse, 1978, "Multidimensional Numerical Modelling of Estuaries and Coastal Seas", *Adv. Hydrosciences*, Vol. 11, pp. 95–164.

Lulksch, J. and J. Wolf, 1892, "Physitalische Untrsuchungen in Oestlichen Mittelmeer III Reise", *Berichte d.Kommission zur Erforschung des oestlichen Muttelmeers* VIII.

Maderich, V. S., and V. Efroimson, 1990, "Theory for Water Exchange Across a Strait", *Oceanology*, Vol. 30, pp. 415–420.

Madericha, V.and S. Konstantinov, 2002, "Seasonal Dynamics of the System Sea-Strait: Black Sea–Bosphorus Case Study", *Estuarine, Coastal and Shelf Science*, Vol. 55, pp. 183–196.

Magnaghi, G. B., 1894, "Di Alcune Esprience Esequiet Nagli Stretti dei Dardanelli e del Bosphoro per Misurarvi le Correnti a Varie Profondita", *Atti del primo Congr. Geogr. Ital., Genua* 1, Vol. 2, pp. 440-453.

Makaroff, S., 1885, "On the Water Exchange Between Black Sea and Mediterran Seas", in Russian.

Makaroff, S., 1899, "On Some Oceanogharhic Problems", *Proceed. of Royal Soc. of Edinburgh*, pp. 391-400.

Marsilli, L. F., 1861, Osservazioni Interno al Bosforo Traio overo Canale di Contantinopoli, Roma.

Merz, A., 1921, Stroemungen von Bosphorus und Dardanellen. S. A. aus Verhandlungen 20, *Deutsch. Geogr. Tages.*, Berlin.

Merz, A., 1928, Hydrographische Untersuchungen in Bosphorus und Dardanellen. Bearbeitet von L. Moeller, Veroeff. des Inst. fuer Meereskunde an der Univ. Berlin.

Moller, L., 1928, "Alfred Merz Hydrographische Untersuchungen im Bosphorus und Dardanellesen," Veroff. Inst. Meeresk, Berlin, Vol. 18.

Moody, J., and J. Darken, 1989, "Fast Learning in Networks of Locally-Tuned Processing Units" *Neural Computation*, Vol. 1, pp. 281–294.

Murray, S. and W. Johns, 1997, "Direct Observations of Seasonal Exchange Through the Bab el Mandab Strait", *Geophys. Res.*, Lett. Vol. 24, pp. 2557-2560.

NASA, 2003, "*Stallite image number 12596*", National Aeronautics and Space Administration, http://www.nasa.gov.

Natterer, K., 1894, Chemische Untersuchungen in Oestlichen Mittelmeer, (in Merz u. Muller).

Natterer, K., 1895, "Tiefseeforschungen in Marrara Meer auf S. M. Shiff Taurus" in Mai 1894. Denkschriften Kais. Akad. Wiss. Wien. Math. Nat. Kl., 62. In "*Berichte der Kommission zur Erforcshung des oestlichen Mittelmeeres*", 4 Reihe, Abschnit XIV.

Neumann, G., 1952, "On the Complex Nature of Ocean Waves and the Growth of the Sea under the Action of Wind", *Gravity Waves*, NBS Circular 521.

Neumann, G., and W. J. Pierson, Jr., 1966, *Principals of Physical Oceanoraphy*, Prentice-Hall, New Jersey.

Nielsen, J. N., 1912, "Report on the Danish Oceanographical Expedition 1908-1910 to the Mediterranean and Adjacent Seas", Report Vol. 1, pp. 77-191.

Oğuz, T. and H. Sur, 1989, "A Two-Layer Model of Water Exchange Through the Dardanelles Strait", *Oceanol. Acta*, Vol. 12, pp. 23-31.

Oğuz, T., E. Özsoy, M. Latif, H. Sur and U. Ünlüata, 1990, "Modeling of Hydraulically Controlled Exchange Flow in the Bosphorus Strait", *J. Phys. Oceanogr*, Vol. 20, pp. 945-965.

Ottesen Hansen, N. and J. Moller, 1990, "Zero Blocking Solution for the Great Belt Link" in *the Physical Oceanography of Sea Straits* edited by L. Pratt, Vol. 318 of NATO ASI series C, pp. 153-170.

Özsoy, E., M. A. Latif, H. Sur and Y. Goryachkin, 1996, "A Review of the Exchange Flow Regime and Mixing in the Bosphorus Strait" in *Mediterranean Tributary Seas*. Bull. de l'Inst. Oceanogr. Monacono. Vol. 17, CIESM Science Series, Monaco, pp. 187–204.

Pektaş, H., 1953, "*Surface Currents in the Bosphorus and the Sea of Marmara*," Publications of the Hydrobiological Research Instutute, Faculty of Science, University of Istanbul, Ser. A, Vol. 1, No. 4, pp. 154-169.

Pektaş, H., 1954, Bogazicinde Satih-Alti Akintilari ve Su Karisimlari, I. bid., Cilt 2, sayı 1.

Pektaş, H., 1956, "The Influence of the Mediterranean Water on the Hydrology of the Black Sea", *4th Tech. Papers Meeting Fisheries Center of Istanbul*, Mediterranean General Fisheries Council.

Powell, M. J. D., 1992, "The Theory of Radial Basis Function Approximation in 1990", *Wavelets, Subdivision Algorithm and Radial Basis Functions*, ed. Will Light, Chapter 3, Vol. II, Oxford University Press, pp. 105-210.

Pratt, L., 1986, "Hydraulic Control of Sill Flow with Bottom Friction", *J. Phys. Oceanog*, Vol. 16, pp. 1970-1980.

Schijf, T. B., and J. C. Schönfeld, 1953, "Theoretical Considerations on the Motion of Salt and Fresh Water", *Proc. of the Minn. Intl Hydraulics Conv.*, Joint meeting IAHR and Hyd. Div., ASCE, pp. 321-333.

Shu, C., H. Ding and K. S. Yeo, 2004, "Solution of Partial Differential Equations by a Global Radial Basis Function-Based Differential Quadrature Method", *Engineering Analysis with Boundary Elements*, Vol. 28, pp. 1217-1226.

Simonov, A. I. and E. N. Altman, (eds.), 1991, "Hydrometeorology and Hydrochemistry of Seas of USSR. IV, Black Sea, pt. 1, Hydrometeorological Conditions", *Hydrometeorological Publishers*, pp. 430-450, S. Petersburg.

Spratt, 1870, "On the Under Current Theory of the Ocean as Propounded by Recent Explorers", *Procced. of the Royal Geog. Soc. of London.*

Sprindler, J., 1894, "Russische Untersuchungen im Marmara Meer auf den Turkischen Dempfer "Selanik", *Ann. d. Hydr. Mar. Met.*, pp. 313-323.

Sprindler, J., 1898, "Materials on the Hydrology of the Sea of Marmara. Sapiski d. Kaiss", *Russ. Geogr. Soc. Proceed.*, Vol. 33.

Sümer, B. M. and M. Bakioğlu, 1981, "Sea-Strait Flow with Special Reference to Bosphorus", Istanbul Technical University, Faculty of Civil Engineering, pp. 25-34.

Tolmazin, D., 1985, "Changing Coastal Oceanography of the Black Sea", *II. Mediterranean Effluent Prog. Oceanog.*, Vol. 15, pp. 277-316.

Turkish Navy Department of Navigation, *Hydrography and Oceanography (TNHO) Map* No: 2921 a, b.

Ullyott, P., 1953, "Conditions of Flow in the Bosphorus", Publications of the Hydrobiological Research Instutute, Faculty of Science, University of Istanbul, Ser. B., No. 3, pp. 199-214.

Ullyott, P. and H. Pektaş, 1952, "A Note on the Yearly Temperature and Salinity Cycle in the Dardanelles", *Hidrobiologi Pub. of the Hydrobiol*, Res. Inst. Univ. Istanbul, Seri A, cilt I, Haziran sayı: 1, pp 19-34, Istanbul.

Ullyott, P. and O. Ilgaz, 1943, "*Observations on the Bosphorus II: Geographical and Hydrographical Conditions*", Publications of Faculty of Science, University of Istanbul, Ser. B, Vol. 2.

Ullyott, P. and O. Ilgaz, 1946, "*Observations on the Bosphorus III: The Degree of Turbulence*", Publications of Faculty of Science, University of Istanbul, Ser. B, Vol. 11.

United States Navy Hydrographic Office, 1967, *Oceanographic Atlas of the North Atlantic Section 2*, Physical Properties, Washington, DC

Uyguner, B., 1957, La Dosage du Nitrite dans less Eaux du Bosphore, Dardanelles et Trabuzonde. Considerations sur la Production Biologique du Nitrite et le Cycle d" *Azote. Hidrobiologie*, Serie B., Tome IV., Fasc. 2-3 Univ. Istanbul.

Ünlüata, Ü. and T. Oğuz, 1983, "A Review of the Dynamical Aspects of the Bosphorus", Instutute of Marine Sciences, METU, *NATO Advanced Workshop on Atmospheric and Oceanic Circulation in Mediterranean*, La Spezia, Italy, September.

Ünlüata, Ü., T. Oğuz, M. A. Latif and E. Özsoy, 1990, "On the Physical Oceanography of the Turkish Straits" in *the Physical Oceanography of Sea Straits* (Pratt, L. J., ed.). NATO/ASI Series, pp. 25–60, Kluwer Academic, Netherlands.

Wang, J. D., 1990, "Numerical Modelling of Bay Circulation", *The Sea and Ocean Engineering Science*, Vol. 9, Part B, Wiley-Luterscience.

Wang, J. D. and G. R. Liu, 2002, "A Point Interpolation Meshless Method Based on Radial Basis Functions", *Int. J. Numer Meth Engrg*, Vol. 54, No. 11, pp.1623-1648.

Wendland, H., 1995, "Piecewise Polynomial, Positive Definite and Compactly Supported Radial Functions of Minimal Degree", *Advances In Computational Mathematics*, Vol. 4, pp. 389-396.

Wharton, W. J. L., 1886, "Report on the Currents of the Dardanelles and Bosphorus", Published by order of the Lord Commissioners of the Admiralty, London.

Wharton, W. J. L., 1899, Undercurrents, *Nature LX.*, pp. 316-350.

Wong, S. M., Y. C. Hon and M. A. Golberg, 2002, "Compactly Supported Radial Basis Functions For the Shallow Water Equations", *Appl. Math. Comput.*, Vol. 127, pp. 79-101.

Yüce, H., 1996, "Mediterranean Water in the Strait of Istanbul (Bosphorus) and the Black Sea Exit", *Estuarine, Coastal and Shelf Science,* Vol. 43, pp. 597–616.

Zaremba L. J. and G. A. Lawrance and R. Pieters, 2003, "Frictional Two-Layer Exchange Flow", *J. Fluid Mech.*, Vol. 474, pp. 339-354.